TG-752
NOVEMBER 1965
Copy No. 45

AD630342

Technical Memorandum

AN ENGINEERING METHOD FOR RAPID CALCULATION OF SUPERSONIC-HYPERSONIC PRESSURE DISTRIBUTIONS ON LIFTING AND NON-LIFTING POINTED BODIES OF REVOLUTION AND SEVERAL SPECIAL CASES OF BLUNT-NOSED BODIES OF REVOLUTION

by R. J. VENDEMIA, Jr.

THE JOHNS HOPKINS UNIVERSITY • APPLIED PHYSICS LABORATORY

TG–752

NOVEMBER 1965

Technical Memorandum

AN ENGINEERING METHOD FOR RAPID CALCULATION OF SUPERSONIC-HYPERSONIC PRESSURE DISTRIBUTIONS ON LIFTING AND NON-LIFTING POINTED BODIES OF REVOLUTION AND SEVERAL SPECIAL CASES OF BLUNT-NOSED BODIES OF REVOLUTION

by R. J. VENDEMIA, Jr.

THE JOHNS HOPKINS UNIVERSITY • APPLIED PHYSICS LABORATORY
8621 Georgia Avenue, Silver Spring, Maryland 20910

Operating under Contract NOw 62-0604-c, Bureau of Naval Weapons, Department of the Navy

SUMMARY

This report prescribes a method for calculating pressure coefficients and local Mach numbers for lifting and non-lifting pointed bodies of revolution and for several special cases of blunt-nosed bodies. The method, which utilizes hybrid tandem solutions involving Generalized Newtonian and Shock-Expansion theories, provides accurate results for a variety of nose shapes and fineness ratios over a range of supersonic/hypersonic Mach numbers. The numerical simplicity of the method, which makes it readily applicable for quick hand-calculational procedures, was the prime factor in its selection and publication; the few existing methods which yield accurate results over a comparable range of application, such as the method of characteristics, are not used extensively because of the lengthy numerical calculations involved.

The present method has been compared with exact solutions, various pertinent theories, and experimental data where available and the overall agreement of the results is quite favorable. The investigation for lifting bodies indicates the present method is applicable for bodies of revolution at angles of attack up to about ten degrees.

This report presents numerical examples showing stepwise calculational procedures for obtaining pressure coefficient and local Mach number distributions along the meridians of a body of revolution at angle of attack. In order to make the report immediately useful to the engineer desiring such information, all of the necessary tables and look-up parameters are included in the appendices.

Table of Contents

Page

Summary ii
List of Figures v
List of Tables vii

I. Introduction 1

II. Symbols and Nomenclature 2

III. Analysis and Results 5

A. Flow Regime 5

B. Methods of Calculating Pressure Distributions 5

1. Generalized Newtonian Theory 5

2. Shock Expansion Method 7

3. Method of Characteristics 8

4. Tangent-Cone Method 8

5. Other Methods 9

6. Present Method 9

C. Method of Correlating Pressure Distributions 9

D. Pressure Distributions for Non-Lifting "Pointed Bodies" of Revolution - Shock Attached 11

1. Tangent Ogives 11

2. Secant Ogives 18

3. Triple Cone-Tangent Ogive Combination 20

4. von Karman Minimum Drag Nose Shapes 21

5. Power Series Minimum Drag Nose Shapes 25

6. Isentropic Spikes 26

E. Pressure Distributions for Non-Lifting Blunt-Nosed Bodies of Revolution 30

1. Hemisphere 30

2. Hemisphere-Cone Combination 32

F. Pressure Distributions on Non-Lifting Cylindrical Afterbodies 34

Page

G. Application of Present Method to Lifting Pointed Bodies of Revolution 36

1. Bodies of Revolution at Small Angles of Attack. . . . 36

2. Bodies of Revolution at Large Angles of Attack. . . . 40

Appendix 1. Calculation of Pressure Coefficient Distribution for a Tangent Ogive-Cylindrical Afterbody Combination at an Angle of Attack of 5 Degrees 44

Appendix 2. Calculation of Pressure Coefficient Distribution for a Tangent Ogive-Cylindrical Afterbody Combination at an Angle of Attack of 10 Degrees 54

Appendix 3. Prandtl-Meyer Flow Table 62

References 64

Acknowledgement 66

List of Figures

Figure		Page
1.	Comparison of Newtonian and Generalized Newtonian Theory with Exact Solutions for Ogives	7
2.	Range of Applicability of Similarity Law for Ogives	10
3.	Shock Detachment Mach Number for Bodies of Revolution with Conical Tip Noses	13
4.	Tangent Ogive Geometric Characteristics	13
5.	$C_{p_{max}}$ for Tangent Ogives	14
6.	Matching Point Value of x/l for Tangent Ogives at All Mach Numbers Considered	16
7.	Tangent Ogive Pressure Coefficient Distribution, $K = 0.5$, 1.0, and 2.0	17
8.	Correlation of Pressure Coefficient Distributions on Tangent Ogives Using the Hypersonic Similarity Parameter, K	19
9.	Pressure Coefficient Distribution on a Triple Cone-Tangent Ogive Combination	20
10.	Tangency Point for Cones Fitted to von Karman Nose Shapes	22
11.	$C_{p_{max}}$ for von Karman Nose Shapes	22
12.	Matching Point Value of x/l for von Karman Nose Shapes	22
13.	Pressure Coefficient Distribution for von Karman Minimum Drag Nose Shape, $l/d = 2.10$, 2.32, and 2.72	23
14.	Pressure Coefficient Distribution for von Karman Minimum Drag Nose Shape, $l/d = 2.10$	24
15.	$C_{p_{max}}$ for 3/4 Power Nose Shapes	25
16.	Tangency Point for Cones Fitted to 3/4 Power Nose Shapes	25
17.	Pressure Coefficient Distribution for 3/4 Power Minimum Drag Nose Shape, $l/d = 3$, 5, and 7	27
18.	Ratio of Matching Point Θ to Nose Semi-Vertex Angle Versus Free Stream Mach Number for Isentropic Spikes	28
19.	Pressure Coefficient Distribution for a 15° Isentropic Spike, $M_o = 2.5$, 3.0, and 4.0	29

Figure		Page
20.	$C_{p_{max}}$ for Hemisphere or Hemisphere-Cone	31
21.	Matching Point Value of Θ for Hemisphere or Hemisphere-Cone	33
22.	Hemisphere Pressure Coefficient Distribution, M_o = 1.82, 2.81, 3.74, 4.76, and 7.7	33
23.	Pressure Coefficient Distribution for a Tangent Ogive-Cylindrical Afterbody Combination at α = 5°, ψ = 0°, 30°, 60°, 90°, 120°, 150°, and 180°	39
24.	Pressure Coefficient Distribution for a Tangent Ogive-Cylindrical Afterbody Combination at α = 10°, ψ = 0°, 30°, 60°, 90°, 120°, 150°, and 180°	43

List of Tables

Table		Page
1.	Percent Error in Drag	18
2.	Pressure Coefficient and Mach Number Starting Values, $x/\ell = 0$, $\alpha = 5°$	45
3.	Values of Sine δ, $\alpha = 5°$	45
4.	Pressure Coefficient Distribution and Mach Number Along $\psi = 180°$ Meridian, $\alpha = 5°$	46
5.	Pressure Coefficient Distribution on Cylindrical Afterbody, $\alpha = 5°$	47
6.	Values of Surface Pressure Coefficient, C_{p_N}, at $\alpha = 0°$	48
7.	Values of M on Cone Surface at $\alpha = 0°$	49
8.	Values of p/p_o at $\alpha = 0°$	50
9.	Values of $M_1{}^*$ on Cone Surface at $\alpha = 0°$	51
10.	Surface Values of $M_2{}^*$	52
11.	Values of S_2/R	53
12.	Pressure Coefficient Starting Values, $x/\ell = 0$, $\alpha = 10°$	55
13.	Mach Number Starting Values, $x/\ell = 0$, $\alpha = 10°$	56
14.	Values of Sine δ, $\alpha = 10°$	56
15.	Pressure Coefficient Distribution and Mach Number Along $\psi = 180°$ Meridian, $\alpha = 10°$	57
16.	Pressure Coefficient Distribution on Cylindrical Afterbody, $\alpha = 10°$	58
17.	Parameters Given in MIT Cone Tables	
	a. $\theta_s = 5°$	59
	b. $\theta_s = 7.5°$	59
	c. $\theta_s = 10°$	60
	d. $\theta_s = 12.5°$	60
	e. $\theta_s = 15°$	61
	f. $\theta_s = 20°$	61
	g. $\theta_s = 25°$	61
18.	Prandtl-Meyer Flow Table	62

BLANK PAGE

I. INTRODUCTION

There are a variety of methods available for the calculation of pressure distributions over lifting and non-lifting bodies of revolution in the supersonic-hypersonic speed regime. The usefulness and range of applicability of these methods have been widely discussed in available literature and are briefly summarized herein.

In general it can be said that the methods having the most extensive range of applicability involve lengthy calculational procedures. Impact theory provides a quick and easy-to-apply method for calculating surface pressures in the supersonic-hypersonic régime if the surface is normal or sufficiently oblique to the flow. The generalized shock-expansion method for steady two dimensional flows is also quick and easy to apply. Its useful range of application is for Mach numbers greater than 2.0 and for values of the hypersonic similarity parameter, $M_o d/\ell$, greater than about 1.2.

The method presented herein is a hybrid combination of modified impact and shock-expansion theories which permits the facile and rapid hand calculation of the pressure and local Mach number distributions along any meridian on the surface of a lifting or non-lifting pointed body of revolution and many of the blunt nosed shapes. This method, which has a wide range of application, is intended for use in handbook fashion by engineers needing such information for studies concerned with aerodynamic heating, structural loads, drag, etc.

Wind tunnel test data in the Mach number range 2.0 to 4.0 are presented and are compared with the theory. These data show the pressure distributions on a secant ogive nose, a triple-cone ogive combination, a von Karman nose shape, and on hemispheres. These nose sections are attached to cylindrical afterbodies.

II. SYMBOLS AND NOMENCLATURE

a	sound speed
c	limiting speed due to expansion into a vacuum
C_p	pressure coefficient
c_p	specific heat at constant pressure
c_v	specific heat at constant volume
d	diameter
GN	Generalized Newtonian
K	hypersonic similarity parameter, $M_o d/\ell$
ℓ	nose length
M	Mach number
M^*	critical Mach number
N	nose caliber
p	static pressure
p_t	total pressure
q	dynamic pressure
R	generating radius for ogival shapes
$\mathcal{R}$	universal gas constant
r	nose radius
r	radius of focal point
S	entropy
$S_2/\mathcal{R}$	parameter, entropy/universal gas constant
SEM	shock-expansion method
s	segment length
V	velocity
x,y	body-fixed rectangular coordinate system
x,r,ϕ	body-fixed cylindrical coordinate system
$\bar{y}$	vertical distance from the tangent ogive generating point to the centerline of the ogive

α	angle of attack; angle between free stream velocity and body centerline
γ	ratio of specific heats
Δ	increment
δ	angle between the free stream velocity and the tangent to the body surface
θ	angle between the body surface and the longitudinal axis of the body
ν	Prandtl-Meyer flow deflection angle
π	radian measure
ρ	density
ϕ	$\cos^{-1}(1 - 2x/\ell)$ by definition
ψ	radial meridian along body surface
∞	infinity

SUBSCRIPTS

o	free stream conditions
1	flow quantities for the zero angle of attack condition
2	flow quantities related to the effect of angle of attack
b	base
c	cone
cn	conditions on the equivalent tangent cone for a specific segment
m	matching point
max	maximum
N	conditions at nose vertex
n	specific segment of equivalent tangent body
s.o.	secant ogive
stag.	stagnation
t	total
'	primed value; conditions at the most forward point of a segment of the equivalent tangent body (s = 0)

Nomenclature used in Appendix 2 corresponding to References 26, 27, and 28.

$\bar{u}/c$, $\bar{a}^{*}/c^{2}$, p_s/p_w, p_w/p_1	parameters given in Reference 26
$\eta/\bar{p}$, $\xi/\bar{\rho}$	parameters given in Reference 27
$p_o/\bar{p}$, $p_2/\bar{p}$, $\rho_o/\bar{\rho}$, $\rho_2/\bar{\rho}$	parameters given in Reference 28
A_1, B_1, S_1	coefficients related to first order effects of angle of attack
A_2, A_3, B_2, B_3, S_2, S_3	coefficients related to second order effects of angle of attack

Subscripts

1	free stream conditions
s	body surface
w	conditions immediately behind shock wave
–	barred quantities; conditions for zero angle of attack

The remaining nomenclature used in Appendix 2 are compatible with values previously defined.

III. ANALYSIS AND RESULTS

A. FLOW REGIME

The flow regime considered herein covers the Mach number range from 1.5 to approximately 8. In general, the Mach number range most seriously considered was from $M_o = 2$ to 6; thus only a small portion of the hypersonic flow regime ($M_o > 5$) has been investigated. The hypersonic regime, however, is basically an extension of the supersonic regime and if the fluid retains the properties of an ideal gas and the ratio of specific heats (c_p/c_v) remains constant, the theories developed for the supersonic continuum should be valid in the hypersonic regime. For extremely high Mach numbers, of course, the properties of the gas may change radically and consequently the theory which was valid at the lower Mach numbers must be modified accordingly.

B. METHODS OF CALCULATING PRESSURE DISTRIBUTIONS

1. Generalized Newtonian Theory

The Newtonian impact theory provides the engineer with a simple, rapid, and easy-to-apply method for determining the local pressure and Mach number distributions over a wide variety of nose shapes. The flow concept as formulated by Newton assumes that the shock wave lies on the body surface and that the component of momentum normal to the body surface is transferred to the body while the tangential component remains unchanged; a condition which is reached in the limit as M_o approaches infinity and γ approaches 1. This concept provides a force or force coefficient (C_p) which is dependent only on the local slope of the surface, i.e.,

$$C_p = 2 \sin^2 \Theta$$

The above expression for C_p reduces to that of the hypersonic small disturbance theory,

$$C_p = (\gamma + 1) \Theta^2 = 2 \Theta^2$$

where the assumption of very slender bodies at high Mach numbers yields:

$$\gamma \rightarrow 1 \text{ as } M_o \rightarrow \infty$$

and $\qquad \sin \Theta = \Theta$ for small angles.

The Newtonian concept of flow as stated above neglects the effects of centrifugal forces which arise due to body curvature. When the body curvature is small in the free stream direction, the centrifugal forces in the thin layer of air between the shock wave and body surface should not affect the impact pressures appreciably. When the body curvature is large, however, the impact pressures might be significantly altered by the centrifugal forces which tend to relieve the impact pressures. Various authors have attempted to modify the simple impact theory expression to account for centrifugal forces and have done so with little or moderate success. #Busemann[1] presents the problem in some detail with encouraging results, but the equation for determining the local pressure coefficient becomes somewhat more complicated than that given by the original simple impact theory.

Since the Newtonian theory offers a convenient, easy-to-apply method of determining pressure distributions, further attempts were made to improve upon the original C_p equation; these efforts proved to be acceptable only when used with values of the hypersonic similarity parameter (K) greater than two. To this extent, Lees[2] suggested the modified form

$$C_p = C_{p_{max}} \sin^2\theta$$

for use with blunt bodies where $C_{p_{max}}$ is derived from the normal shock relations. By generalizing Lees' modified form, Love[3] indicated the above equation could be made to include pointed-nosed bodies when used in the form:

$$C_p = C_{p_N} \frac{\sin^2\theta}{\sin^2\theta_N}$$

where N refers to conditions at the nose vertex. For $\theta_N = 90°$, of course, Love's generalization reverts to Lees' modified form but for θ_N values less than 90°, an expression is obtained which exhibits advantages over the use of simple impact theory ($C_p = 2 \sin^2\theta$). To illustrate graphically, Love's Generalized Newtonian theory has been compared with the Newtonian theory and exact (method of characteristics) solutions for several tangent ogives in Figure 1. The exact solutions were obtained from Rossow[4] and include the effects due to rotation. As shown in Figure 1, the Generalized Newtonian theory offers excellent agreement with the exact solutions up to approximately an x/ℓ value equal to 0.6; of equal interest is the theory's apparent independence of K, the hypersonic similarity parameter. In contrast, the Newtonian theory is markedly affected by K as indicated by the shaded portion of the figure wherein K varies from 0.5 to 4; from this, the Newtonian theory would appear to approach the exact solutions only for $K \gg 1$.

#Reference numbers will always appear as a superscript numeral to the right of the subject and the footnote symbol (#) will always appear as a superscript to the left of the subject.

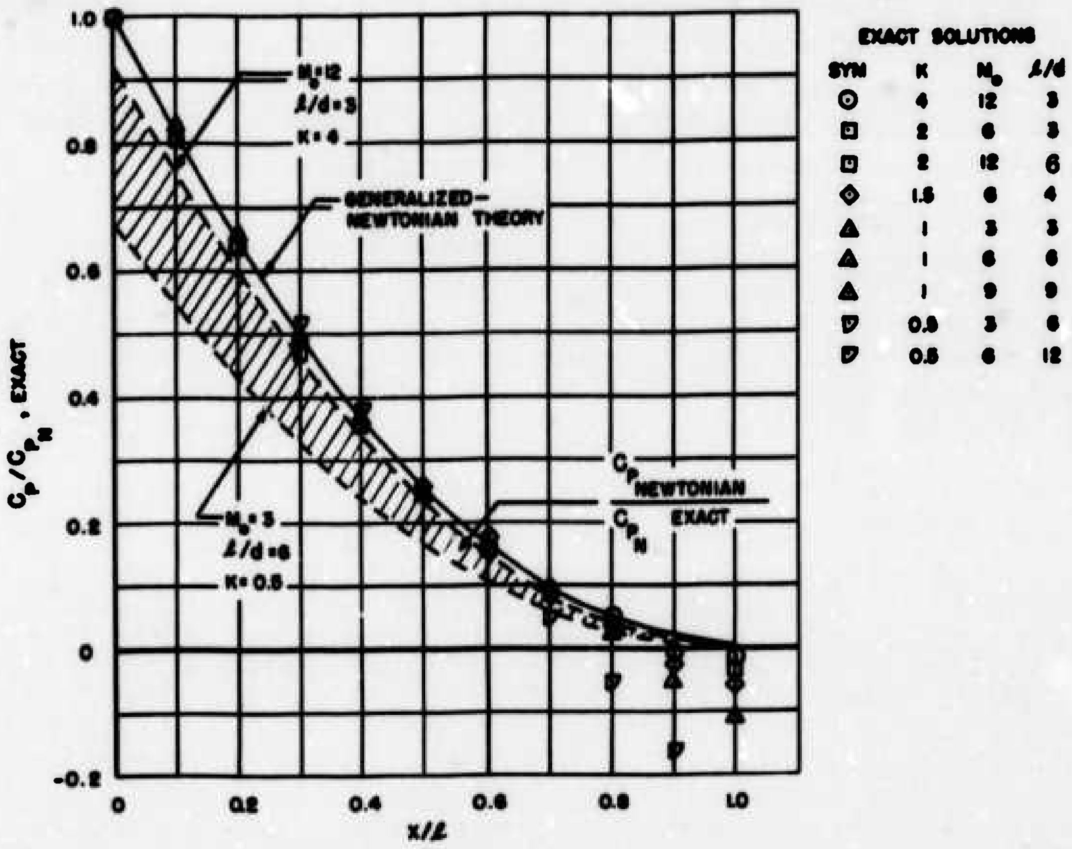

Fig. 1 COMPARISON OF NEWTONIAN AND GENERALIZED-NEWTONIAN THEORY WITH EXACT SOLUTIONS FOR OGIVES

These results indicate the Generalized Newtonian theory would be highly suitable for use in calculating pressure distributions on ogival shapes if one further improvement could be made, i.e., refinement of the theory to better predict the pressure (especially for the lower K values) over the after 40 percent of the nose length (an important region for drag consideration). In the interests of rapid calculational use, however, the relative simplicity of the theory should be maintained, and on this basis, further improvement of this type appears remote.

2. Shock-Expansion Method

The shock-expansion method[5] is an extremely simple method for determining the flow fields about bodies in supersonic flow, but the range of Mach numbers and fineness ratios which can be treated by this method are limited. To apply the method, the flow conditions at the nose vertex of the body are obtained from conical flow solutions (charts or tables) and for flow downstream of the nose vertex, the Prandtl-Meyer flow equations or tables are used.

Comparing solutions obtained by the shock-expansion method with exact solutions indicates that accurate pressure distributions over ogival nose shapes can be predicted by the shock-expansion method provided the hypersonic similarity parameter, K, is greater than approximately 1.2 (comparisons of this method with other methods will be discussed further in Section D).

3. Method of Characteristics

The method of characteristics[4] provides accurate solutions to the complete differential equations of flow by the use of numerical and graphical integration. The accuracy of the method is dependent upon the fineness of the "mesh" employed and since the solution by hand calculation requires much tedious work, the time required per solution becomes prohibitive for most generalized design studies.

The method of characteristics has been applied to many basic types of flow fields including many of those associated with the configurations contained herein. As a result, this method has been used as a basis for comparison when either experimental data or pertinent theoretical solutions are unavailable. The validity of using pressure distributions from characteristic solutions as standards has been well established by its correlation with available experimental data.

4. Tangent-Cone Method

The tangent-cone method[6] estimates pressures on curved bodies by using the flow solutions for cones which have the same slopes as those of the body surface at the points in question. Two applications of this method are available wherein the relative accuracy of either application depends on the Mach number and fineness ratio of the nose. One application of the tangent-cone method is to merely use the pressure coefficient for cones whose semi-vertex angles correspond to those of the body surface. This assumes a different total-head pressure for each segment and, in addition, cannot predict negative pressures. This application is referred to as the tangent-cone method with local total-head ratio.

The second application of the tangent-cone method uses the nose vertex total-head ratio across the bow shock wave of the body in the calculation of the surface pressures where the local Mach numbers correspond to those for cones tangent to the body surface. This application is referred to as the tangent-cone method with vertex total-head ratio.

The tangent-cone method with local total-head ratio has been used briefly herein for comparison purposes and this particular application was selected since it offers better agreement with exact solutions.

5. Other Methods

There are various other methods or theories available for calculating pressure distributions such as Linearized theory[7], First Order theory[8], Second Order theory[9], Slender Body theory[10,11], etc., each of which, in general, is applicable for a limited range of Mach numbers and nose fineness ratios. These methods will not be discussed since for the most part, they represent solutions which are not readily adapted to quick hand calculational procedures.

6. Present Method

Various authors in dealing with high supersonic or hypersonic flow over hemispherical noses have successfully used a combination impact-shock expansion theory to predict pressure distributions. This blunt body method is discussed in Section E. The present method extends this hybrid type of approach to "pointed bodies" in that Generalized Newtonian theory is used to obtain the pressure distribution on the forward portion of the nose and the shock-expansion method is used to obtain the pressure distribution on the after section of the nose. The pressure distribution on the cylindrical afterbody is obtained by means of an exponential decay law derived by Fenter[12] from a second order shock-expansion approximation. In the present analysis, a method has been developed for the tandem blending of these solutions to provide a rapid and accurate hand calculational procedure for obtaining the pressure and local Mach number distributions over a variety of nose curvatures. This method will be developed in a stepwise procedure in Part 1 of Section D which describes its application to tangent ogives.

C. METHOD OF CORRELATING PRESSURE DISTRIBUTIONS

The pressure distributions calculated by the "Present Method" for pointed bodies of revolution are correlated on the basis of the Hypersonic Similarity Parameter, K, which represents the ratio of free stream Mach number to nose fineness ratio. The hypersonic similarity rule states that for related, pointed, axially symmetric bodies of revolution, the pressure distributions (in terms of $(p - p_o)/p_o$ or the normalizing parameter C_p/C_{p_N}) depend only on the similarity parameter K. Thus, if the pressure distribution for a given body is known, the pressure distributions for geometrically similar bodies are identical provided the two bodies have the same value of the similarity parameter, K.

The range of application of this rule for ogives[4] is shown in Figure 2 and as noted, the rule is normally not valid for Mach numbers or fineness ratios less than approximately 2. The present method illustrates this limit may be relaxed slightly to include a nose fineness ratio of 1.5 for $K = 2$.

The hypersonic similarity rule has been successfully applied to several special cases included herein which theoretically have blunt noses (infinite slope at the nose vertex) but for most practical purposes are considered pointed bodies. Blunt-nosed bodies, of course, violate the basic assumptions made in the development of the rule, i.e., slender bodies and hypersonic flow. In addition, application of the rule requires that for similarity in pressure or drag, these parameters must be a function of K alone at any point along the body surface. The pressure at the nose tip of a blunt body is the stagnation pressure which is solely a function of M_o instead of K. Thus for truly blunt bodies, like the hemisphere, values of C_p have not been correlated on the basis of the hypersonic similarity parameter.

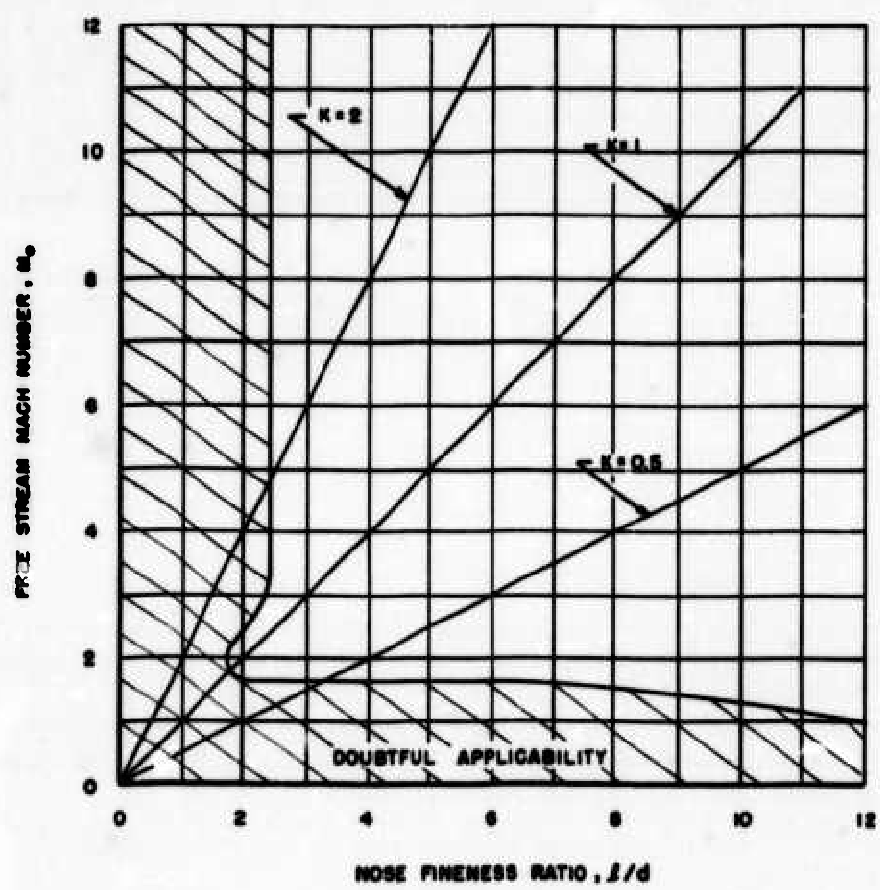

Fig. 2 RANGE OF APPLICABILITY OF SIMILARITY LAW FOR OGIVES

D. PRESSURE DISTRIBUTIONS FOR NON-LIFTING "POINTED BODIES" OF REVOLUTION - SHOCK ATTACHED

1. Tangent Ogives

The tangent ogive nose shape is used quite extensively in the design of high speed aircraft and guided missiles. Tangent ogives have the advantage of a larger nose vertex angle and higher volume than that of an inscribed cone having the same length-to-diameter ratio, but the disadvantage of slightly increased drag. This disadvantage is usually overshadowed, however, particularly with reference to those fixed length guided missiles which normally use the nose to house a radar dish or scanner as far forward on the missile as possible.

The analysis required for the development of the "Present Method" was initially formulated for the tangent ogive nose shapes and before proceeding with the method description, a brief discussion of the geometric characteristics of the tangent ogive is presented.

The tangent ogive is a pointed (for $R > r_b$) convex surface of revolution generated by rotation of the radius vector R to produce a circular arc with the tangent at the maximum radius (r_b) being parallel to the axis of symmetry of the body of revolution.

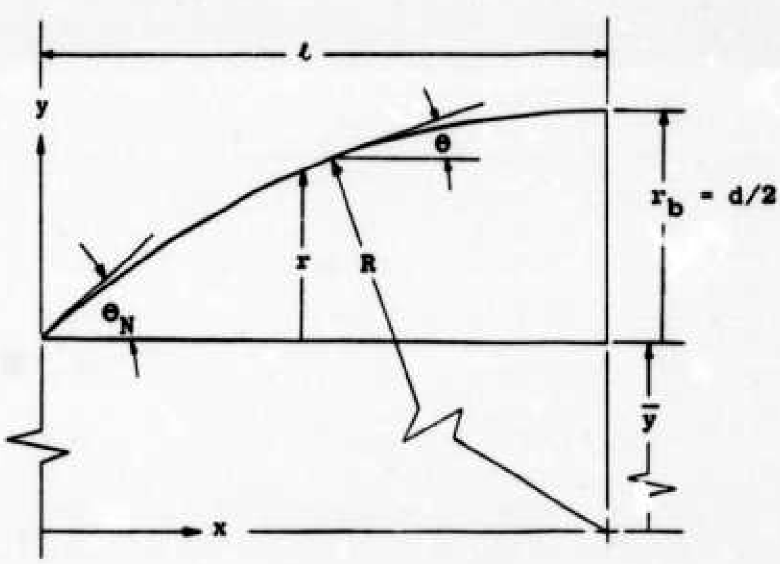

The following relations are used to define the geometric characteristics of the tangent ogives:

a. Body Surface curvature angle, θ

$$\sin\theta = \frac{\ell - x}{R}, \quad \theta = \sin^{-1}\left(\frac{\ell - x}{R}\right)$$

at the nose vertex, $\theta_N = \sin^{-1}\left(\frac{\ell}{R}\right)$

b. Caliber, N

$$N = R/d$$

In terms of fineness ratio, ℓ/d

$$N = \frac{R}{\ell}\frac{\ell}{d} = \frac{1}{4} + \left(\frac{\ell}{d}\right)^2$$

c. Relation for fraction of axial distance along nose centerline, x/ℓ

$$x/\ell = 1 - \frac{\sqrt{R^2 - (\bar{y} + r)^2}}{\ell}$$

Once an ℓ/d value has been selected for the tangent ogive, the above geometric relations can quickly provide the caliber, if desired, and the variations in body surface angle, Θ.

This section considers only pointed bodies of revolution with shock attached. The tangent ogive may or may not have shock detachment depending on the Mach number and nose vertex angle of the ogive. For this reason, a plot of free stream Mach number versus ogive semi-vertex angle, Θ_N, has been presented in Figure 3 wherein the shock detachment region has been defined. An additional plot of the tangent ogive geometric characteristics (Θ_N, ℓ/d, N) has also been presented in Figure 4. This additional plot provides a rapid means of determining the shock region into which any one tangent ogive will fall.

The prescribed method of this study for calculating pressure coefficients, C_p, represents a combination of the Generalized Newtonian theory and the shock-expansion method. The application of this method begins with the Generalized Newtonian theory, i.e.,

$$^{\#}C_p = C_{p_{max}} \sin^2\Theta \qquad (1)$$

where $$C_{p_{max}} = C_{p_N}/\sin^2\Theta_N \qquad (2)$$

and Θ = local body surface inclination angle

Θ_N = nose semi-vertex angle

C_{p_N} = pressure coefficient at nose vertex

\# For the special case of tangent ogives, a more convenient form of the C_p equation might be:

$$C_p = C_{p_{max}} \sin^2\Theta = C_{p_N}\frac{\sin^2\Theta}{\sin^2\Theta_N} = C_{p_N}(1 - x/\ell)^2 \qquad (1a)$$

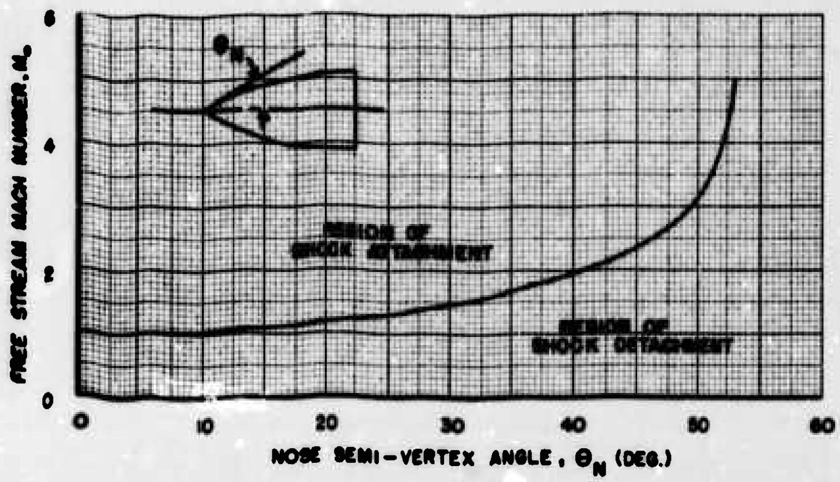

Fig. 3 SHOCK DETACHMENT MACH NUMBER FOR BODIES OF REVOLUTION WITH CONICAL TIP NOSES

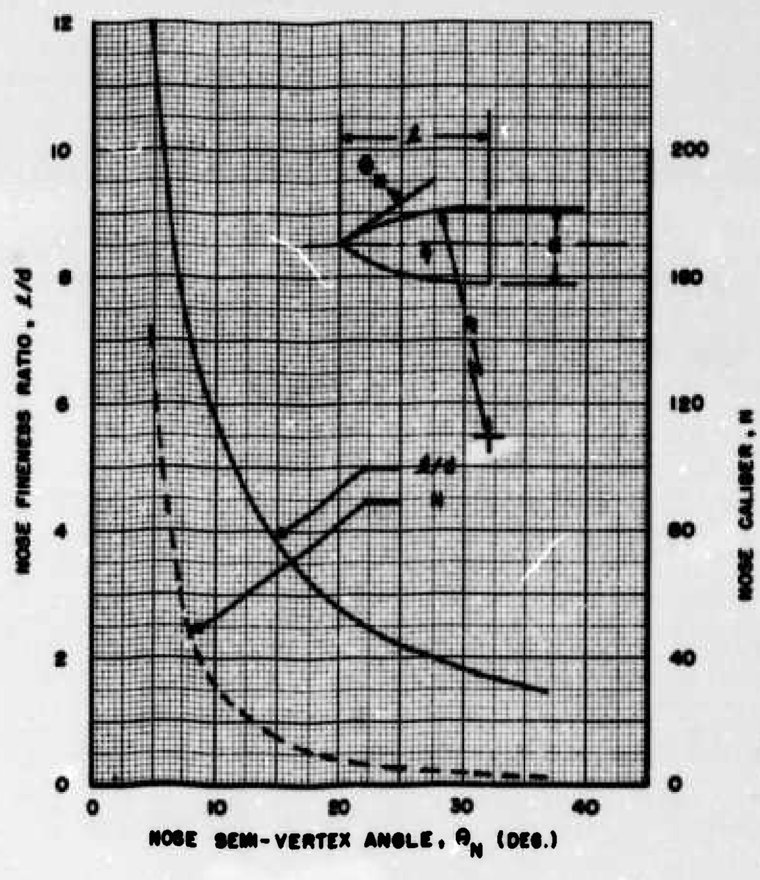

Fig. 4 TANGENT OGIVE GEOMETRIC CHARACTERISTICS

Using the appropriate value of nose semi-vertex angle, θ_N, enter the conical flow tables, such as those given in Table 6 of Appendix 1, and obtain a value of C_{p_N} at $\alpha = 0°$ for a cone of equivalent semi-vertex angle. $C_{p_{max}}$, a constant, can now be determined and the pressure coefficient distribution along the body surface can be calculated since θ is a known quantity at any x/ℓ value. A plot of $C_{p_{max}}$ vs. K for tangent ogives with M_o as a parameter is shown in Figure 5.

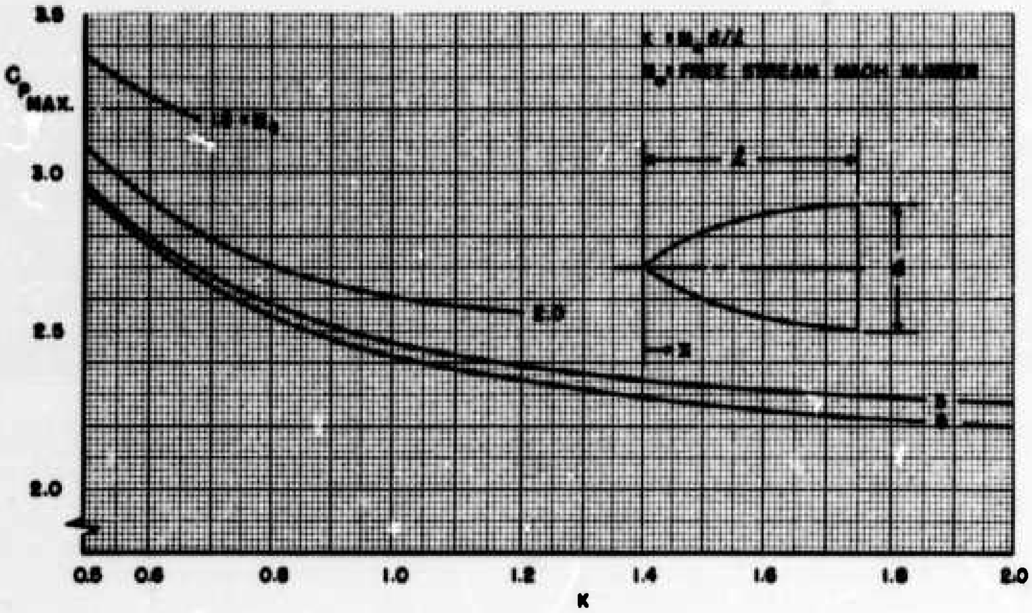

Fig. 5 $C_{p_{max}}$ FOR TANGENT OGIVES

The local Mach number distribution along the surface of the body may be obtained directly from Table 18 of Appendix 3 once a value of p/p_t has been determined as follows:

$$C_p = \frac{p - p_o}{q_o} = \frac{p}{p_t} \frac{p_{t_N}}{q_o} - \frac{p_o}{q_o}$$

where $p_t = p_{t_N}$ along a body surface meridian.

Now $$C_{p_N} = \frac{p_N - p_o}{q_o} = \frac{(p/p_t)_N - (p_o/p_{t_N})}{q_o/p_{t_N}}$$

so $$\frac{p_{t_N}}{q_o} = \frac{C_{p_N} + p_o/q_o}{(p/p_t)_N}$$

$$\therefore \quad C_p = p/p_t \, \frac{C_{p_N} + p_o/q_o}{(p/p_t)_N} - p_o/q_o \tag{3}$$

and $$p/p_t = (C_p + p_o/q_o)\, \frac{(p/p_t)_N}{C_{p_N} + p_o/q_o} \tag{3a}$$

where $(p/p_t)_N$ is determined by first using the cone tables (such as Table 7 of Appendix 1) to obtain a value of M_N corresponding to a particular value of Θ_N and M_o; $(p/p_t)_N$ can then be obtained directly from Table 18 of Appendix 3 (Prandtl-Meyer flow table) for the given value of M_N.

At some point along the body, the C_p calculated by the Generalized Newtonian theory will offer poor agreement with the exact solutions. At or near the value of x/ℓ where the C_p from impact theory begins to deviate from the exact solution, the shock-expansion method is used to extend the solution by matching, at that point, the surface *pressure coefficients and preserving the surface streamline total head.

The x/ℓ point at which the impact theory should be terminated for the case of tangent ogives was found by correlating the C_p values obtained from the Generalized Newtonian theory with those from exact solutions and this point was found to be a function of the hypersonic similarity parameter, K. By investigating a wide range of K values, an empirical expression was determined for the x/ℓ value at which the two methods should be matched:

$$(x/\ell)_m = 0.15\,K + 0.60 \quad \text{for } K \leq 2.667$$

---

*An attempt was made to match both the pressure and pressure gradient for the pointed bodies but the pressure gradient, which is a function of body curvature angle, could not be matched in the region of small curvature changes considered. It will be shown later, however, that the pressure gradient can be matched on the hemisphere nose in the region where the two methods are to be matched since the body curvature changes are large.

This equation has been plotted in Figure 6.

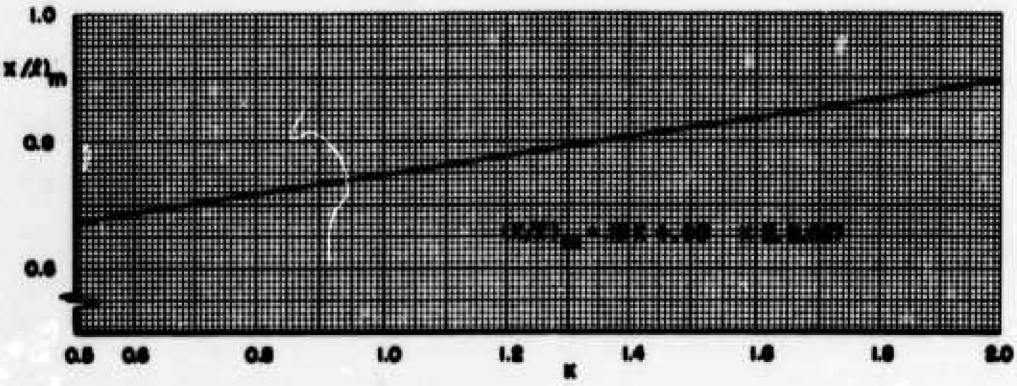

Fig. 6 MATCHING POINT VALUE OF x/ℓ FOR TANGENT OGIVES AT ALL MACH NUMBERS CONSIDERED

Once x/ℓ is known, the value of C_p at which the shock-expansion method starts ($C_{p_{SEM}}$) is found from equation 1a. In order to continue the SEM aft of the matching point, the following procedure must be used:

a. calculate a value of p/p_t at the matching point by using equation 3a;

b. from the Prandtl-Meyer flow equations or tables[13] (Table 18 herein), determine the value of ν (flow deflection angle from $M = 1$) corresponding to p/p_t above; this ν is used as ν_m in the following step;

c. knowing the body surface angle at the matching point, Θ_m, and at other points downstream, Θ, additional values of p/p_t and M aft of the matching point may be obtained by entering Table 18 with a known value of ν ($\nu = \nu_m + \Theta_m - \Theta = \nu_m + \Delta\Theta$) and proceeding in steps of $\nu = \nu_m + \Delta\Theta$ over the remainder of the body surface;

d. the additional values of p/p_t may now be substituted into equation 3 and C_p values aft of the matching point can be calculated.

(To illustrate the application of the "Present Method", numerical examples have been presented in Appendix 1 and Appendix 2 for a tangent ogive of fineness ratio 3 at $M_o = 2$. The afterbody pressure distribution, which is discussed in Section F, has also been included as part of the numerical examples.)

Using the procedure outlined above, pressure coefficient distributions have been calculated using the present method for five tangent ogives with ℓ/d values of 1.5, 2, 3, 6, and 12 and for Mach numbers of 1.5, 2, 3, and 6. These results have been compared with the method of characteristics, the shock-expansion method, and the tangent-cone method in Figure 7. The agreement of the present method with exact solutions is exceptional for all values of the hypersonic similarity parameter K. (The only instance where deviation was apparent was for $M_o = 1.5$ at $K = 0.5$ where the C_p values from the present method matched those from the exact solutions only when faired.) Notable disagreement was exhibited by the tangent-cone and shock-expansion methods for $M_o = 1.5$ at $K = 0.5$, $M_o = 2$ at $K = 1$, and $M_o = 3$ at $K = 2$; the remaining cases indicated markedly improved agreement with exact solutions, i.e., the high Mach number and fineness ratio cases approached the accuracy provided by the present method.

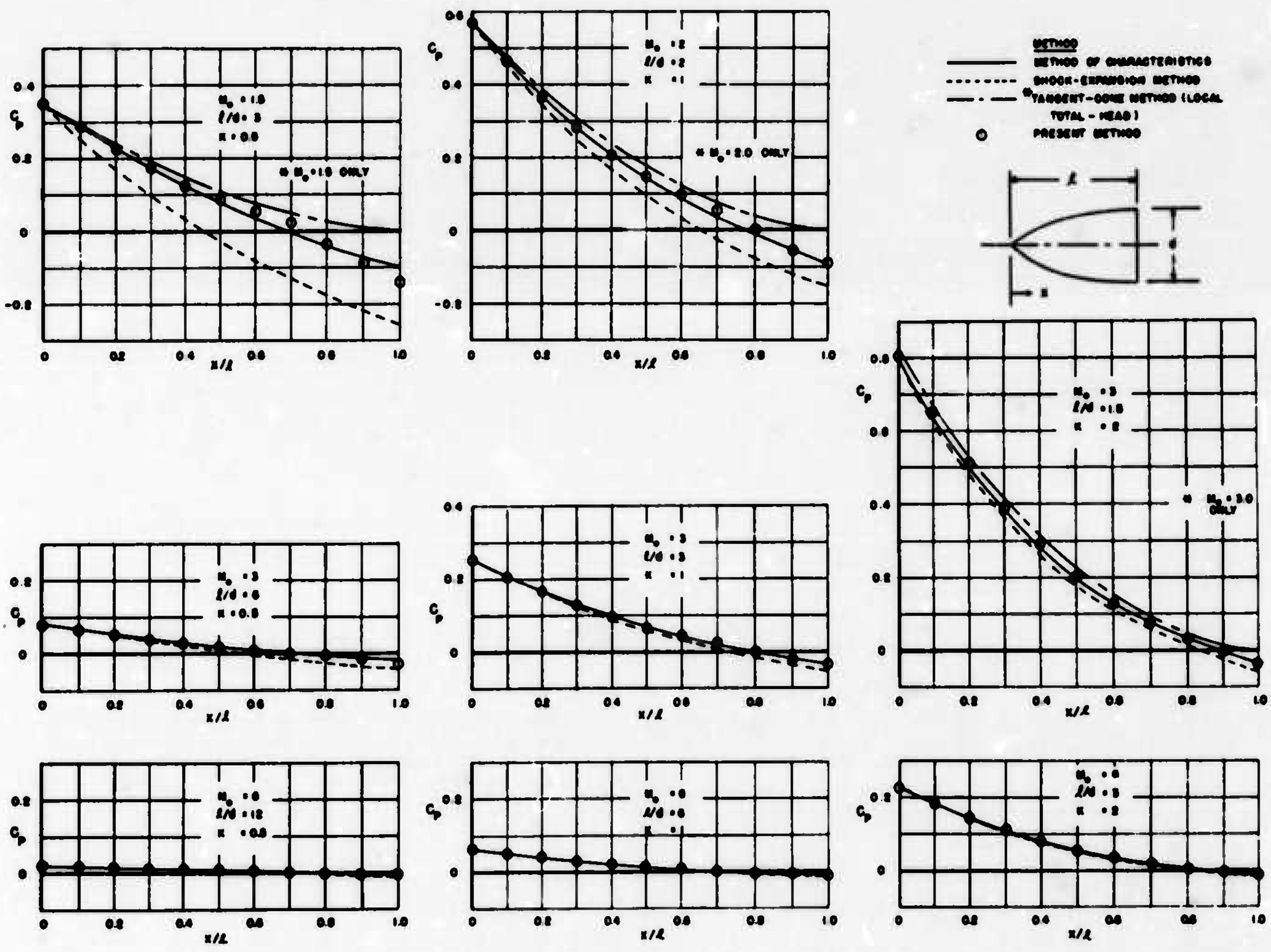

Fig. 7 TANGENT OGIVE PRESSURE COEFFICIENT DISTRIBUTION, $K = 0.5$, 1.0, and 2.0

The percent error in drag due to the disagreement of the C_p values from the above three methods with the C_p values obtained from exact solutions has been presented in table form below for the lowest Mach number of each K value. These particular cases were selected because they represent the poorest conditions for the three methods; in spite of this, the present method yields near perfect agreement while the tangent-cone and shock-expansion methods offer considerable disagreement when each method is compared with exact solutions.

Table 1. Percent Error in Drag

Method	M_o	ℓ/d	K	% Error in Drag
Present	1.5	3	0.5	2
Shock Expansion	"	"	"	-84
Tangent-Cone	"	"	"	29
Present	2.0	2	1.0	0
Shock Expansion	"	"	"	-29
Tangent-Cone	"	"	"	12
Present	3.0	1.5	2.0	0
Shock Expansion	"	"	"	-6
Tangent-Cone	"	"	"	9

Ordinarily, a presentation of "percent error in drag" only would not be sufficient to define the accuracy to which the method might predict the pressure distribution over the body. This, of course, refers to the possibility of some one method predicting higher pressures at the vertex and lower pressures near the base (or vice versa) and as a result, the compensating errors in pressure would serve to lower the error in drag which is merely an integration of the pressure distribution values. Fortunately, this condition did not prevail for the methods used as comparisons; a small compensating error was noted, however, for the present method at $M_o = 1.5$ and $\ell/d = 3$.

As mentioned earlier, the results obtained using the present method were correlated on the basis of the hypersonic similarity parameter, K. Figure 8 illustrates the validity of this correlation.

2. Secant Ogives

Secant ogive is the name applied to an ogival nose cut off in length, $\ell_{s.o.}$, from its related tangent ogive length, ℓ, by passing a plane normal to the longitudinal axis of the ogival shape. A family of secant ogives related to the tangent ogive (see pages 11 and 12 for sketch and nomenclature)

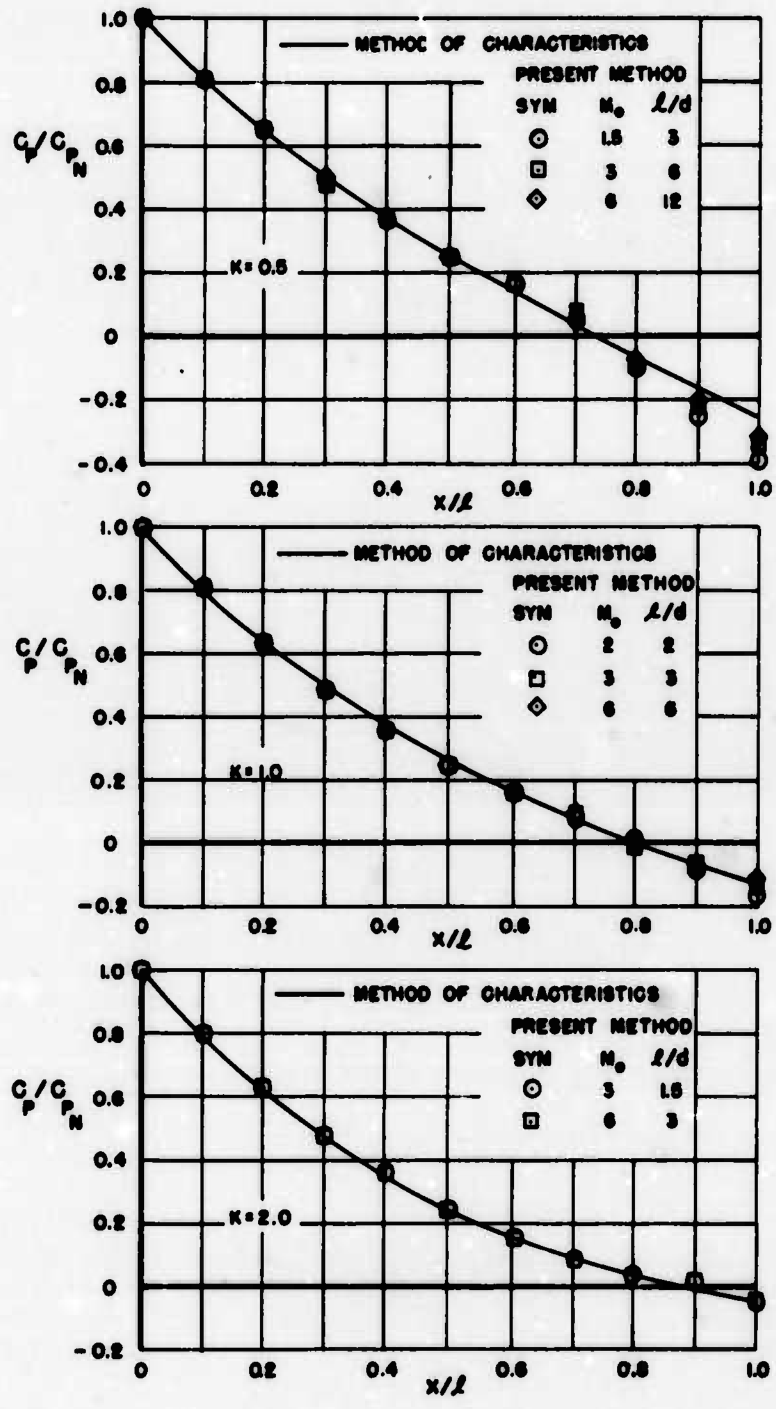

Fig. 8 CORRELATION OF PRESSURE COEFFICIENT DISTRIBUTIONS ON TANGENT OGIVES USING THE HYPERSONIC SIMILARITY PARAMETER K

of caliber N and nose curvature angle, Θ, can be expressed in particular by the following equation:

$$x/\ell = 1 - \frac{\sqrt{R^2 - (\bar{y} + r)^2}}{\ell} \qquad \text{where} \quad x \leq \ell_{s.o.} < \ell$$

These shapes (for equal fineness ratios) offer high volume approaching that provided by the tangent ogives with the further advantage of exhibiting less drag than either the related tangent ogive or inscribed cone of the same fineness ratio. Pressure coefficient distributions have not been presented for secant ogives, as such, since they are merely forward segments of the tangent ogives discussed in Section D, Part 1.

3. Triple Cone-Tangent Ogive Combination

This composite nose design has been considered for two reasons: the nose shape is an unusual one wherein a triple cone segment preceeds a tangent ogive section and secondly, experimental data were available for comparison purposes. Experimental data, of course, provide an excellent basis for comparison studies but often times the reliability or availability of such information is quite limited.

Figure 9 presents a comparison of the C_p values obtained using the present method, the shock-expansion method, and the experimental data. The

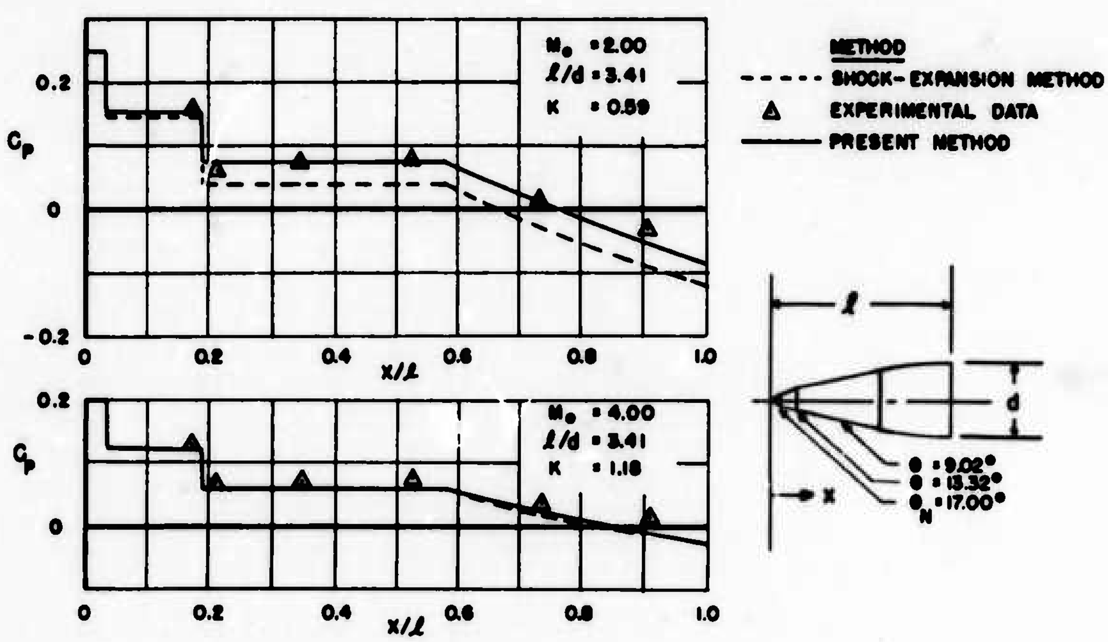

Fig. 9 PRESSURE COEFFICIENT DISTRIBUTION ON A TRIPLE CONE-TANGENT OGIVE COMBINATION

present method indicates favorable agreement at both $M_o = 2$ and 4 whereas the shock-expansion method is quite poor at $M_o = 2$ but like the present method, shows favorable agreement at $M_o = 4$. The failure of the shock-expansion method in predicting the proper C_p values at $M_o = 2$ was to be expected since the value of the hypersonic similarity parameter, $K = 0.59$, was far too low for this method.

4. von Karman Minimum Drag Nose Shapes

The von Karman nose shapes are high volume-low drag nose shapes developed by von Karman for a given length and diameter for practical fineness ratios and moderate supersonic Mach numbers. The nose shapes are defined by the equation:

$$r = \frac{r_b}{\sqrt{\pi}} \sqrt{\phi - 1/2 \sin 2\phi}$$

where $\phi = \cos^{-1} (1 - 2x/\ell)$.

These nose shapes have mathematically infinite slopes at their vertices yet for most practical purposes are considered pointed bodies. Using the present method for predicting C_p, however, these noses require special consideration in that they cannot be treated as either blunted or pointed bodies of revolution and the difficulty arises in the proper determination of $C_{p_{max}}$. In an effort to obtain starting values of $C_{p_{max}}$ to use with the Generalized Newtonian theory, equation 1, a systematic study was initiated whereby cones were fitted to each von Karman nose shape tangent to the nose at some x_c/ℓ value. Using the cone tables at a given free stream Mach number, $C_{p_{max}}$ was determined and pressure distributions were calculated using the Generalized Newtonian theory and compared with the theoretical values[14]. When the present method matched the theory, the x_c/ℓ and Mach number values were noted and the entire process repeated using various other fineness ratios and Mach numbers. Ultimately, this study provided the curve of Figure 10 wherein #x_c/ℓ versus K has been plotted. Accompanying this curve is a plot of $C_{p_{max}}$ versus K as shown in Figure 11. This is a fictitious $C_{p_{max}}$ value to be used with the Generalized Newtonian equation (Eq. 1),

$$C_p = C_{p_{max}} \sin^2\theta ,$$

for calculating pressures on von Karman noses.

#Solutions may be carried forward of x_c/ℓ using the θ at the desired point, x, and the empirically determined value of $C_{p_{max}}$; the error incurred is negligible as indicated by the results.

As in the cases for the previously discussed nose shapes, the Generalized Newtonian theory has been extended using the shock-expansion method. The matching point for the two methods was determined analytically and has been plotted as $(x/\ell)_m$ versus K in Figure 12. These values differ somewhat from those for the ogival shapes (see Fig. 6).

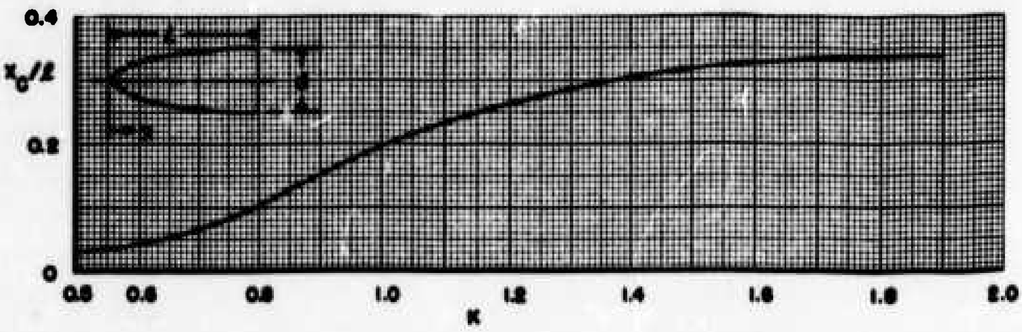

Fig. 10 TANGENCY POINT FOR CONES FITTED TO VON KARMAN NOSE SHAPES

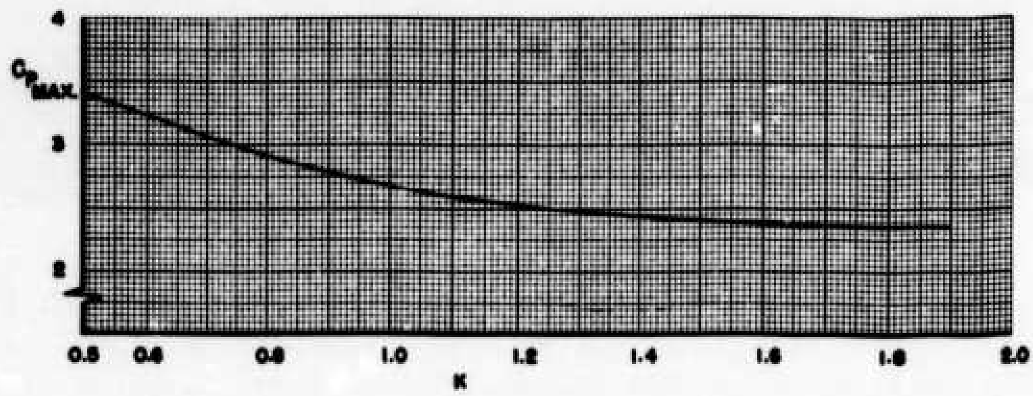

Fig. 11 $C_{p_{max}}$ FOR VON KARMAN NOSE SHAPES

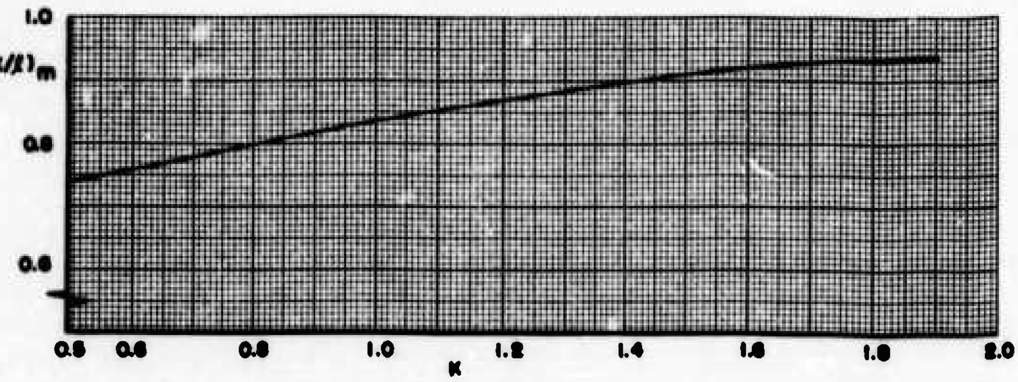

Fig. 12 MATCHING POINT VALUE OF x/ℓ FOR VON KARMAN NOSE SHAPES

The pressure distributions calculated using the present method were compared with the theoretical[14] values at M_o = 1.5 and 2 (approximately) for the K region in which the theory is applicable, i.e., from K = 0.55 to 0.922. Figure 13 presents these comparisons and the agreement appears quite favorable.

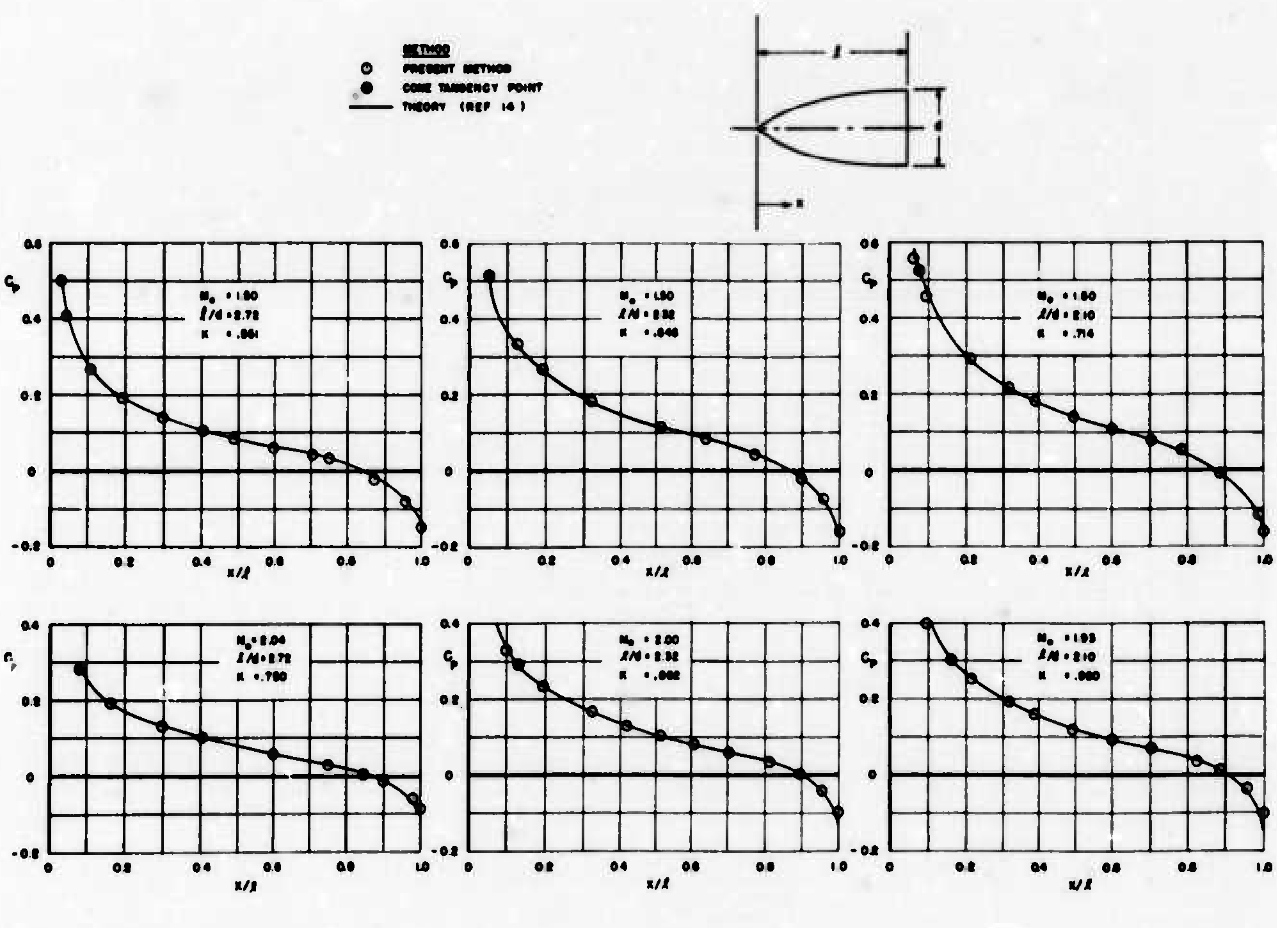

Fig. 13 PRESSURE COEFFICIENT DISTRIBUTION FOR VON KARMAN MINIMUM DRAG NOSE SHAPE, ℓ/d = 2.10, 2.32, and 2.72

The use of the present method has provided a means of extending the restricted K region characteristic of the von Karman nose shapes. The $C_{p_{max}}$, x_c/ℓ, and $(x/\ell)_m$ curves were extrapolated to K values of almost 2 and pressure distributions were calculated and compared with experimental data[15] gathered at M_o = 1.61, 2.80, and 4.00. This comparison is presented in Figure 14 and the agreement appears very good, indicating the useful range of the K values can now be more than doubled when applying the solutions offered by the present method.

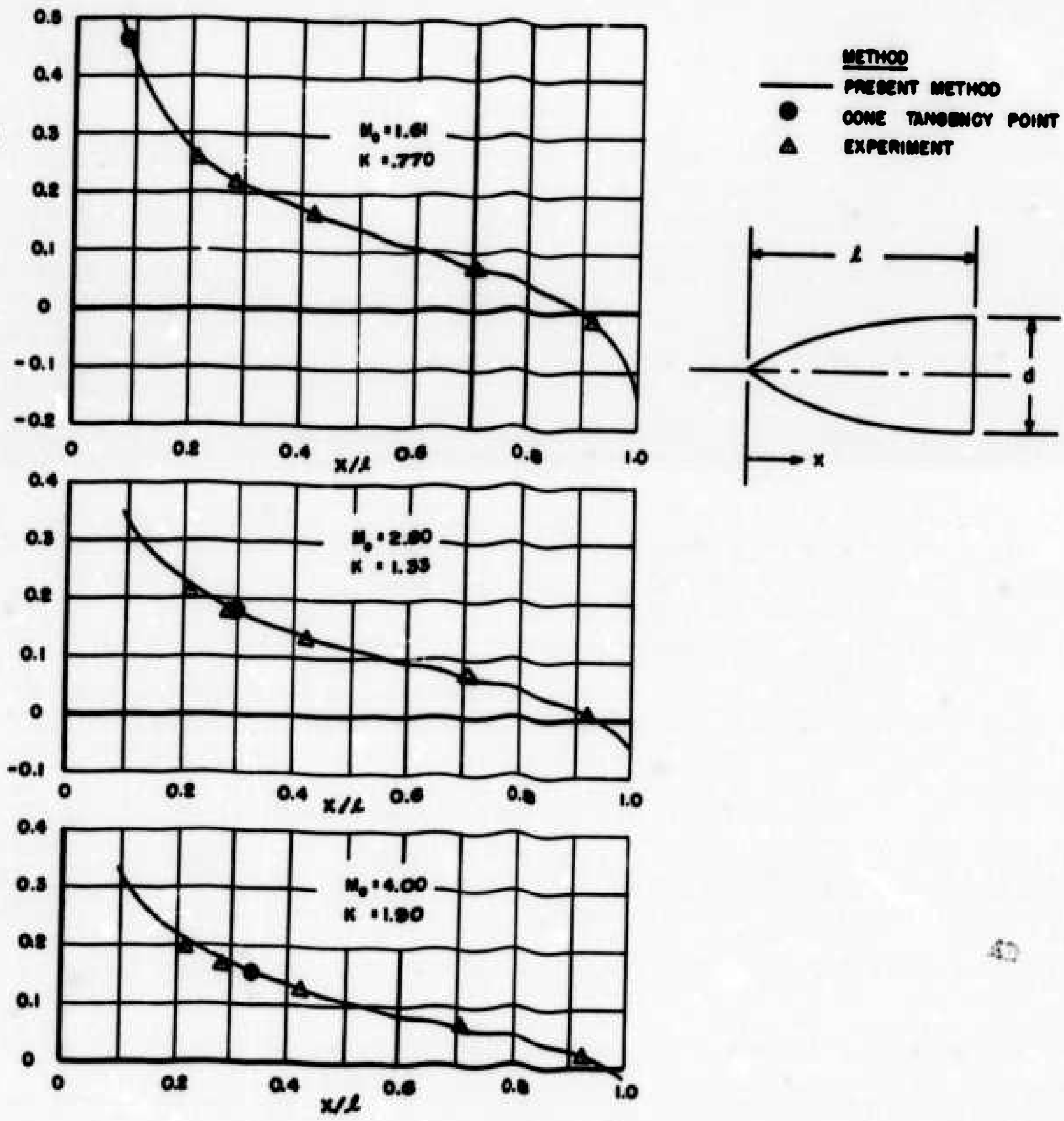

Fig. 14 PRESSURE COEFFICIENT DISTRIBUTION FOR VON KARMAN MINIMUM DRAG NOSE SHAPE, ℓ/d = 2.10

5. Power Series Minimum Drag Nose Shapes

The minimum drag power series nose, often referred to as the hypersonic optimum nose since it closely approximates the profile of Newton's hypersonic optimum nose, is defined by the equation:

$$r = r_b \ (x/\ell)^{3/4}$$

These nose shapes, like the von Karman noses, have mathematically infinite slopes at the vertex and calculational procedures similar to those performed for the von Karman shapes had to be carried out for the 3/4 power noses with one notable exception, i.e., the Generalized Newtonian theory predicts the pressure distribution very accurately along the entire surface of the nose. Worthy of note in this instance is the geometry of the power series nose shapes which have a finite slope at the shoulder or base. This eliminates the need for extending the theory using the SEM since this type of body has no shallow angle section wherein the Generalized Newtonian theory is inapplicable. Thus only plots of $C_{p_{max}}$ and x_c/ℓ were predetermined for these nose shapes and are presented in Figures 15 and 16.

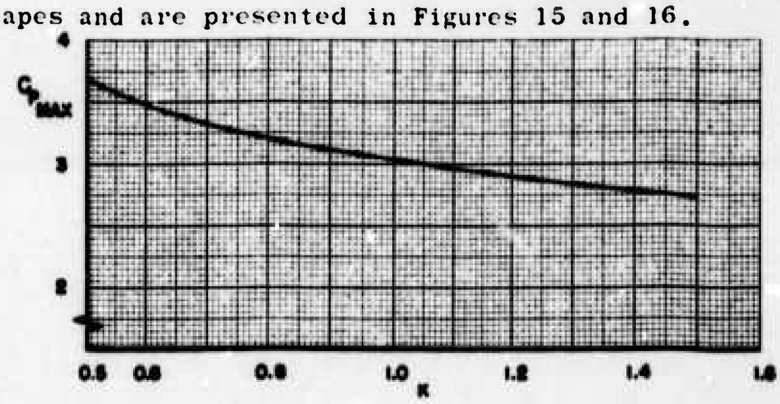

Fig. 15 $C_{p_{max}}$ FOR 3/4 POWER NOSE SHAPES

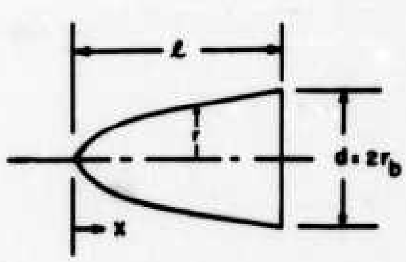

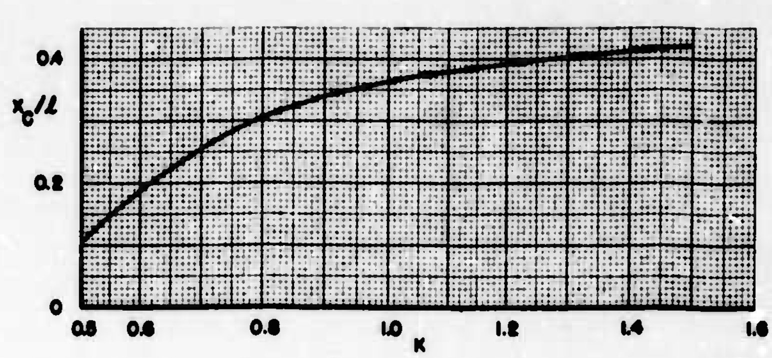

Fig. 16 TANGENCY POINT FOR CONES FITTED TO 3/4 POWER NOSE SHAPES

Pressure distribution coefficients were calculated using the present method for three different 3/4 power noses of fineness ratio 3, 5, and 7, for Mach numbers from 2 to 7.5. These values were compared with theoretical[14] C_p values in Figure 17 and once again, the agreement is exceptional. Note that solutions were carried forward of the x_c/ℓ value using the corresponding $C_{p_{max}}$ value in the Generalized Newtonian theory and the resulting error is negligible.

6. Isentropic Spikes

Brief consideration has been given these shapes even though they are primarily used as supersonic diffusers for ramjet engines. The function of the diffuser is to decelerate the air from its free stream velocity at the ramjet intake to a velocity at the combustor which is compatible with the available flame velocity.

The true isentropic spike would ideally have a total pressure recovery factor of one but the length of such a spike would make it impractical for use. The long needle-like nose would, of course, make it structurally unsound and the boundary layer build-up along the spike would destroy its effectiveness. Due to these conditions, conical tips are usually attached forward of the "isentropic surfaces" with the end result of some loss in total pressure recovery attributed to the bow shock-wave. The spikes are usually designed such that the bow shock wave and the Mach lines from the compression surfaces coalesce at a point called the focal point. This point, by design, usually lies at or very near the cowl lip of the ramjet engine depending on the desired conditions at the combustor. Because of the design mobility in focal point and possible compromises in total pressure recovery for a given condition, isentropic spikes of basically two designs are available: those which yield a constant total pressure recovery factor by merely varying the cone angle and free stream Mach number and secondly, those which have a fixed cone tip angle thereby causing the total pressure recovery to decrease with increasing Mach number. These two designs[16,17] were investigated in the Mach number range from 2 to 4 and pressure distributions were calculated using the present method and compared with exact solutions. The matching point value of θ for the present method was arrived

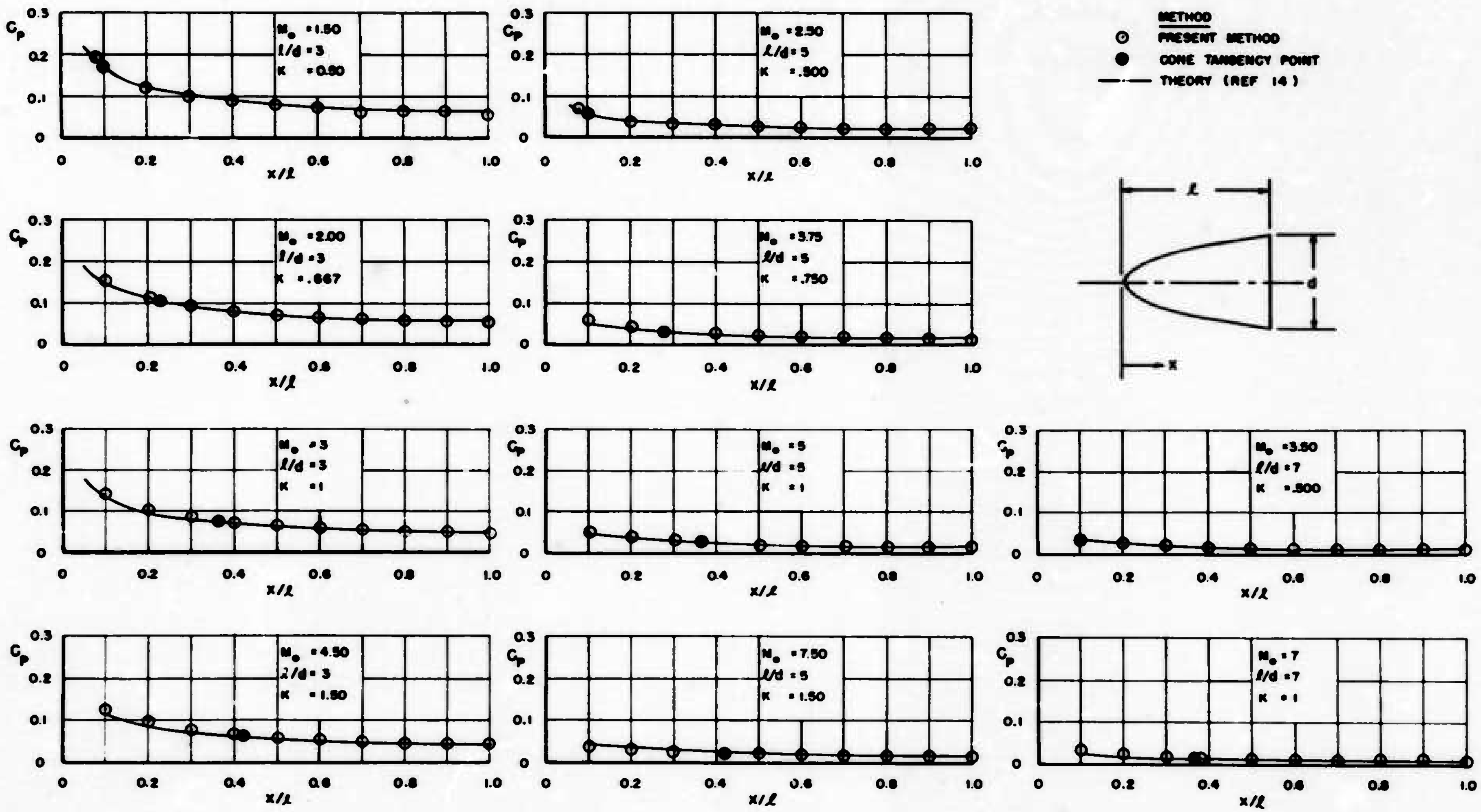

Fig. 17 PRESSURE COEFFICIENT DISTRIBUTION FOR 3/4 POWER MINIMUM DRAG NOSE SHAPE, ℓ/d = 3, 5, and 7.

at analytically and has been presented in Figure 18 as a function of free stream Mach number. As noted the matching point Θ has been non-dimensionalized and given as Θ_m/Θ_N in order to eliminate the variable Θ_N; in effect, the matching point Θ has been normalized with respect to Θ_N thereby eliminating the need for a family of curves to represent spikes of different conical tip angles.

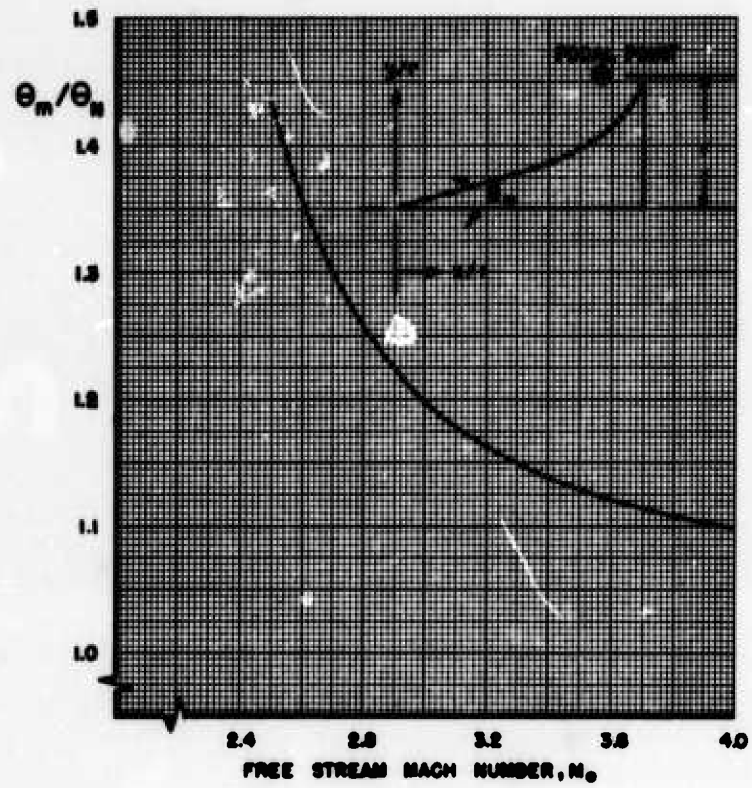

Fig. 18 RATIO OF MATCHING POINT Θ TO NOSE SEMI-VERTEX ANGLE VERSUS FREE STREAM MACH NUMBER FOR ISENTROPIC SPIKES

Figure 19 presents the results of the C_p comparison between the present method and exact solutions for an isentropic spike with a 15° conical tip at $M_o = 2.5$, 3.0, and 4.0. The agreement appears good at all Mach numbers and exceptional at $M_o = 4.0$. It should be emphasized at this point, however, that the usefulness of the present method diminishes with increasing Mach number as noted in Figure 18, i.e., the value of Θ_m/Θ_N has reached 1.1 at $M_o = 4$ indicating the matching point lies very near the conical tip. In essence, this condition indicates the shock-expansion method alone would be adequate (for most engineering purposes) in determining C_p at the higher Mach numbers for isentropic spikes.

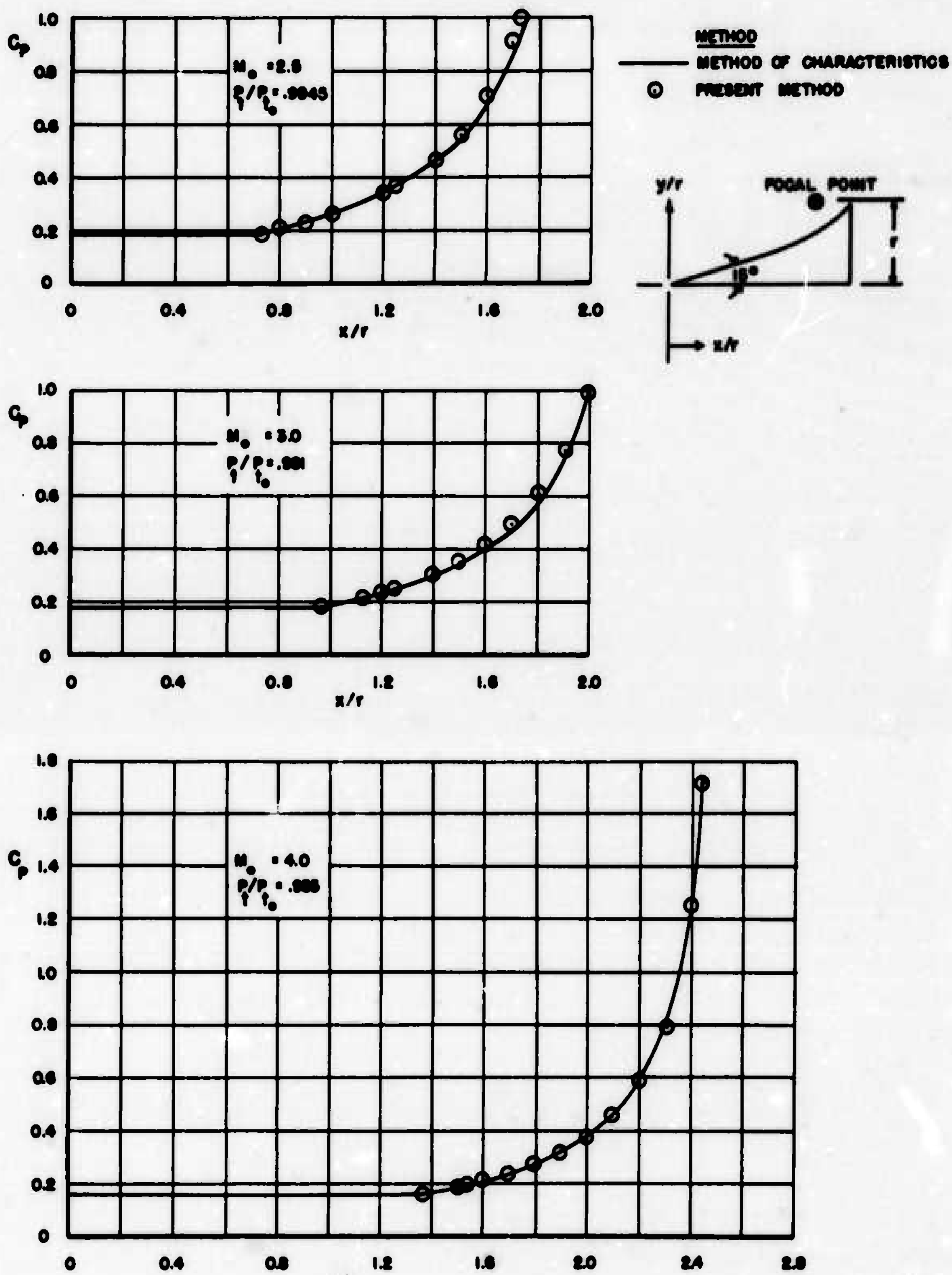

Fig. 19 PRESSURE COEFFICIENT DISTRIBUTION FOR A 15° ISENTROPIC SPIKE, M_o = 2.5, 3.0, and 4.0

E. PRESSURE DISTRIBUTIONS FOR NON-LIFTING BLUNT-NOSED BODIES OF REVOLUTION

1. Hemisphere

The hemispherical-type nose shape exhibits certain advantages for supersonic flight vehicles that are lacking for the generally accepted optimum pointed-nose bodies of revolution. Two possible features of the hemisphere type nose shape are its ability to readily accommodate radome systems and secondly, the reduced heat-transfer effects at high speeds which are characteristic of this type body. The latter feature, of course, is of utmost importance for re-entry bodies.

The use of impact-shock-expansion theory in determining the pressure distributions for hemisphere type noses has been used in Reference 18 for very high Mach numbers ($M_o \geq 7.7$) and shown to be of great value. Reference 18, however, defines the matching point only for M_o approaching infinity whereas the present analysis will consider variations in the matching point which result for free stream Mach numbers less than approximately 8.

Solutions for the pressure distribution on the hemisphere nose are initiated using the Generalized Newtonian theory:

$$C_p = C_{p_{max}} \sin^2\theta$$

where $$C_{p_{max}} = C_{p_N}/\sin^2\theta_N$$

Since $\sin^2\theta_N$ equals 1 at the nose vertex, $C_{p_{max}} = C_{p_N}$. For the blunt-nosed bodies, a detached shock appears at the nose and the value of C_{p_N} becomes the stagnation value behind the normal shock. This stagnation value is a function of free stream Mach number only (for γ = constant) and can be readily calculated using the Rayleigh formula:

$$C_{p_{max}} = C_{p_N} = \frac{2}{\gamma M_o^2}\left[\left(\frac{\gamma+1}{2} M_o^2\right)^{\frac{\gamma}{\gamma-1}} \left(\frac{\gamma+1}{2\gamma M_o^2 - \gamma + 1}\right)^{\frac{1}{\gamma-1}} - 1\right]$$

For convenience, this equation has been plotted in Figure 20 and as illustrated reaches a limiting value of 1.84.

At some point along the surface of the hemisphere, the Generalized Newtonian theory begins to show marked disagreement with comparison data and it is at this point that the shock-expansion method (which utilizes the Prandtl-Meyer

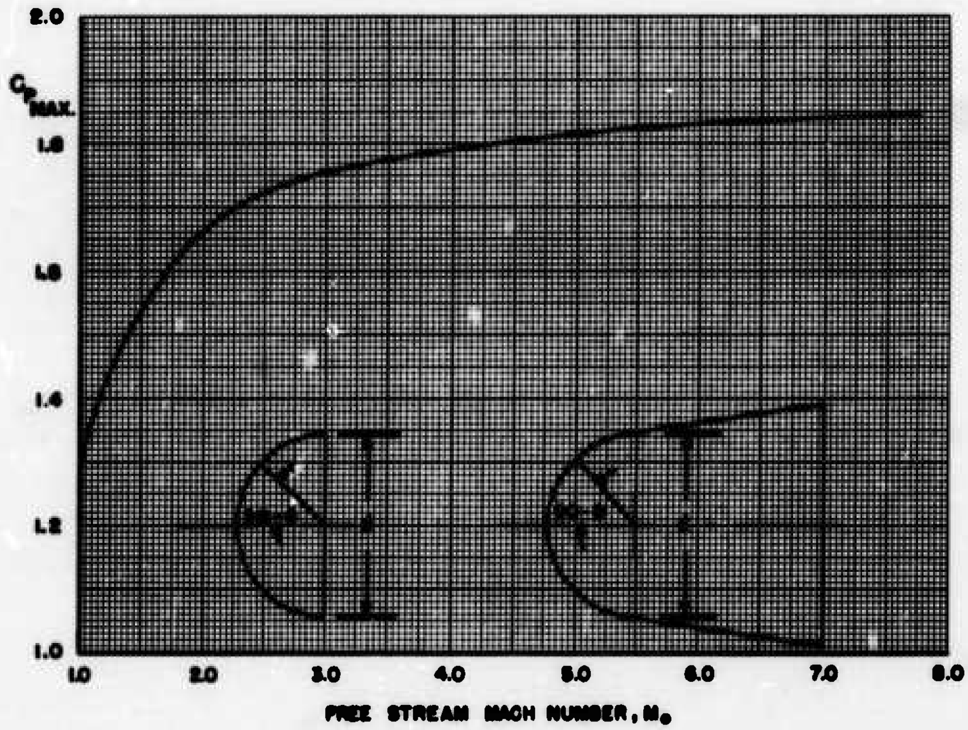

Fig. 20 $C_{p_{max}}$ FOR HEMISPHERE OR HEMISPHERE-CONE

relations) is used to extend the impact theory. This is accomplished by matching the C_p values for the two methods at the point of deviation; this point is determined by equating the pressure and pressure gradient given by the Generalized Newtonian theory and the Prandtl-Meyer relations as follows:

From Generalized Newtonian theory,

$$C_p = C_{p_{max}} \sin^2\theta = \frac{p - p_o}{(\gamma/2)p_o M_o^2}$$

Solving for p

$$p = p_o + (\gamma/2)p_o M_o^2 \; C_{p_{max}} \sin^2\theta$$

$$\frac{dp}{d\theta} = (\gamma/2)p_o M_o^2 \; C_{p_{max}} \sin 2\theta$$

and

$$\frac{1}{p}\frac{dp}{d\theta} = \frac{(\gamma/2)M_o^2 \; C_{p_{max}} \sin 2\theta}{1+(\gamma/2)M_o^2 \; C_{p_{max}} \sin^2\theta}$$

From the Prandtl-Meyer relations,

$$\frac{1}{p}\frac{dp}{d\Theta} = \frac{\gamma M^2}{\sqrt{M^2 - 1}}$$

By equating the above product of $\frac{1}{p}\frac{dp}{d\Theta}$ from the two methods, the matching point Θ can be determined. It is apparent that the value of Θ at the matching point is a function of M_o and a plot of M_o versus matching point Θ has been presented in Figure 21. (Note that for very low Mach numbers, there is no point at which both the pressure and pressure gradient are the same for the two methods and the curve has been extrapolated in this region.) For sufficiently high Mach numbers ($M > 21$), the matching point Θ reaches a limiting value of approximately 35.4°. This fact is borne out by Vaglio-Laurin and Trella[18] as they indicate the matching point Θ for M_o approaching infinity can be obtained by the following expression:

$$\cot \Theta = \frac{\gamma}{\gamma-1}\left[(\sin \Theta)^{\frac{2(1-\gamma)}{\gamma}} - 1\right]\left\{\frac{2}{\gamma-1}\left[(\sin \Theta)^{\frac{2(1-\gamma)}{\gamma}} - 1\right] - 1\right\}^{-1/2}$$

Once the matching point Θ has been determined, the remainder of the solution is quite simple since p/p_t can be calculated using:

$$C_p = p/p_t \frac{C_{p_N} + p_o/q_o}{(p/p_t)_N} - p_o/q_o$$

Knowing p/p_t, the Prandtl-Meyer relations or tables provide the local Mach number and flow deflection angles (from $M = 1$) so that one may proceed along the surface of the body according to $\nu + \Delta\Theta$ (see page 16).

Pressure coefficient distributions were calculated for the hemisphere nose using the present analysis and compared with experimental data[19] at $M_o = 1.82$, 2.81, 3.74, and 4.76 and a theoretical treatment using numerical analysis[18] at $M_o = 7.7$. The agreement of the present analysis with the comparison data is quite favorable as illustrated in Figure 22.

2. Hemisphere-Cone Combination

The hemisphere-cone type nose has found extensive use among high speed vehicles for much the same reasons as the hemisphere nose. The hemisphere-cone nose, although not exhibiting the high volume of a hemisphere, does have the advantage of reducing the heat-transfer effects at high speeds and in addition provides somewhat more stability than that of the hemisphere. Recent studies by

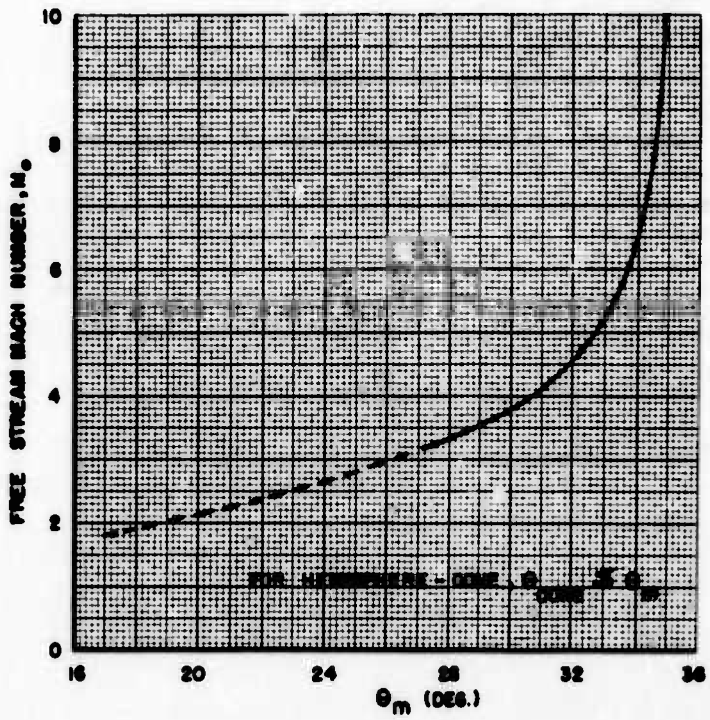

Fig. 21 MATCHING POINT VALUE OF θ FOR HEMISPHERE OR HEMISPHERE-CONE

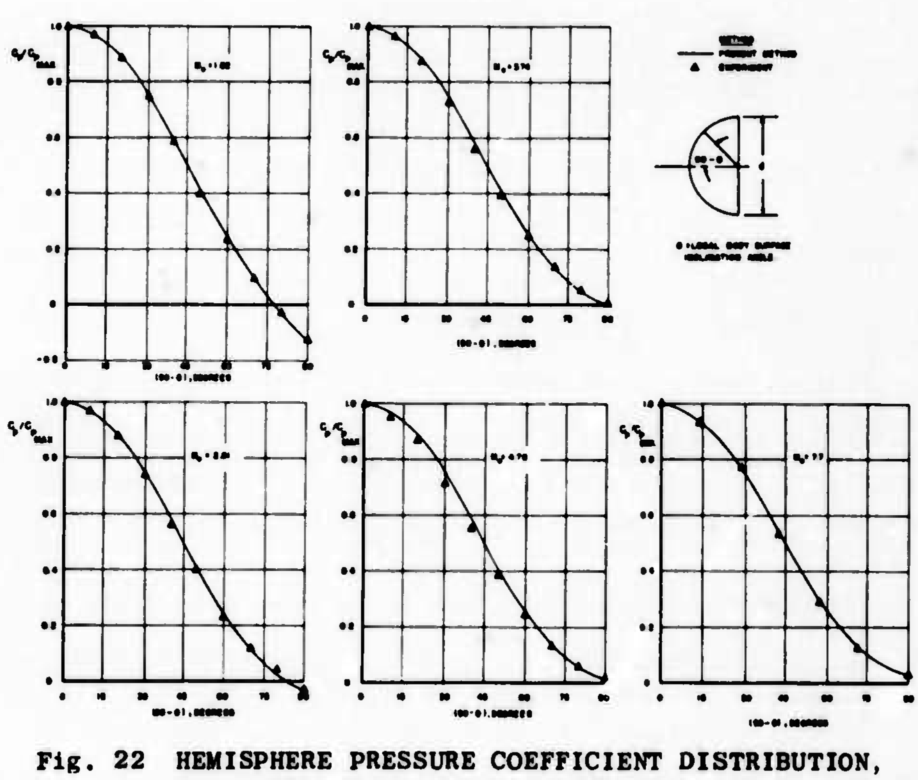

Fig. 22 HEMISPHERE PRESSURE COEFFICIENT DISTRIBUTION, M_o = 1.82, 2.81, 3.74, 4.76, and 7.7

Perkins, Jorgensen and Sommer[20] have also indicated that the drag of a nose shape consisting of a hemispherical surface faired into an expanding conical surface can be less than that of a sharp cone of the same fineness ratio at all supersonic Mach numbers.

Pressure distributions have not been calculated for the hemisphere-cone nose shapes since the procedure would be similar to that of the hemisphere. Moreover, the present analysis will not predict the over-expansion of the flow at the hemisphere-cone juncture which occurs for Mach numbers less than about 3. Above $M_o = 3$, however, the present analysis should predict the pressure coefficients accurately enough for engineering needs since the expanding flow over the hemispherical tip does not reach a lower pressure than the exact value for a cone having the same slope as the conical afterbody and, in addition, this pressure remains essentially constant over the entire conical afterbody as would be predicted by impact-shock expansion theory.

Reference 20 presents experimental data which illustrate the flow over-expansion phenomenon associated with the hemisphere-cone type nose shapes for Mach numbers less than 3. The extent of the over-expansion as pointed out in this reference is dependent primarily on the slope of the conical afterbody surface; as the slope decreases, the over-expansion of the flow appears more prominent. At all Mach numbers, however, the pressure on the conical afterbody returns almost to the exact value of a cone with a slope corresponding to that of the conical afterbody. With this in mind, a first approximation for predicting the pressure coefficients of hemisphere-cone noses by the present analysis for M_o less than 3 is quite possible. It has been shown that the present analysis would give accurate results over the hemisphere portion of the nose and since experimental data have indicated the conical afterbody pressure approaches that of the equivalent cone, it would be within the acceptable accuracy limits of most engineering methods to merely fair the present analysis solution into the equivalent cone solution.

F. PRESSURE DISTRIBUTIONS ON NON-LIFTING CYLINDRICAL AFTERBODIES

Fenter's[13] method has been used to predict the pressure distributions over cylindrical afterbodies. This method, which is a simplification of the second-order shock expansion method, yields the following relation for pressure distribution:

$$p_n/p_o = p_{cn}/p_o + (p_n'/p_o - p_{cn}/p_o)\, e^{-\frac{s}{K\ell}}$$

where s = segment length

ℓ = nose length

K = hypersonic similarity parameter, $M_o d/\ell$

d = diameter of body

with subscripts and superscripts

n = specific segment of equivalent tangent body

cn = condition on the equivalent tangent cone of a specific segment

$'$ = condition at the most forward point of an equivalent tangent body segment ($s = 0$)

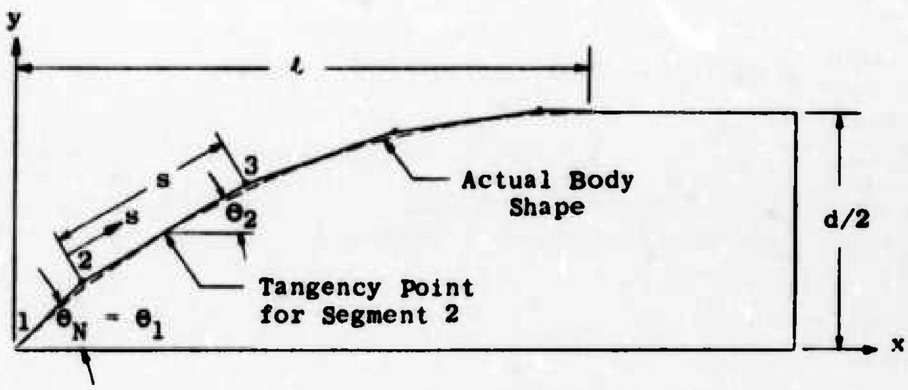

The values of p_n/p_o and p_{cn}/p_o are the actual pressures on the ogive (tangency points) whereas the primed values p_n'/p_o represent conditions at the most forward point of any segment and are obtained using the Prandtl-Meyer relations or tables for expansions through $\theta_n - \theta_{n+1}$, etc.

Since the Fenter method is being used on the cylindrical afterbody alone, the relation for pressure distribution reduces to:

$$\frac{p_n}{p_o} = 1 + \left(\frac{p_n'}{p_o} - 1\right) e^{-\frac{\Delta x/\ell}{K}} \tag{4}$$

where: Δx = segment length

ℓ = nose length

and $\frac{p_{cn}}{p_o} = 1$ since the equivalent tangent cone angle = 0° and $C_{p_{cn}} = 0$

Using equation 4, the pressure coefficient becomes:

$$C_p = \frac{p_o}{q_o}\left(\frac{p_n}{p_o} - 1\right) \tag{5a}$$

or

$$C_p = C_{p_{(x/\ell = 1)}} e^{-\frac{\Delta x/\ell}{K}} \tag{5b}$$

where $\Delta x/\ell$ = non-dimensional distance from base of nose, where $x/\ell = 1$, to the desired point on the afterbody.

G. APPLICATION OF PRESENT METHOD TO LIFTING POINTED BODIES OF REVOLUTION

Reliable theory amenable to rapid hand calculational procedures for describing the pressure distributions along lifting bodies of revolution is practically non-existent, especially for higher angles of attack. The pressure distributions provided by the present method for angles of attack up to 10 degrees yield results which are comparable and at times better than various other available methods. Theoretical treatment of the problem at higher angles of attack is hampered by the effects of cross-flow separation on the leeward side of the body and compressibility effects when at high cross-flow Mach numbers.

In the following two sub-sections, the application of the present method to bodies of revolution at low and moderate angles of attack is described and numerical examples are presented in the appendices.

1. Bodies of Revolution at Small Angles of Attack

The present method for predicting pressure distributions on non-lifting bodies will also be used on the lifting bodies of revolution. The combination of Generalized Newtonian theory and the shock-expansion method will be used to define C_p for the nose section and the method of Fenter[18] will be used to continue the solution over the cylindrical afterbody. Beginning with the Generalized Newtonian theory, Equation 1 is modified to read:

$$C_p = C_{p_{max}} \sin^2\delta \tag{6}$$

where

$$C_{p_{max}} = C_{p_N}/\sin^2\delta_N \tag{7}$$

$$\sin\delta = \sin\Theta\cos\alpha - \cos\psi\cos\Theta\sin\alpha \tag{8}$$

and Θ = body surface inclination angle

ψ = radial meridian along body surface

α = angle of attack

δ = angle between free stream and tangent to the body surface

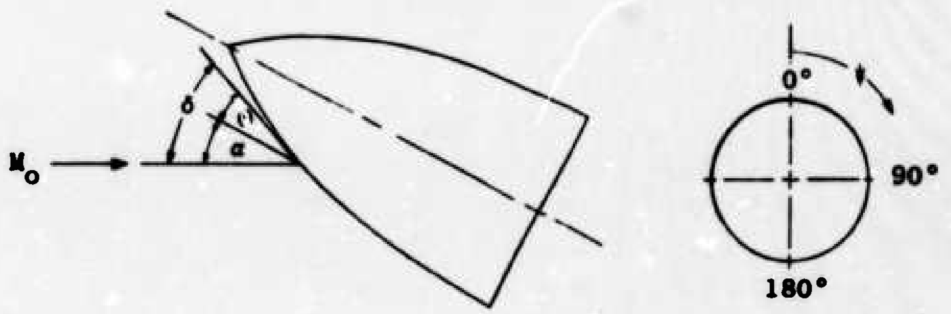

For $\alpha = 0°$, $\sin \delta = \sin \Theta$.

The value for $C_{p_{max}}$ on the desired meridian, ψ, may be determined either experimentally or theoretically. The NASA[21,22] zero and small angle of attack cone #tables can be used for the starting values on a cone fitted to the nose vertex if experimental data are lacking; the procedure is as follows: The general expression for pressure coefficient is:

$$C_p = \frac{p_o}{q_o}\left(\frac{p}{p_o} - 1\right) \text{ and } \frac{p}{p_o} = \frac{p}{p_1}\frac{p_1}{p_o}$$

where p_1 refers to conditions at zero angle of attack and the quantity p_1/p_o may be obtained directly from the zero angle of attack cone tables[22]. The ratio of p/p_1 which is the ratio of static pressure at angle of attack to static pressure at zero angle of attack can be calculated using the theory of Stone[23] wherein the velocity, pressure, and density are expanded in the following series and higher order terms in α are neglected:

$$M^* = M_1^* - \alpha M_2^* \cos \psi$$

$$p = p_1 + \alpha p_2 \cos \psi$$

$$\rho = \rho_1 + \alpha \rho_2 \cos \psi$$

where the flow quantities M_1^*, p_1, and ρ_1 refer to conditions at zero angle of attack and M_2^*, p_2, and ρ_2 are the flow quantities related to the effect of angle of attack. Reference 23 provides solutions for the above equations yielding,

#The necessary tables required in the calculational procedures of this subsection have been reproduced from the references and included in Appendix 1.

among others, the following expression:

$$p/p_1 = \left[\frac{(\gamma+1) - (\gamma-1)\, M^{*2}}{(\gamma+1) - (\gamma-1)\, M_1^{*2}}\right]^{\frac{\gamma}{\gamma-1}} e^{-\alpha\, (S_2/R)\, \cos\psi}$$

References 21 and 22 have provided tabulated values of M_1^*, M_2^*, and S_2/R for use in determining p/p_1 and subsequently, C_p. Since conditions at the nose vertex were used to calculate the pressure coefficient, this value of C_p becomes C_{p_N} from whence $C_{p_{max}}$, Equation (7), may be determined. Starting values of $C_{p_{max}}$ must be calculated for each value of ψ at the desired angle of attack. Once this is done, the Generalized Newtonian theory, Equation (6), is used to calculate the values of C_p along each meridian up to the point where the shock expansion method is used to extend the impact theory; for the cylindrical afterbody, Equation (5a) or (5b) is used for the pressure coefficient distribution.

The local Mach number at the nose vertex (where $M = M_N$) may be determined from the relation[24]:

$$M^2 = \frac{2\, M^{*2}}{(\gamma+1) - (\gamma-1)\, M^{*2}}$$

On the leeward side of the body, certain portions of the surface will lie in the "aerodynamic shadow" and the Newtonian theory cannot predict the pressures in this region. This shadow area on the body, shown pictorially here.

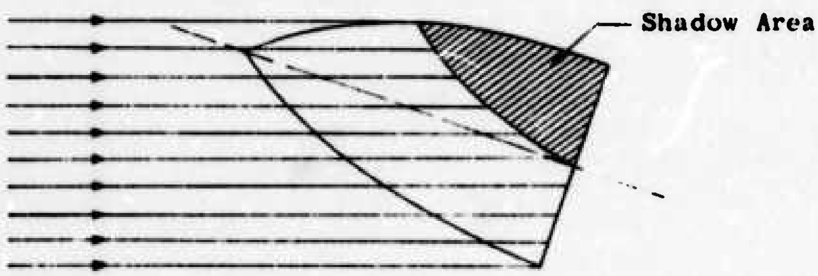

can be determined quite easily along any leeward meridian by setting $\sin\delta = 0$ and solving for Θ. For any meridian in general, the Θ at which the shadowed area starts is:

$$\Theta = \tan^{-1}(\tan\alpha \cos\psi)$$

for $\psi = 0°$ $\qquad \Theta = \alpha$

Thus the shadow area begins along the $\psi = 0°$ meridian at the point where the body surface angle is equal to the angle of attack.

On all meridians, the matching point (where the shock-expansion method is used to extend the impact theory) is obtained directly from plots presented in prior sections of this report, e.g., Fig. 6, page 16. When the matching point lies within the shadowed area, the shock-expansion method should be started at the x/ℓ value where $\sin \delta = 0$.

A numerical example is presented in Appendix 1 wherein the pressure coefficient distribution has been calculated for a tangent ogive-cylindrical afterbody combination at $M_o = 2.0$ and $\ell/d = 3$ at an angle of attack of 5 degrees. Tables are included which provide the necessary parameters for determining the pressure and local Mach number distribution. For the numerical example, starting values of C_{p_N} were determined for seven meridians beginning at $\psi = 0°$ and proceeding in 30 degree increments up to $\psi = 180°$. The pressure distribution along the $\psi = 180°$ meridian is the only one for which the C_p calculation is shown since the procedure is similar for each meridian. The calculation of the cylindrical afterbody pressure distribution using Equation (5b) has also been included for the $\psi = 180°$ meridian.

The pressure distributions calculated by the present method for the numerical example of Appendix 1 are presented in Figure 23 where experimental

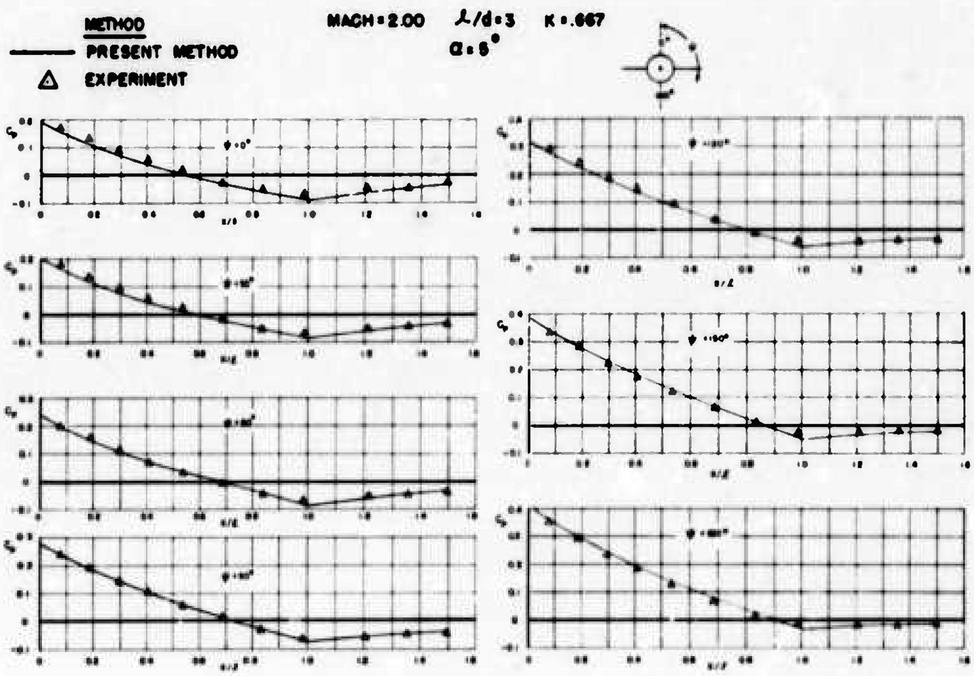

Fig. 23 PRESSURE COEFFICIENT DISTRIBUTION FOR A TANGENT OGIVE-CYLINDRICAL AFTERBODY COMBINATION AT $\alpha = 5°$, $\psi = 0°$, 30°, 60°, 90°, 120°, 150°, and 180°

values[25] have been included for comparison purposes with the subsequent indication of good agreement.

2. Bodies of Revolution at Large Angles of Attack

The calculation of pressure distributions for angles of attack greater than about 5 degrees requires somewhat more time since the starting values of C_{p_N} must be determined from the MIT[26,27,28] cone tables (or comparable information) unless experimental data are available. Once the starting values have been obtained, the procedure is similar to that used for the small angles of attack.

Since the MIT cone tables are being used to obtain starting values at the nose vertex, the symbols and nomenclature adopted by this widely used reference will not be altered to conform to the nomenclature of this report. Any attempt to redefine or re-reference the parameters would inevitably tend to compound the existing complexity of the equations. The symbols and nomenclature from the MIT cone tables which are used in the present study are defined on page 4 of this report. In addition, the parameters required for calculating C_{p_N} have been picked from the MIT cone tables and are tabulated in Appendix 2 for ready use. If any intermediate values of the parameters are required, they can be obtained much more readily when nomenclature consistent with the reference source is used.

The theory of Stone[33] is used once again to determine the flow parameters which have been expanded in the following series; for large angles of attack, the higher order terms in α cannot be neglected, i.e.,

$$p/\bar{p} = 1 + \alpha A_1 \cos\psi + \alpha^2 (A_2 + A_3 \cos 2\psi)$$

$$\rho/\bar{\rho} = 1 + \alpha B_1 \cos\psi + \alpha^2 (B_2 + B_3 \cos 2\psi)$$

where $p/\bar{p}$ and $\rho/\bar{\rho}$ are the pressure and density on the cone surface at angle of attack divided by the corresponding values at zero angle of attack, A_1 and B_1 specify the first order effects of α, and A_2, A_3, B_2, and B_3 represent the second order effects of α. Proceeding further:

$$A_1 = -\eta/\bar{p}$$

$$A_2 = p_o/\bar{p} + \frac{\gamma}{2}\frac{\bar{u}^2}{\bar{a}^2} + \frac{\eta}{2\bar{p}} \cot \theta_s$$

$$A_3 = p_2/\bar{p} + \frac{\gamma}{2}\frac{\bar{u}^2}{\bar{a}^2} - \frac{\eta}{2\bar{p}} \cot \theta_s$$

$$B_1 = -\xi/\bar{\rho}$$

$$B_2 = \rho_o/\bar{\rho} + \frac{1}{2}\frac{\bar{u}^2}{\bar{a}^2} + \frac{\xi}{2\bar{\rho}} \cot \theta_s$$

$$B_3 = \rho_2/\bar{\rho} + \frac{1}{2}\frac{\bar{u}^2}{\bar{a}^2} - \frac{\xi}{2\bar{\rho}} \cot \theta_s$$

By entering the cone tables at the desired free stream Mach number (corresponds to M with no subscript in tables) and the nose semi-vertex angle θ_N equal to θ_s, the following quantities may be obtained:

\# $\bar{u}/c$ and $\bar{a}^2/c^2$

$\eta/\bar{p}$ and $\xi/\bar{\rho}$

$p_o/\bar{p}$, $p_2/\bar{p}$, $\rho_o/\bar{\rho}$ and $\rho_2/\bar{\rho}$

With these quantities, A_1, A_2, A_3, B_1, B_2, and B_3 may be evaluated and subsequently $p/\bar{p}$ can be obtained. This value of $p/\bar{p}$ must now be referred to the free stream in order to calculate the surface pressure coefficient, i.e.,

$$\frac{p}{p_1} = \frac{p}{\bar{p}}\,\frac{\bar{p}}{p_1} \quad \text{(subscript 1 denotes free stream in tables)}$$

where $\frac{\bar{p}}{p_1} = \frac{\bar{p}}{p_w}\,\frac{p_w}{p_1}$ and the quantities $\bar{p}/p_w$ and p_w/p_1 are taken directly from the tables herein. The quantity $\bar{p}/p_w$ will be listed as p_s/p_w (p_s is the cone surface static pressure and p_w is the static pressure immediately behind the shock wave).

Knowing p/p_1, the pressure coefficient at any meridian, ϕ, on the cone surface can be calculated using:

$$C_p = p_1/q_1\left(\frac{p}{p_1} - 1\right) = \frac{2}{\gamma M_1^{\,2}}\left(\frac{p}{p_1} - 1\right)$$

Since the value of C_p for a given ϕ is determined at the nose vertex, this represents the starting value of C_{p_N}.

To compute the local Mach number at the nose vertex, we begin by expressing the entropy in powers of α similar to that for pressure and density:

$$S = \bar{S} - \alpha S_1 + \alpha^2 (S_2 + S_3)$$

\# These values appear as u and a^2 in Reference 26.

where
$$S_1 = c_v \left[A_1 - \gamma B_1\right]$$
$$S_2 = c_v \left[\gamma B_1^2/4 - A_1^2/4 + A_2 - \gamma B_2\right]$$
$$S_3 = c_v \left[\gamma B_1^2/4 - A_1^2/4 + A_3 - \gamma B_3\right]$$

Now from the equation of state,

$$\rho/\bar{\rho} = (p/\bar{p})^{1/\gamma} \; e^{-\frac{(S-\bar{S})}{\gamma c_v}}$$

$p/\bar{p}$ has already been determined and $(S-\bar{S})/\gamma c_v$ may be calculated using the aforementioned entropy distribution equations wherein the quantities A_1, A_2, A_3, B_1, B_2, and B_3 have also been determined ($\rho/\bar{\rho}$ can also be calculated using the equation on page 40). Finally, from Bernoulli's equation,

$$V^2 + \frac{2\gamma p}{\rho(\gamma-1)} = c^2 \quad \text{where } c = \text{limit speed.}$$

Dividing by a^2 and simplifying,

$$M^2 = \frac{c^2}{a^2} - \frac{2}{\gamma-1} = \frac{c^2}{\bar{a}^2}\frac{\bar{a}^2}{a^2} - \frac{2}{\gamma-1}$$

where: $\dfrac{\bar{a}^2}{a^2} = \dfrac{\bar{p}/p}{\bar{\rho}/\rho}$ and $c^2/\bar{a}^2$ is obtained from Table 17 herein.

A numerical example has been provided in Appendix 2 which illustrates the manner in which C_p was obtained for a tangent ogive-cylindrical afterbody combination at $M_o = 2.0$, $\ell/d = 3$ and $\alpha = 10°$. As was done for the numerical example at 5 degrees, starting values of C_{p_N} were calculated and are shown for $\psi = 0°$ to $180°$ in $30°$ increments. Only the calculation for C_p values along the $\psi = 180°$ meridian (including the pressure distribution on the cylindrical afterbody) are shown in the numerical example.

Figure 24 presents the pressure distribution coefficients calculated by the present method and experimental values[25] which were used for comparison purposes. The agreement at $\alpha = 10°$ is not as good as that for the $\alpha = 5°$ case especially on the leeward meridian but this was more or less to be expected since flow separation may now be present. The more windward meridians indicate good agreement with the experimental values.

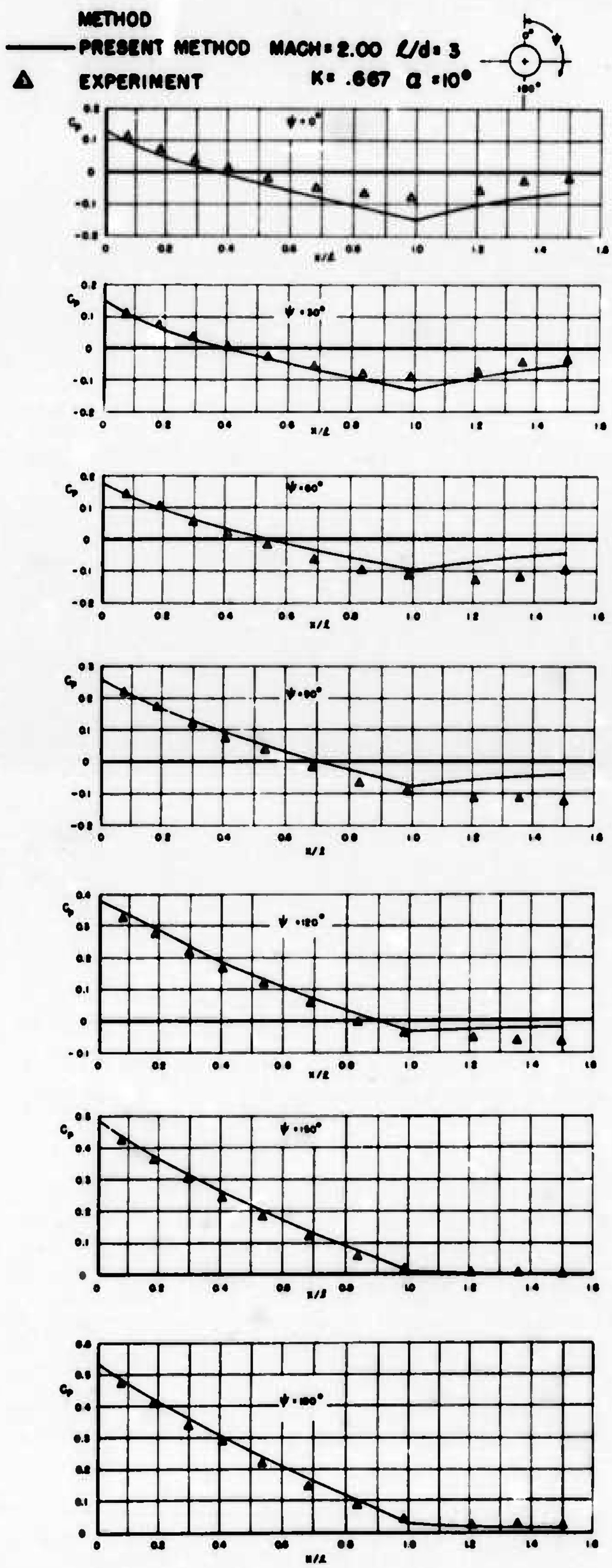

Fig. 24 PRESSURE COEFFICIENT DISTRIBUTION FOR A TANGENT OGIVE-CYLINDRICAL AFTERBODY COMBINATION AT $\alpha = 10°$, $\psi = 0°$, 30°, 60°, 90°, 120°, 150°, and 180°

APPENDIX I

CALCULATION OF PRESSURE COEFFICIENT DISTRIBUTION FOR A TANGENT OGIVE-CYLINDRICAL AFTERBODY COMBINATION AT AN ANGLE OF ATTACK OF 5 DEGREES

A. CONDITIONS

FREE STREAM MACH NUMBER	—	$M_o = 2$
NOSE FINENESS RATIO	—	$\ell/d = 3$
NOSE SEMI-VERTEX ANGLE	—	$\theta_N = 18.925^\circ$
HYPERSONIC SIMILARITY PARAMETER	—	$K = .67$
RATIO OF SPECIFIC HEATS	—	$\gamma = 1.405$

B. PRESSURE COEFFICIENT AND MACH NUMBER STARTING VALUES, $X/\ell = 0$

$$C_p = (P_o/q_o)(P/P_o - 1) = (P_o/q_o)\left[(P/P_1)(P_1/P_o) - 1\right] \qquad \text{EQ. AI-1}$$

$$P/P_1 = \left[\frac{(\gamma+1) - (\gamma-1)M^{*2}}{(\gamma+1) - (\gamma-1)M_1^{*2}}\right]^{\frac{\gamma}{\gamma-1}} e^{-\alpha(S_2/R)\cos\psi} \qquad \text{EQ. AI-2}$$

$$M^* = M_1^* - \alpha M_2^* \cos\psi, \qquad \alpha \text{ IN RADIANS} \qquad \text{EQ. AI-3}$$

$$M = \left[\frac{2M^{*2}}{(\gamma+1) - (\gamma-1)M^{*2}}\right]^{1/2} \qquad \text{EQ. AI-4}$$

WHERE

P_1/P_o	$= 1.8335$	FROM	APPENDIX I,	TABLE 8,	PAGE	50	.
M_1^*	$= 1.4241$	"	"	TABLE 9,	"	51	.
M_2^*	$= -.7258$	"	"	TABLE 10,	"	52	.
S_2/R	$= .0651$	"	"	TABLE 11,	"	53	.

$$P_o/q_o = .3571 = \frac{2}{\gamma M_o^2}$$

NUMERICAL SOLUTIONS FOR EQUATIONS AI-1, AI-2, AI-3, AND AI-4 ARE SHOWN IN COLUMNS 8, 6, 4, AND 9 RESPECTIVELY OF TABLE 2, PAGE 45.

TABLE 2. PRESSURE COEFFICIENT AND MACH NUMBER STARTING VALUES, $X/\ell = 0$, $\alpha = 5°$

1	2	3	4	5	6	7	8	9	10
ψ	$\cos\psi$	$\alpha M_2^* \cos\psi$	M^* EQ. AI-3	$e^{-\alpha(S_2/R)\cos\psi}$	P/P_1 EQ. AI-2	P/P_0 = 1.8335 ⑥	$C_p = C_{p_N}$ EQ. AI-1	$M = M_N$ EQ. AI-4	*$(P/P_t)_N$ TABLE 18
0	1.0000	-.0633	1.4874	.9926	.8393	1.5389	.1924	1.713	.1987
30	.8660	-.0549	1.4790	.9936	.8599	1.5766	.2060	1.697	.2035
60	.5000	-.0317	1.4558	.9963	.9180	1.6831	.2439	1.656	.2164
90	0	0	1.4241	1.0000	1.0000	1.8335	.2976	1.606	.2332
120	-.5000	.0317	1.3925	1.0037	1.0854	1.9901	.3536	1.547	.2544
150	-.8660	.0549	1.3693	1.0065	1.1501	2.1086	.3959	1.510	.2685
180	-1.0000	.0633	1.3608	1.0075	1.1743	2.1530	.4117	1.496	.2740

C. SINE OF FLOW DEFLECTION ANGLE, δ, ALONG $\psi = 180°$ MERIDIAN

$$\sin\delta = \sin\theta\cos\alpha - \cos\psi\cos\theta\sin\alpha$$

TABLE 3. VALUES OF SINE δ, $\alpha = 5°$

1	2	3	4	5	6	7
X/ℓ	θ	$\sin\theta$	$\cos\theta$	$\sin\theta\cos\alpha$	$\cos\psi\cos\theta\sin\alpha$	$\sin\delta$
0	18.925	.32433	.94594	.32309	-.08245	.40554
.1	16.972	.29190	.95646	.29079	-.08336	.37415
.2	15.038	.25946	.96575	.25847	-.08417	.34264
.3	13.122	.22703	.97388	.22617	-.08488	.31105
.4	11.221	.19460	.98088	.19386	-.08549	.27935
.5	9.333	.16217	.98676	.16155	-.08601	.24756
.6	7.454	.12973	.99155	.12924	-.08642	.21566
.7	5.584	.09730	.99525	.09693	-.08675	.18368
.8	3.719	.06487	.99789	.06462	-.08698	.15160
.9	1.859	.03243	.99947	.03231	-.08711	.11942
1.0	0	0	1.00000	0	-.08716	.08716

* VALUES OF $(P/P_t)_N$ ARE OBTAINED FROM TABLE 18 USING THE APPROPRIATE VALUES OF M_N IN COLUMN 9, TABLE 2.

APPENDIX I

D. PRESSURE COEFFICIENT AND LOCAL MACH NUMBER DISTRIBUTIONS ALONG $\psi = 180°$ MERIDIAN (SEE FIGURE 23)

CONDITIONS AT NOSE VERTEX

M_N	$= 1.496$	—	COLUMN 9, TABLE 2
$(P/P_t)_N$	$= .2740$	—	" 10, "
C_{P_N}	$= .4117$	—	" 8, "
$C_{P_{MAX}}$	$= 2.5033$	—	EQ. 7

1. C_p VALUES (COLUMN 3, TABLE 4) FROM THE NOSE VERTEX UP TO THE MATCHING POINT, $(X/\ell)_m$, ARE OBTAINED USING EQ. 6. (THE MATCHING POINT SOLUTION IS DISCUSSED ON PAGE 15).
2. C_p VALUES (COLUMN 4, TABLE 4) FROM $(X/\ell)_m$ TO $X/\ell = 1$ ARE CALCULATED USING THE PROCEDURE OUTLINED ON PAGES 15 AND 16. FOR THIS PARTICULAR EXAMPLE, $C_p = 2.8058\ (P/P_t) - .3571$ (EQ. 3)
3. ALL LOCAL MACH NUMBER VALUES (COLUMN 9, TABLE 4) ARE OBTAINED FROM TABLE 18, APPENDIX 3, USING THE APPROPRIATE VALUE OF P/P_t (COLUMN 8, TABLE 4) CALCULATED FROM EQ. 3a.

TABLE 4. PRESSURE COEFFICIENT DISTRIBUTION AND MACH NUMBER ALONG $\psi = 180°$ MERIDIAN, $\alpha = 5°$

1	2	3	4	5	6	7	8	9
X/ℓ	$\sin^2\delta$	C_p GN EQ. 6	C_p SEM EQ. 3	θ	$\Delta\theta$	ν	P/P_t	M TABLE 18
0	.16446	.4117	—	—	—	—	.2740	1.496
.1	.13999	.3504	—	—	—	—	.2522	1.553
.2	.11740	.2939	—	—	—	—	.2320	1.609
.3	.09675	.2422	—	—	—	—	.2136	1.665
.4	.07804	.1954	—	—	—	—	.1969	1.719
.5	.06129	.1534	—	—	—	—	.1819	1.771
.6	.04651	.1164	—	—	—	—	.1688	1.820
$.7_m$	.03374	.0845	.0845	5.584	—	22.604	.1574	1.865
.8	—	—	.0418	3.719	1.865	24.469	.1422	1.931
.9	—	—	.0028	1.859	1.860	26.329	.1282	1.996
1.0	—	—	-.0336	0	1.859	28.188	.1153	2.066

GN = GENERALIZED NEWTONIAN
SEM = SHOCK EXPANSION METHOD
θ = BODY SURFACE ANGLE
$.7_m$ = MATCHING POINT OF GENERALIZED NEWTONIAN AND SHOCK EXPANSION METHOD
M = M CORRESPONDING TO P/P_t FROM PRANDTL-MEYER TABLES
ν = PRANDTL-MEYER FLOW DEFLECTION ANGLE CORRESPONDING TO M

APPENDIX I

E. CYLINDRICAL AFTERBODY PRESSURE COEFFICIENT DISTRIBUTION ALONG $\psi = 180°$ MERIDIAN

USING EQ. 5b

$$C_p = C_{p(x/\ell=1)}\, e^{-\frac{\Delta x/\ell}{K}}$$

VALUES OF C_p ON THE CY' NDRICAL AFTERBODY ARE CALCULATED AS SHOWN IN TABLE 5.

$C_{p(x/\ell=1)} = -.0336$, FROM COLUMN 4, TABLE 4.

TABLE 5. PRESSURE COEFFICIENT DISTRIBUTION ON CYLINDRICAL AFTERBODY, $\alpha = 5°$

1	2	3	4
x/ℓ	$\Delta x/\ell$	$e^{-\frac{(2)}{K}}$	$C_p = -.0336$ (3)
1.0	0	1.0000	-.0336
1.1	.1	.8607	-.0289
1.2	.2	.7408	-.0249
1.3	.3	.6376	-.0214
1.4	.4	.5488	-.0184
1.5	.5	.4724	-.0159

TABLE 6. Values of Surface Pressure Coefficient, C_{p_N}, at $\alpha = 0°$

M_o \ θ_N	2.5	5.0	7.5	10.0	12.5	15.0	17.5	20.0	22.5	25.0	27.5	30.0
1.5	.012338	.039662	.077386	.123798	.178117	.240031	.309545	.386979	.473154	.569989		
1.75	.011441	.036329	.070429	.112270	.161201	.216923	.279290	.348246	.423819	.506190	.595857	.694052
2.0	.010786	.033946	.065581	.104458	.150085	.202234	.260761	.325531	.396413	.473302	.556160	.645120
2.5	.009830	.030586	.058960	.094131	.135861	.184034	.238526	.299159	.365710	.437919	.515504	.598189
3.0	.009135	.028240	.054519	.087475	.127024	.173101	.225581	.284262	.348884	.419129	.494637	.575031
3.5	.008592	.026475	.051302	.082818	.121020	.165859	.217199	.274818	.338425	.407669	.482154	.561453
4.0	.008149	.025088	.048865	.079393	.116712	.160770	.211415	.268404	.331425	.400103	.474018	.552714
4.5	.007779	.023968	.046962	.076789	.113504	.157044	.207243	.263837	.326496	.394830	.468399	.546733
5.0	.007462	.023047	.045443	.074757	.111045	.154232	.204131	.260466	.322892	.391003	.464350	.542452
6.0	.006947	.021623	.043189	.071829	.107580	.150338	.199887	.255923	.318080	.385936	.459028	.536858
7.0	.006544	.020585	.041621	.069858	.105309	.147838	.197204	.253086	.315105	.382829	.455786	.533474
8.0	.006221	.019802	.040486	.068472	.103744	.146141	.195404	.251200	.313140	.380789	.453669	.531271
10.0	.005736	.018718	.038988	.066703	.101792	.144060	.193221	.248931	.310793	.378363	.451160	.528672
12.0	.005392	.018021	.038076	.065665	.100674	.142885	.192002	.247675	.309500	.377032	.449790	.527256
15.0	.005038	.017365	.037263	.064766	.099723	.141897	.190986	.246631	.308431	.375937	.448664	.526095
20.0	.004681	.016779	.036577	.064031	.098960	.141113	.190185	.245813	.307594	.375079	.447785	.525193

TABLE 7. Values of M on Cone Surface at $\alpha = 0°$

M_o \ θ_N	2.5	5.0	7.5	10.0	12.5	15.0	17.5	20.0	22.5	25.0	27.5	30.0
1.5	1.4867	1.4579	1.4197	1.3749	1.3249	1.2707	1.2127	1.1506	1.0837	1.0101		
1.75	1.7340	1.7005	1.6568	1.6064	1.5513	1.4925	1.4306	1.3657	1.2977	1.2259	1.1496	1.0669
2.0	1.9809	1.9415	1.8912	1.8340	1.7722	1.7069	1.6387	1.5678	1.4941	1.4175	1.3375	1.2536
2.5	2.4729	2.4194	2.3529	2.2789	2.2002	2.1179	2.0328	1.9449	1.8544	1.7614	1.6660	1.5681
3.0	2.9628	2.8914	2.8048	2.[illegible]1	2.6104	2.5068	2.3998	2.2900	2.1777	2.0636	1.9479	1.8310
3.5	3.4501	3.3572	3.2467	3.1275	3.0026	2.8731	2.7401	2.6043	2.4669	2.3287	2.1904	2.0527
4.0	3.9348	3.8165	3.6784	3.5306	3.3761	3.2167	3.0538	2.8890	2.7240	2.5601	2.3983	2.2394
4.5	4.4166	4.2691	4.0995	3.9189	3.7308	3.5374	3.3414	3.1453	2.9514	2.7612	2.5761	2.3965
5.0	4.8955	4.7148	4.5097	4.2922	4.0663	3.8356	3.6041	3.3752	3.1518	2.9357	2.7279	2.5289
6.0	5.8441	5.5852	5.2969	4.9928	4.6802	4.3668	4.0597	3.7641	3.4830	3.2178	2.9688	2.7353
7.0	6.7797	6.4269	6.0385	5.6318	5.2205	4.8178	4.4335	4.0731	3.7388	3.4303	3.1463	2.8844
8.0	7.7019	7.2391	6.7337	6.2104	5.6923	5.1982	4.7390	4.3188	3.9373	3.5919	3.2788	2.9940
10.0	9.5046	8.7725	7.9852	7.1978	6.4568	5.7868	5.1934	4.6724	4.2154	3.8131	3.4569	3.1392
12.0	11.2504	10.1821	9.0583	7.9858	7.0291	6.2043	5.5020	4.9043	4.3927	3.9511	3.5660	3.2268
15.0	13.7591	12.0635	10.3683	8.8728	7.6324	6.6229	5.7998	5.1216	4.5553	4.0754	3.6629	3.3037
20.0	17.6379	14.6135	11.9195	9.8177	8.2281	7.0145	6.0679	5.3120	4.6947	4.1803	3.7438	3.3673

TABLE 8. #Values of p/p_o at $\alpha = 0°$

M_o \ θ_N	2.5	5.0	7.5	10.0	12.5	15.0	17.5	20.0	22.5	25.0	27.5	30.0
1.5	1.0194	1.0625	1.1219	1.1950	1.2805	1.3780	1.4875	1.6095	1.7452	1.8977		
1.75	1.0245	1.0779	1.1510	1.2407	1.3456	1.4650	1.5987	1.7466	1.9086	2.0851	2.2774	2.4879
2.0	1.0302	1.0950	1.1836	1.2925	1.4202	1.5663	1.7301	1.9115	2.1100	2.3252	2.5572	2.8063
2.5	1.0430	1.1338	1.2579	1.4118	1.5944	1.8052	2.0436	2.3088	2.6000	2.9159	3.2553	3.6171
3.0	1.0576	1.1779	1.3435	1.5511	1.8003	2.0905	2.4212	2.7909	3.1980	3.6405	4.1162	4.6227
3.5	1.0737	1.2270	1.4400	1.7102	2.0377	2.4222	2.8625	3.3566	3.9020	4.4958	5.1345	5.8145
4.0	1.0913	1.2810	1.5473	1.8892	2.3072	2.8006	3.3678	4.0061	4.7120	5.4812	6.3090	7.1904
4.5	1.1103	1.3398	1.6657	2.0885	2.6089	3.2261	3.9377	4.7399	5.6281	6.5967	7.6395	8.7499
5.0	1.1306	1.4033	1.7952	2.3082	2.9433	3.6991	4.5723	5.5582	6.6506	7.8426	9.1261	10.4929
6.0	1.1751	1.5449	2.0884	2.8101	3.7110	4.7885	6.0371	7.4493	9.0156	10.7256	12.5675	14.5288
7.0	1.2245	1.7061	2.4276	3.3961	4.6121	6.0709	7.7641	9.6809	11.8081	14.1310	16.6335	19.2982
8.0	1.2787	1.8871	2.8138	4.0675	5.6477	7.5471	9.7541	12.2538	15.0287	18.0594	21.3244	24.8009
10.0	1.4015	2.3103	3.7292	5.6692	8.1255	11.0842	14.5255	18.4252	22.7555	27.4854	32.5812	38.0071
12.0	1.5436	2.8165	4.8381	7.6190	11.1480	15.4028	20.3538	25.9656	32.1976	39.0049	46.3388	54.1474
15.0	1.7934	3.7349	6.8689	11.2006	16.7064	23.3488	31.0803	39.8443	49.5779	60.2101	71.6646	83.8600
20.0	2.3108	5.6981	11.2417	18.9287	28.7087	40.5116	54.2519	69.8276	87.1262	106.0220	126.3799	148.0542

#Equals p_1/p_o for Small Angle of Attack Calculations.

TABLE 9. Values of M_1^* on Cone Surface at $\alpha = 0°$

M_o \ θ_N	2.5	5.0	7.5	10.0	12.5	15.0	17.5	20.0	22.5	25.0	27.5	30.0
1.5	1.35619	1.33784	1.31295	1.28297	1.24863	1.21025	1.16778	1.12079	1.06831	1.00837		
1.75	1.50107	1.48273	1.45826	1.42918	1.39627	1.35989	1.32012	1.27678	1.22947	1.17755	1.11996	1.05485
2.0	1.62426	1.60595	1.58183	1.55341	1.52145	1.48627	1.44790	1.40620	1.36086	1.31146	1.25740	1.19785
2.5	1.81688	1.79886	1.77556	1.74839	1.71797	1.68444	1.64769	1.60751	1.56362	1.51572	1.46345	1.40639
3.0	1.95515	1.93766	1.91532	1.88940	1.86029	1.82793	1.79210	1.75255	1.70901	1.66123	1.60895	1.55187
3.5	2.05552	2.03867	2.01734	1.99259	1.96456	1.93305	1.89777	1.85846	1.81488	1.76683	1.71410	1.65647
4.0	2.12963	2.11345	2.09310	2.06936	2.04219	2.01128	1.97632	1.93705	1.89329	1.84486	1.79159	1.73333
4.5	2.18537	2.16986	2.15040	2.12752	2.10102	2.07051	2.03572	1.99641	1.95241	1.90359	1.84982	1.79097
5.0	2.22807	2.21320	2.19453	2.17237	2.14637	2.11614	2.08143	2.04202	1.99778	1.94861	1.89440	1.83504
6.0	2.28775	2.27402	2.25665	2.23553	2.21019	2.18027	2.14556	2.10592	2.06126	2.01151	1.95659	1.89644
7.0	2.32623	2.31347	2.29706	2.27661	2.25164	2.22184	2.18707	2.14721	2.10221	2.05202	1.99660	1.93589
8.0	2.35236	2.34038	2.32467	2.30466	2.27989	2.25014	2.21527	2.17522	2.12997	2.07946	2.02368	1.96257
10.0	2.38439	2.37360	2.35875	2.33921	2.31462	2.28484	2.24981	2.20950	2.16389	2.11298	2.05672	1.99510
12.0	2.40250	2.39248	2.37810	2.35877	2.33423	2.30440	2.26924	2.22876	2.18294	2.13177	2.07525	2.01332
15.0	2.41777	2.40846	2.39444	2.37522	2.35069	2.32078	2.28551	2.24487	2.19886	2.14748	2.09071	2.02854
20.0	2.43004	2.42131	2.40749	2.38833	2.36376	2.33378	2.29840	2.25762	2.21145	2.15990	2.10295	2.04056

TABLE 10. Surface Values of M_2^*

M_o \ θ_N	2.5	5.0	7.5	10.0	12.5	15.0	17.5	20.0	22.5	25.0	27.5	30.0
1.5	-.11690	-.22548	-.32371	-.41200	-.49187	-.56551	-.63554	-.70482	-.77662	-.85544		
1.75	-.12856	-.24547	-.34870	-.43946	-.52026	-.59421	-.66449	-.73391	-.80483	-.87953	-.96079	-1.05319
2.0	-.13817	-.26115	-.36721	-.45873	-.53951	-.61377	-.68518	-.75646	-.82953	-.90584	-.98689	-1.07470
2.5	-.15237	-.28214	-.38935	-.47960	-.55987	-.63607	-.71196	-.78955	-.86979	-.95314	-1.03999	-1.13098
3.0	-.16150	-.29311	-.39799	-.48606	-.56706	-.64717	-.72923	-.81416	-.90202	-.99267	-1.08601	-1.18221
3.5	-.16712	-.29752	-.39881	-.48556	-.56892	-.65408	-.74253	-.83421	-.92861	-1.02526	-1.12387	-1.22445
4.0	-.17032	-.29778	-.39553	-.48233	-.56916	-.65957	-.75380	-.85110	-.95066	-1.05189	-1.15445	-1.25833
4.5	-.17187	-.29549	-.39045	-.47851	-.56928	-.66458	-.76368	-.86544	-.96894	-1.07356	-1.17903	-1.28535
5.0	-.17226	-.29174	-.38490	-.47506	-.56979	-.66936	-.77241	-.87762	-.98407	-1.09122	-1.19882	-1.30693
6.0	-.17085	-.28246	-.37477	-.47028	-.57202	-.67819	-.78686	-.89675	-1.00710	-1.11753	-1.22791	-1.33836
7.0	-.16780	-.27315	-.36722	-.46811	-.57523	-.68530	-.79795	-.91061	-1.02323	-1.13557	-1.24758	-1.35941
8.0	-.16398	-.26504	-.36214	-.46768	-.57866	-.69212	-.80645	-.92080	-1.03481	-1.14831	-1.26132	-1.37402
10.0	-.15571	-.25325	-.35712	-.46924	-.58484	-.70147	-.81809	-.93423	-1.04969	-1.16446	-1.27858	-1.39226
12.0	-.14799	-.24628	-.35576	-.47170	-.58958	-.70767	-.82532	-.94227	-1.05843	-1.17381	-1.28850	-1.40268
15.0	-.13864	-.24125	-.35624	-.47505	-.59444	-.71346	-.83178	-.94930	-1.06596	-1.18180	-1.29691	-1.41148
20.0	-.12887	-.23907	-.35831	-.47880	-.59898	-.71849	-.83720	-.95507	-1.07206	-1.18823	-1.30365	-1.41852

TABLE 11. Values of S_2/R

M_o \ θ_N	2.5	5.0	7.5	10.0	12.5	15.0	17.5	20.0	22.5	25.0	27.5	30.0
1.5	0	0	0	.0001	.0009	.0036	.0101	.0218	.0393	.0621		
1.75	0	0	0	.0004	.0029	.0105	.0263	.0515	.0854	.1261	.1709	.2172
2.0	0	0	.0001	.0015	.0082	.0261	.0585	.1053	.1634	.2285	.2962	.3623
2.5	0	0	.0009	.0097	.0403	.1020	.1933	.3058	.4287	.5524	.6689	.7730
3.0	0	.0001	.0051	.0380	.1241	.2650	.4442	.6401	.8341	1.0127	1.1675	1.2942
3.5	0	.0006	.0186	.1042	.2828	.5323	.8140	1.0938	1.3485	1.5650	1.7377	1.8660
4.0	0	.0024	.0504	.2253	.5293	.9036	1.2870	1.6374	1.9326	2.1642	2.3325	2.4426
4.5	0	.0074	.1114	.4133	.8658	1.3672	1.8390	2.2386	2.5504	2.7744	2.9188	2.9950
5.0	0	.0184	.2115	.6740	1.2863	1.9054	2.4446	2.8687	3.1736	3.3704	3.4758	3.5073
6.0	.0002	.0755	.5587	1.4111	2.3328	3.1283	3.7273	4.1295	4.3633	4.4640	4.4640	4.3905
7.0	.0012	.2112	1.1253	2.3977	3.5634	4.4349	4.9981	5.3041	5.4168	5.3919	5.2730	5.0919
8.0	.0047	.4601	1.9079	3.5668	4.8783	5.7270	6.1804	6.3447	6.3133	6.1560	5.9213	5.6414
10.0	.0364	1.3816	4.0018	6.1821	7.4817	8.0631	8.1737	8.0054	7.6832	7.2835	6.8510	6.4113
12.0	.1510	2.8904	6.5379	8.8289	9.8049	9.9624	9.6838	9.1968	8.6252	8.0333	7.4530	6.8993
15.0	.6424	6.0565	10.5718	12.3884	12.5914	12.0629	11.2583	10.3859	9.5348	8.7392	8.0087	7.3426
20.0	2.7803	12.5896	16.6551	16.8366	15.6737	14.2026	12.7728	11.4837	10.3496	9.3573	8.4869	7.7190

* APPENDIX 2

CALCULATION OF PRESSURE COEFFICIENT DISTRIBUTION FOR A TANGENT OGIVE-CYLINDRICAL AFTERBODY COMBINATION AT AN ANGLE OF ATTACK OF 10 DEGREES

A. CONDITIONS

FREE STREAM MACH NUMBER	— $M_1 = 2$
NOSE FINENESS RATIO	— $\ell/d = 3$
NOSE SEMI-VERTEX ANGLE	— $\theta_s = \theta_N = 18.925°$
HYPERSONIC SIMILARITY PARAMETER	— $K = .87$
RATIO OF SPECIFIC HEATS	— $\gamma = 1.405$

B. PRESSURE COEFFICIENT STARTING VALUES, $X/\ell = 0$

$$C_p = (p_1/q_1)(p/p_1 - 1) = (p_1/q_1)\left[(p/\bar{p})(\bar{p}/p_1) - 1\right] \qquad \text{EQ. A2-1}$$

$$p/\bar{p} = 1 + \alpha A_1 \cos\psi + \alpha^2 (A_2 + A_3 \cos 2\psi), \qquad \alpha \text{ IN RADIANS} \qquad \text{EQ. A2-2}$$

WHERE: $A_1 = -\eta/\bar{p}$

$$A_2 = p_0/\bar{p} + (\gamma/2)\bar{u}^2/\bar{a}^2 + (\eta/2\bar{p})\cot\theta_s$$

$$A_3 = p_2/\bar{p} + (\gamma/2)\bar{u}^2/\bar{a}^2 - (\eta/2\bar{p})\cot\theta_s$$

AND:

$\eta/\bar{p}$	$= 1.7363$	FROM APPENDIX 2,	TABLE 17,	PAGES 59,	60,	AND 61.
$p_0/\bar{p}$	$= -4.39$	"	"	"	"	"
$p_2/\bar{p}$	$= 2.723$	"	"	"	"	"
$\bar{u}^2/c^2$	$= .33963$	"	"	"	"	"
$\bar{a}^2/c^2$	$= .13365$	"	"	"	"	"
$\bar{p}/p_1$	$= 1.8389$	"	"	"	"	"
p_1/q_1	$= .3571 = \dfrac{2}{\gamma M_1^2}$					

SO $A_1 = -1.7363$ $\qquad A_2 = -.07328$ $\qquad A_3 = 1.9756$

NUMERICAL SOLUTIONS FOR EQUATIONS A2-1, AND A2-2 ARE SHOWN IN COLUMNS 9 AND 7 RESPECTIVELY OF TABLE 12, PAGE 55.

* THE NOMENCLATURE USED IN APPENDIX 2 CORRESPONDS TO THAT USED IN THE MIT CONE TABLES OF REFERENCES 26, 27, AND 28.

APPENDIX 2

TABLE 12. PRESSURE COEFFICIENT STARTING VALUES, $X/\ell = 0$, $\alpha = 10°$

1	2	3	4	5	6	7	8	9
ψ	$\cos\psi$	$\cos 2\psi$	$\alpha A_1 \cos\psi$	$\alpha^2 A_2$	$\alpha^2 A_3 \cos 2\psi$	$P/\bar{P}$ $= 1 + (4) + (5) + (6)$ EQ. A2-2	$P/P_1 =$ 1.8889 (7)	$C_P = C_{P_N}$ EQ A2-1
0	1.0000	1.0000	-.3030	-.0022	.0602	.7549	1.3882	.1386
30	.8660	.5000	-.2624	"	.0301	.7654	1.4075	.1455
60	.5000	-.5000	-.1515	"	-.0301	.8162	1.5008	.1780
90	0	-1.0000	0	"	-.0602	.9376	1.7241	.2586
120	-.5000	-.5000	.1515	"	-.0301	1.1192	2.0581	.3778
150	-.8660	.5000	.2624	"	.0301	1.2903	2.3727	.4902
180	-1.0000	1.0000	.3030	"	.0602	1.3610	2.5027	.5366

C. MACH NUMBER STARTING VALUES, $X/\ell = 0$

$$M^2 = \frac{c^2}{\bar{a}^2}\,\frac{\bar{a}^2}{a^2} - \frac{2}{\gamma - 1} \qquad \frac{c^2}{\bar{a}^2} = \frac{1}{.13366} = 7.4822 \quad \text{FROM APPENDIX 2, TABLE 17.}$$

$$\frac{\bar{a}^2}{a^2} = \frac{\rho/\bar{\rho}}{P/\bar{P}} \quad \text{WHERE} \quad \rho/\bar{\rho} = \left(\frac{P}{\bar{P}}\right)^{1/\gamma} e^{-\left(\frac{S-\bar{S}}{\gamma c_v}\right)}$$

a.) DETERMINE $(S-\bar{S})/\gamma c_v$ $\qquad S = \bar{S} - \alpha S_1 + \alpha^2 (S_2 + S_3)$

WHERE $S_1 = c_v \left[A_1 - \gamma B_1\right]$

$$S_2 = c_v \left[(\gamma B_1^2/4) - (A_1^2/4) + A_2 - \gamma B_2\right]$$

$$S_3 = c_v \left[(\gamma B_1^2/4) - (A_1^2/4) + A_3 - \gamma B_3\right]$$

FROM PART B, $A_1 = -1.7363$ $\quad A_2 = -.07328$ $\quad A_3 = 1.9756$

$$B_1 = -\xi/\bar{P}$$

$$B_2 = P_0/\bar{P} + (1/2)\,\bar{u}^2/\bar{a}^2 + (\xi/2\bar{P}) \cot \theta_s$$

$$B_3 = P_2/\bar{P} + (1/2)\,\bar{u}^2/\bar{a}^2 - (\xi/2\bar{P}) \cot \theta_s$$

$\xi/\bar{P} = 1.2089$ FROM APPENDIX 2, TABLE 17.

$P_0/\bar{P} = -3.44$ " " "

$P_2/\bar{P} = 1.839$ " " "

SO $\quad B_1 = -1.2089 \qquad B_2 = -.4070 \qquad B_3 = 1.3463$

NOW $\quad S - \bar{S} = -\alpha S_1 + \alpha^2 (S_2 + S_3)$

$$(S-\bar{S})/\gamma c_v = -\alpha\left[(A_1/\gamma) - B_1\right] + \alpha^2\left[-(A_1^2/2\gamma) + (B_1^2/2) + (A_2 + A_3)/\gamma - (B_2 + B_3)\right]$$

$$(S-\bar{S})/\gamma c_v = .0069037$$

$$e^{\frac{-(S-\bar{S})}{\gamma c_v}} = .99312$$

APPENDIX 2

TABLE 13. MACH NUMBER STARTING VALUES $X/\ell = 0$, $\alpha = 10°$

1	2	3	4	5	6	7	8	9
ψ	$(P/\bar{P})$	$(P/\bar{P})^{1/\gamma}$	$\rho/\bar{\rho}$ = .98312 (3)	$\bar{a}^2/a^2$ (4)/(2)	$(\bar{a}^2/a^2)(c^2/\bar{a}^2)$ = 7.4822 (5)	M^2 (6) $-2/(\gamma-1)$	$M = M_N$	* $(P/P_t)_N$ TABLE 18
0	.7549	.8186	.8130	1.0070	8.0581	3.1198	1.7663	.1833
30	.7654	.8267	.8210	1.0727	8.0260	3.0877	1.7572	.1858
60	.8162	.8654	.8594	1.0530	7.8789	2.9406	1.7148	.1981
90	.9376	.9552	.9486	1.0117	7.5701	2.6318	1.6223	.2277
120	1.1192	1.0835	1.0760	.9614	7.1934	2.2551	1.5017	.2716
150	1.2903	1.1990	1.1907	.9228	6.9044	1.9661	1.4022	.3134
180	1.3610	1.2453	1.2367	.9087	6.7991	1.8608	1.3641	.3308

D. SINE OF FLOW DEFLECTION ANGLE, δ, ALONG $\psi = 180°$ MERIDIAN

$$\sin \delta = \sin \theta \cos \alpha - \cos \psi \cos \theta \sin \alpha$$

TABLE 14. VALUES OF SINE δ, $\alpha = 10°$

1	2	3	4	5	6	7
X/ℓ	θ	$\sin\theta$	$\cos\theta$	$\sin\theta\cos\alpha$	$\cos\psi\cos\theta\sin\alpha$	$\sin\delta$
0	18.925	.32433	.94594	.31940	−.16426	.48366
.1	16.972	.29190	.95645	.28747	−.16609	.45356
.2	15.038	.25946	.96575	.25552	−.16770	.42322
.3	13.122	.22703	.97388	.22358	−.16911	.39269
.4	11.221	.19460	.98088	.19164	−.17033	.36197
.5	9.333	.16217	.98676	.15971	−.17135	.33106
.6	7.454	.12973	.99155	.12776	−.17218	.29994
.7	5.584	.09730	.99525	.09582	−.17283	.26865
.8	3.719	.06487	.99789	.06388	−.17328	.23716
.9	1.859	.03243	.99947	.03194	−.17356	.20550
1.0	0	0	1.00000	0	−.17365	.17365

*VALUES OF $(P/P_t)_N$ ARE OBTAINED FROM TABLE 18 USING THE APPROPRIATE VALUES OF M_N IN COLUMN 8, TABLE 13.

APPENDIX 2

E. PRESSURE COEFFICIENT AND LOCAL MACH NUMBER DISTRIBUTIONS ALONG $\psi = 180°$ MERIDIAN (SEE FIGURE 24)

THE SAME PROCEDURE OUTLINED FOR THE EXAMPLE OF APPENDIX I HAS BEEN USED IN THE FOLLOWING EXAMPLE TO OBTAIN THE PRESSURE AND LOCAL MACH NUMBER DISTRIBUTIONS ON THE NOSE AND CYLINDRICAL AFTERBODY; THE RESULTS HAVE BEEN SUMMARIZED IN TABLES 15 AND 16.

CONDITIONS AT NOSE VERTEX

$M_N = 1.364$ — COLUMN 9, TABLE 13

$(P/P_t)_N = .3305$ — " 9, " "

$C_{P_N} = .5366$ — " 9, " 12

$C_{P_{MAX}} = 2.2938$ EQ. 7

$C_P = 2.7041\ (P/P_t) - .3571$ EQ. 3

TABLE 15. PRESSURE COEFFICIENT DISTRIBUTION AND MACH NUMBER ALONG $\psi = 180°$ MERIDIAN, $\alpha = 10°$

1	2	3	4	5	6	7	8	9
X/ℓ	$\sin^2\delta$	C_P GN EQ. 6	C_P SEM EQ. 3	θ	$\Delta\theta$	ν	P/P_t	M TABLE 16
0	.23393	.5366	–	–	–	–	.3305	1.364
.1	.20572	.4719	–	–	–	–	.3066	1.417
.2	.17912	.4109	–	–	–	–	.2840	1.471
.3	.15421	.3537	–	–	–	–	.2629	1.524
.4	.13102	.3006	–	–	–	–	.2432	1.578
.5	.10960	.2514	–	–	–	–	.2250	1.630
.6	.08996	.2064	–	–	–	–	.2084	1.681
$.7_m$	.07217	.1655	.1655	5.584	–	18.719	.1933	1.731
.8	–	–	.1169	3.719	1.865	20.584	.1753	1.795
.9	–	–	.0720	1.859	1.860	22.444	.1587	1.860
1.0	–	–	.0309	0	1.859	24.303	.1436	1.925

GN = GENERALIZED NEWTONIAN

SEM = SHOCK EXPANSION METHOD

θ = BODY SURFACE ANGLE

$.7_m$ = MATCHING POINT OF GENERALIZED NEWTONIAN AND SHOCK EXPANSION METHOD

M = M CORRESPONDING TO P/P_t FROM PRANDTL-MEYER TABLES

ν = PRANDTL-MEYER FLOW DEFLECTION ANGLE CORRESPONDING TO M

APPENDIX 2

E. CYLINDRICAL AFTERBODY PRESSURE COEFFICIENT DISTRIBUTION ALONG $\psi = 180°$ MERIDIAN

USING EQ. 5b

$$C_p = C_{p(x/\ell=1)}\, e^{-\frac{\Delta x/\ell}{K}}$$

VALUES OF C_p ON THE CYLINDRICAL AFTERBODY ARE CALCULATED AS SHOWN IN TABLE 16.

$C_{p(x/\ell=1)} = .0309$, FROM COLUMN 4, TABLE 15.

TABLE 16. PRESSURE COEFFICIENT DISTRIBUTION ON CYLINDRICAL AFTERBODY , $\alpha = 10°$

1	2	3	4
x/ℓ	$\Delta x/\ell$	$e^{-\frac{②}{K}}$	$C_p = .0309$ ③
1.0	0	1.0000	.0309
1.1	.1	.8607	.0266
1.2	.2	.7408	.0229
1.3	.3	.6376	.0197
1.4	.4	.5488	.0170
1.5	.5	.4724	.0146

TABLE 17 Parameters Given in MIT Cone Tables

a. $\theta_s = 5°$

M	$\bar{u}/c$	$\bar{a}^2/c^2$	p_s/p_w	p_w/p_1	$\eta/\bar{p}$	$\xi/\bar{\rho}$	$p_e/\bar{p}$	$p_2/\bar{p}$	$\rho_e/\bar{\rho}$	$\rho_2/\bar{\rho}$
1.5058	.55000	.14124	1.0601	1.0028	.5070	.3609	- 5.603	4.190	- 4.001	2.969
1.7153	.60000	.12960	1.0716	1.0041	.6478	.4611	- 7.109	5.275	- 5.081	3.733
1.9580	.65000	.11694	1.0857	1.0062	.8281	.5894	- 9.000	6.65	- 6.44	4.70
2.2473	.70000	.10328	1.1028	1.0101	1.0649	.7579	-11.43	8.33	- 8.19	5.87
2.6064	.75000	.08859	1.1240	1.0171	1.3885	.9883	-14.64	10.61	-10.52	7.45
3.0774	.60000	.07290	1.1501	1.0311	1.8555	1.3206	-19.14	13.69	-13.80	9.57
3.7495	.85000	.05619	1.1812	1.0620	2.5892	1.8424	-25.83	18.16	-18.74	12.58
4.8602	.90000	.03848	1.2124	1.1435	3.9201	2.7859	-37.51	25.22	-27.62	17.18
7.4152	.95000	.01974	1.2167	1.4646	7.148	5.001	-64.96	37.29	-51.51	24.30
10.146	.97000	.01197	1.1860	1.9813	10.282	6.893	-95.28	41.12	-82.64	23.31

b. $\theta_s = 7.5°$

M	$\bar{u}/c$	$\bar{a}^2/c^2$	p_s/p_w	p_w/p_1	$\eta/\bar{p}$	$\xi/\bar{\rho}$	$p_e/\bar{p}$	$p_2/\bar{p}$	$\rho_e/\bar{\rho}$	$\rho_2/\bar{\rho}$
1.5462	.55000	.14124	1.1111	1.0147	.7377	.5251	- 5.319	3.926	- 3.807	2.770
1.7610	.60000	.12960	1.1289	1.0214	.9320	.6633	- 6.586	4.829	- 4.733	3.392
2.0108	.65000	.11694	1.1487	1.0324	1.1768	.8376	- 8.148	5.911	- 5.873	4.138
2.3105	.70000	.10328	1.1699	1.0508	1.4928	1.0624	-10.11	7.33	- 7.32	5.10
2.6847	.75000	.08859	1.1914	1.0822	1.9154	1.3627	-12.69	8.90	- 9.25	6.15
3.1795	.80000	.07290	1.2105	1.1386	2.5085	1.7830	-16.11	10.95	-11.85	7.49
3.8946	.85000	.05619	1.2216	1.2489	3.4039	2.4106	-21.15	13.70	-15.87	9.15
5.1033	.90000	.03848	1.2143	1.5043	4.9174	3.4312	-29.88	16.97	-23.72	10.86
8.0589	.95000	.01974	1.1638	2.4450	8.0430	5.1596	-52.15	17.91	-47.78	8.64

TABLE 17 (continued) Parameters Given in MIT Cone Tables

c. $\theta_s = 10°$

M	$\bar{u}/c$	$\bar{a}^2/c^2$	p_s/p_w	p_w/p_1	$\eta/\bar{p}$	$\xi/\bar{\rho}$	$p_o/\bar{p}$	$p_2/\bar{p}$	$\rho_o/\bar{\rho}$	$\rho_2/\bar{\rho}$
1.4028	.50000	.15188	1.1415	1.0338	.7562	.5382	- 4.031	2.995	- 2.898	2.103
1.5957	.55000	.14124	1.1594	1.0458	.9499	.6760	- 4.962	3.633	- 3.579	2.539
1.8165	.60000	.12960	1.1778	1.0655	1.1864	.8442	- 6.074	4.368	- 4.399	3.038
2.0750	.65000	.11694	1.1952	1.0962	1.4798	1.0527	- 7.406	5.209	- 5.390	3.594
2.3869	.70000	.10328	1.2099	1.1443	1.8515	1.3159	- 9.019	6.192	- 6.624	4.235
2.7794	.75000	.08859	1.2195	1.2210	2.3365	1.16567	-11.091	7.328	- 8.267	4.943
3.3041	.80000	.07290	1.2208	1.3501	2.9950	2.1107	-13.87	8.610	-10.67	5.73

d. $\theta_s = 12.5°$

M	$\bar{u}/c$	$\bar{a}^2/c^2$	p_s/p_w	p_w/p_1	$\eta/\bar{p}$	$\xi/\bar{\rho}$	$p_o/\bar{p}$	$p_2/\bar{p}$	$\rho_o/\bar{\rho}$	$\rho_2/\bar{\rho}$
1.4552	.50000	.15188	1.1787	1.0784	.9204	.6549	- 3.826	2.814	- 2.769	1.961
1.6530	.55000	.14124	1.1944	1.1054	1.1429	.8129	- 4.644	3.334	- 3.379	2.308
1.8810	.60000	.12960	1.2076	1.1469	1.4112	1.0029	- 5.589	3.903	- 4.099	2.680
2.1496	.65000	.11694	1.2169	1.2086	1.7380	1.2330	- 6.716	4.538	- 4.980	3.079
2.4760	.70000	.10327	1.2203	1.3009	2.1432	1.5144	- 8.087	5.228	- 6.111	3.494
2.8907	.75000	.08859	1.2164	1.4432	2.6566	1.8619	- 9.851	5.934	- 7.677	3.876
4.3002	.85000	.05619	1.1785	2.1130	4.2281	2.8014	-16.06	6.82	-14.14	3.91

TABLE 17 (concluded) Parameters Given in MIT Cone Tables

e. $\theta_s = 15°$

M	$\bar{u}/c$	$\bar{a}^2/c^2$	P_s/P_w	P_w/P_1	$\eta/\bar{p}$	$\xi/\bar{\rho}$	$P_o/\bar{p}$	$P_2/\bar{p}$	$\rho_o/\bar{\rho}$	$\rho_2/\bar{\rho}$
1.5144	.50000	.15188	1.2027	1.1508	1.0725	.7622	- 3.620	2.622	-2.639	1.810
1.7178	.55000	.14124	1.2126	1.1996	1.3164	.9343	- 4.337	3.041	-3.208	2.110
1.9541	.60000	.12960	1.2180	1.2716	1.6055	1.1362	- 5.07	3.37	-3.80	2.30
2.2345	.65000	.11694	1.2178	1.3755	1.9510	1.3734	- 6.143	3.903	-4.735	2.628
2.5787	.70000	.10327	1.2112	1.5276	2.3682	1.6505	- 7.357	4.332	-5.85	2.85
3.6345	.80000	.07290	1.1766	2.1462	3.5151	2.3224	-11.19	4.80	-9.90	2.80

f. $\theta_s = 20°$

M	$\bar{u}/c$	$\bar{a}^2/c^2$	P_s/P_w	P_w/P_1	$\eta/\bar{p}$	$\xi/\bar{\rho}$	$P_o/\bar{p}$	$P_2/\bar{p}$	$\rho_o/\bar{\rho}$	$\rho_2/\bar{\rho}$
1.4672	.45000	.16149	1.2100	1.3197	1.1054	.7811	- 2.715	2.006	-2.046	1.388
1.6531	.50000	.15188	1.2124	1.3959	1.3347	.9391	- 3.244	2.227	-2.491	1.528
1.8714	.55000	.14124	1.2093	1.5106	1.5978	1.1158	- 3.84	2.45	-3.02	1.66
2.1297	.60000	.12960	1.2012	1.6735	1.8979	1.3090	- 4.51	2.63	-3.68	1.76
2.4431	.65000	.11694	1.1884	1.9053	2.2395	1.5142	- 5.35	2.78	-4.58	1.82
2.8387	.70000	.10328	1.1713	2.2476	2.6291	1.7219	- 6.42	2.84	-5.86	1.85

g. $\theta_s = 25°$

M	$\bar{u}/c$	$\bar{a}^2/c^2$	P_s/P_w	P_w/P_1	$\eta/\bar{p}$	$\xi/\bar{\rho}$	$P_o/\bar{p}$	$P_2/\bar{p}$	$\rho_o/\bar{\rho}$	$\rho_2/\bar{\rho}$
1.4608	.40000	.17010	1.1975	1.5708	1.1014	.7679	- 2.060	1.607	-1.635	1.132
1.6236	.45000	.16149	1.1973	1.6584	1.3021	.9010	- 2.502	1.728	-2.04	1.22
1.8248	.50000	.15187	1.1910	1.8113	1.5305	1.0453	- 2.961	1.818	-2.50	1.28
2.0665	.55000	.14124	1.1802	2.0348	1.7843	1.1942	- 3.45	1.85	-3.05	1.30

APPENDIX 3

TABLE 18. PRANDTL-MEYER FLOW PARAMETERS

M	p/p_t	ν	M	p/p_t	ν
1.00	0.5283	0	6.00	.6334 -3	84.955
1.10	.4684	1.336	6.10	.5721 -3	85.635
1.20	.4124	3.558	6.20	.5173 -3	86.295
1.30	.3609	6.170	6.30	.4684 -3	86.937
1.40	.3142	8.987	6.40	.4247 -3	87.561
1.50	.2724	11.905	6.50	.3855 -3	88.169
1.60	.2353	14.861	6.60	.3503 -3	88.760
1.70	.2026	17.810	6.70	.3187 -3	89.335
1.80	.1740	20.725	6.80	.2902 -3	89.895
1.90	.1492	23.586	6.90	.2646 -3	90.441
2.00	.1278	26.380	7.00	.2416 -3	90.973
2.10	.1094	29.097	7.10	.2207 -3	91.492
2.20	#.9352 -1	31.732	7.20	.2019 -3	91.997
2.30	.7997 -1	34.283	7.30	.1848 -3	92.490
2.40	.6840 -1	36.746	7.40	.1694 -3	92.971
2.50	.5853 -1	39.124	7.50	.1554 -3	93.440
2.60	.5012 -1	41.415	7.60	.1427 -3	93.898
2.70	.4295 -1	43.621	7.70	.1312 -3	94.345
2.80	.3685 -1	45.746	7.80	.1207 -3	94.782
2.90	.3165 -1	47.790	7.90	.1111 -3	95.208
3.00	.2722 -1	49.757	8.00	.1024 -3	95.625
3.10	.2345 -1	51.650	8.10	.9449 -4	96.032
3.20	.2023 -1	53.470	8.20	.8723 -4	96.430
3.30	.1748 -1	55.222	8.30	.8060 -4	96.820
3.40	.1512 -1	56.907	8.40	.7454 -4	97.200
3.50	.1311 -1	58.530	8.50	.6898 -4	97.573
3.60	.1138 -1	60.091	8.60	.6390 -4	97.937
3.70	.9903 -2	61.595	8.70	.5923 -4	98.293
3.80	.8629 -2	63.044	8.80	.5494 -4	98.642
3.90	.7532 -2	64.440	8.90	.5101 -4	98.984
4.00	.6586 -2	65.785	9.00	.4739 -4	99.319
4.10	.5769 -2	67.082	9.10	.4405 -4	99.646
4.20	.5062 -2	68.333	9.20	.4099 -4	99.967
4.30	.4449 -2	69.541	9.30	.3816 -4	100.282
4.40	.3918 -2	70.706	9.40	.3555 -4	100.590
4.50	.3455 -2	71.832	9.50	.3314 -4	100.892
4.60	.3053 -2	72.919	9.60	.3092 -4	101.188
4.70	.2701 -2	73.970	9.70	.2886 -4	101.479
4.80	.2394 -2	74.986	9.80	.2696 -4	101.763
4.90	.2126 -2	75.969	9.90	.2520 -4	102.043
5.00	.1890 -2	76.920	10.00	.2356 -4	102.32
5.10	.1683 -2	77.841	10.10	.2205 -4	102.59
5.20	.1501 -2	78.733	10.20	.2065 -4	102.85
5.30	.1341 -2	79.597	10.30	.1934 -4	103.11
5.40	.1200 -2	80.434	10.40	.1813 -4	103.36
5.50	.1075 -2	81.245	10.50	.1701 -4	103.61
5.60	.9643 -3	82.032	10.60	.1596 -4	103.86
5.70	.8663 -3	82.795	10.70	.1499 -4	104.10
5.80	.7794 -3	83.537	10.80	.1408 -4	104.33
5.90	.7021 -3	84.257	10.90	.1324 -4	104.57

$.9352 \times 10^{-1}$ = .9352 -1

TABLE 18. (Continued)

M	p/p_t	ν
11.00	.1245 -4	104.80
11.10	.1171 -4	105.02
11.20	.1103 -4	105.24
11.30	.1039 -4	105.46
11.40	.9788 -5	105.67
11.50	.9228 -5	105.88
11.60	.8704 -5	106.09
11.70	.8215 -5	106.29
11.80	.7755 -5	106.49
11.90	.7325 -5	106.69
12.00	.6922 -5	106.88
12.10	.6544 -5	107.07
12.20	.6189 -5	107.26
12.30	.5857 -5	107.44
12.40	.5544 -5	107.62
12.50	.5250 -5	107.80
12.60	.4973 -5	107.98
12.70	.4714 -5	108.15
12.80	.4469 -5	108.32
12.90	.4239 -5	108.49
13.00	.4023 -5	108.65
13.10	.3818 -5	108.82
13.20	.3626 -5	108.97
13.30	.3444 -5	109.13
13.40	.3273 -5	109.29
13.50	.3111 -5	109.44
13.60	.2958 -5	109.59
13.70	.2814 -5	109.75
13.80	.2678 -5	109.89
13.90	.2550 -5	110.04
14.00	.2428 -5	110.18
14.10	.2313 -5	110.32
14.20	.2204 -5	110.46
14.30	.2100 -5	110.60
14.40	.2003 -5	110.74
14.50	.1910 -5	110.87
14.60	.1823 -5	111.00
14.70	.1739 -5	111.13
14.80	.1660 -5	111.26
14.90	.1586 -5	111.38
15.00	.1515 -5	111.51
15.10	.1447 -5	111.63
15.20	.1383 -5	111.76
15.30	.1323 -5	111.88
15.40	.1265 -5	112.00
15.50	.1210 -5	112.11
15.60	.1158 -5	112.23
15.70	.1108 -5	112.34
15.80	.1061 -5	112.45
15.90	.1016 -5	112.57
16.00	.9731 -6	112.68
16.10	.9323 -6	112.79
16.20	.8936 -6	112.89
16.30	.8565 -6	113.00
16.40	.8213 -6	113.11
16.50	.7876 -6	113.21
16.60	.7556 -6	113.31
16.70	.7250 -6	113.41
16.80	.6959 -6	113.51
16.90	.6680 -6	113.61
17.00	.6415 -6	113.71
17.10	.6161 -6	113.81
17.20	.5918 -6	113.90
17.30	.5687 -6	114.00
17.40	.5465 -6	114.09
17.50	.5254 -6	114.18
17.60	.5052 -6	114.27
17.70	.4859 -6	114.36
17.80	.4674 -6	114.45
17.90	.4496 -6	114.54
18.00	.4328 -6	114.63
18.10	.4165 -6	114.72
18.20	.4010 -6	114.80
18.30	.3861 -6	114.89
18.40	.3718 -6	114.97
18.50	.3582 -6	115.05
18.60	.3452 -6	115.13
18.70	.3326 -6	115.21
18.80	.3206 -6	115.29
18.90	.3090 -6	115.38
19.00	.2980 -6	115.45
19.10	.2874 -6	115.53
19.20	.2772 -6	115.61
19.30	.2674 -6	115.68
19.40	.2581 -6	115.76
19.50	.2491 -6	115.83
19.60	.2404 -6	115.91
19.70	.2321 -6	115.98
19.80	.2241 -6	116.05
19.90	.2165 -6	116.13
20.00	.2091 -6	116.20

REFERENCES

1. Busemann, A., "Fluid and Gas Dynamics", Handbook of Natural Sciences, 2nd Edition (Gustav Fischer, Jena), 1933, pp. 275-277.

2. Lees, Lester, "Hypersonic Flow", Proceedings IAS-RAeS Fifth International Aeronautical Conference, Los Angeles, Calif., June 20-23, 1955.

3. Love, E. S., "Generalized-Newtonian Theory", Journal of the Aero/Space Sciences, pp. 314 and 315, May, 1959.

4. Rossow, Vernon J., "Applicability of the Hypersonic Similarity Rule to Pressure Distributions Which Include the Effects of Rotation for Bodies of Revolution at Zero Angle of Attack", NACA Technical Note 2399, June, 1951.

5. Savin, Raymond C., "Application of the Generalized Shock-Expansion Method to Inclined Bodies of Revolution Traveling at High Supersonic Airspeeds", NACA Technical Note 3349, April, 1955.

6. Ehret, Dorris M., "Accuracy of Approximate Methods for Predicting Pressures on Pointed Nonlifting Bodies of Revolution in Supersonic Flow", NACA Technical Note 2764, August, 1952.

7. Lighthill, M. J., "Supersonic Flow Past Slender Pointed Bodies of Revolution at Yaw", Quart. Jour. Mech. and Appl. Math., Vol. I, Pt. I, March, 1948, pp. 76-89.

8. Van Dyke, M. D., "First- and Second-Order Theory of Supersonic Flow Past Bodies of Revolution", Jour. Aeronaut. Sci., Vol. 18, March 1951, pp. 161-178.

9. Van Dyke, M. D., "A Study of Second-Order Supersonic Flow Theory", NACA Report 1081, 1952.

10. Laitone, E. V., "The Linearized Subsonic and Supersonic Flow About Inclined Slender Bodies of Revolution", Jour. Aeronaut. Sci., Vol. 14, November, 1947, pp. 631-642.

11. Broderick, J. B., "Supersonic Flow Round Pointed Bodies of Revolution", Quart. Jour. Mech. and Appl. Math., Vol. II, Pt. I, March, 1949, pp. 98-120.

12. Fenter, F. W., "An Approximate Method for the Calculation of the Aerodynamic Characteristics of Ogive-Cylinders Near Zero Lift", DRL Report 390, Defense Research Laboratory, University of Texas, January, 1957.

13. Ames Research Staff, "Equations, Tables, and Charts for Compressible Flow", NACA Report 1135, 1953.

14. Jorgensen, L. H., "Correlation by the Hypersonic Similarity Rule of Pressure Distributions and Wave Drags for Minimum-Drag Nose Shapes at Zero Angle of Attack", NACA Research Memorandum A53F12, August 31, 1953.

15. JHU/APL Sponsored Wind Tunnel Tests Conducted at the General Dynamics/Convair, San Diego, Calif., High Speed Wind Tunnel Facility, HST 011 Series, July, 1960.

16. Applied Physics Laboratory, The Johns Hopkins University, "Supersonic Inlets", Handbook of Supersonic Aerodynamics, NAVWEPS Report 1488, Vol. 6, Sec. 17, 1964.

17. Connors, J. F. and Meyer, R. C., "Design Criteria for Axisymmetric and Two-Dimensional Supersonic Inlets and Exits", NACA Technical Note 3589, January, 1956.

18. Vaglio-Laurin, R. and Trella, M., "A Study of Flow Fields About Some Typical Blunt-Nosed Slender Bodies", Aerospace Engineering, pp. 20, 21, 80-88, August, 1961.

19. Kendall, J. M., Jr., "Experiments on Supersonic Blunt-Body Flows", Progress Report No. 20-372, California Institute of Technology, February 27, 1959.

20. Perkins, E. W., Jorgensen, L. H., and Sommer, S. C., "Investigation of the Drag of Various Axially Symmetric Nose Shapes of Fineness Ratio 3 for Mach Numbers from 1.24 to 7.4", NACA Report 1386, 1958.

21. Sims, J. L., "Tables for Supersonic Flow Around Right Circular Cones at Small Angle of Attack", NASA SP-3007, 1964.

22. Sims, J. L., "Tables for Supersonic Flow Around Right Circular Cones at Zero Angle of Attack", NASA SP-3004, 1964.

23. Stone, A. H., "On Supersonic Flow Past a Slightly Yawing Cone", Jour. Math. and Phys., Vol. 27, 1948, pp. 67-81.

24. Pai, Shih-I, "One-Dimensional Flow of an Inviscid Compressible Fluid", Introduction to the Theory of Compressible Flow, Chap. III, 1959.

25. Perkins, E. W. and Jorgensen, L. H., "Comparison of Experimental and Theoretical Normal-Force Distributions (Including Reynolds Number Effects) on an Ogive-Cylinder Body at Mach Number 1.98", NACA Technical Note 3716, May, 1956.

26. Kopal, Zdenek, "Tables of Supersonic Flow Around Cones", Massachusetts Institute of Technology, Tech. Rep. No. 1, 1947.

27. Kopal, Zdenek, "Tables of Supersonic Flow Around Yawing Cones", Massachusetts Institute of Technology, Tech. Rep. No. 3, 1947.

28. Kopal, Zdenek, "Tables of Supersonic Flow Around Cones of Large Yaw", Massachusetts Institute of Technology, Tech. Rep. No. 5, 1949.

ACKNOWLEDGMENT

The author would like to express his gratitude to Dr. Shih-I Pai for his fine suggestions and guidance in the initial preparation of this report which was submitted to the University of Maryland as a thesis in partial fulfillment of the requirements for the degree of Master of Science. My appreciation is also extended to Mr. E. T. Marley for his technical assistance in reviewing the current manuscript, to Mr. Robert C. Sharbaugh for preparing the illustrations, and to Mrs. Helen F. Tate for typing this report.

INITIAL DISTRIBUTION EXTERNAL TO THE APPLIED PHYSICS LABORATORY*

The work reported in TG-752 was done under Bureau of Naval Weapons Contract NOw-62-0604-c (Task Assignment A31A) supported in part by BuWeps (RMGA).

ORGANIZATION	LOCATION	ATTENTION	No. of Copies
DEPARTMENT OF DEFENSE			
DDC	Alexandria, Va.		20
Department of the Navy			
Department Offices			
Chief, BuWeps	Washington, D. C.	DLI-31	2
		RAAD-34	1
		RMGA-811	1
		RR-25	1
		RRRE-3	1
		RRRE-41	1
BuWepsRep	Silver Spring, Md.		1
Laboratories			
NOL	Corona, Calif.	A. C. Sevy	1
NOL	White Oak, Md.	R. E. Wilson	1
		K. R. Enkenhus	1
		S. M. Hastings	1
NWL	Dahlgren, Va.	P. Daniels	1
		K. A. Larsen	1
Facilities			
David Taylor Model Basin	Washington, D. C.	Dr. S. de los Santos	1
		R. M. Hartley	1
		R. Taylor	1
NOTS	China Lake, Calif.	W. R. Haseltine	1
		R. E. Meeker	1
		E. F. Winkel	1
NMC	Pt. Mugu, Calif.	R. H. Peterson	1
		J. W. Rom	1
Department of the Air Force			
Aero Research Lab.	WPAFB, Dayton, Ohio	Librarian	1
Office of Scientific Research	Washington, D. C.	Dr. M. M. Slawsky	1
U. S. GOVERNMENT AGENCIES			
Library of Congress			
Library of Congress	Washington, D. C.	Librarian	1
National Aero. & Space Adm.			
Ames Research Center	Moffett Field, Calif.	G. T. Chapman	1
Division of Research Information	Washington, D. C.	Librarian	1
Goddard Space Flight Center	Greenbelt, Maryland	Librarian	1
Langley Research Center	Langley Field, Va.	Librarian	1
Lewis Research Center	Cleveland, Ohio	Librarian	1
National Bureau of Standards			
Applied Mathematics Division	Washington, D. C.	Librarian	1
UNIVERSITIES			
California Institute of Tech. (Aero. Dept.)	Pasadena, Calif.	Librarian	1
California Institute of Tech. (Jet Propulsion Lab.)	Pasadena, Calif.	Librarian	1
Cornell University (Dept. Aero Engineering)	Ithaca, N. Y.	Librarian	1
Cornell University (Aero. Lab., Inc.)	Buffalo, N. Y.	Librarian	1
MIT (Dept. Mech. Engineering)	Cambridge, Mass.	Librarian	1
MIT (Naval Supersonic Lab.)	Cambridge, Mass.	Librarian	1
Polytechnic Institute of Brooklyn (Aero. Lab.)	Freeport, N. Y.	Librarian	1

*Initial distribution of this document within the Applied Physics Laboratory has been made in accordance with a list on file in the APL Technical Reports Group.

INITIAL DISTRIBUTION EXTERNAL TO THE APPLIED PHYSICS LABORATORY

ORGANIZATION	LOCATION	ATTENTION	No. of Copies
Polytechnic Institute of Brooklyn	Brooklyn, N. Y.	Librarian	1
Princeton University (Aero. Engineering Dept.)	Princeton, N. J.	Librarian	1
State University of New York (Dept. Thermal Sciences)	Long Island, N. Y.	Librarian	1
University of California (Dept. Engineering)	Los Angeles, Calif.	Librarian	1
University of California (Engineering Res. Projects)	Berkeley, Calif.	Librarian	1
University of Illinois (Aero. Engineering Dept.)	Urbana, Ill.	Librarian	1
University of Maryland (Dept. Aero. Engineering)	College Park, Md.	Prof. A. W. Sherwood	1
University of Maryland (Institute Fluid Dynamics)	College Park, Md.	Prof. Shih-I Pai	1
		Librarian	1
University of Michigan (Aero. Engineering Lab.)	Ann Arbor, Mich.	J. L. Amick	1
University of Minnesota (Dept. Mech. Engineering)	Minneapolis, Minn.	Librarian	1
University of Missouri (Dept. Mech. Engineering)	Columbia, Mo.	P. H. Miller	1
University of Notre Dame (School of Engineering)	Notre Dame, Ind.	Librarian	1
University of Texas (Aero. Engineering Dept.)	Austin, Texas	Librarian	1
University of Texas (Defense Research Lab.)	Austin, Texas	M. J. Thompson	1
		J. C. Westkaemper	1
CONTRACTORS			
Aerospace Corp.	San Bernardino, Calif.	K. L. Henrie	1
AVCO Research Lab.	Everett, Mass.	Librarian	1
Douglas Aircraft Co., Inc.	Santa Monica, Calif.	Librarian	1
General Dynamics	Fort Worth, Texas	Librarian	1
General Dynamics	Pomona, Calif.	C. C. Durand	1
		Librarian	1
General Dynamics	San Diego, Calif.	W. T. MacCarthy	1
		W. H. Lowe	1
General Electric	Philadelphia, Pa.	Librarian	1
Lockheed Missiles & Space Co.	Sunnyvale, Calif.	H. M. Bowers	1
		C. H. Kauffman	1
		Librarian	1
LTV Research Center	Dallas, Texas	F. W. Fenter	1
		J. Harkness	1
McDonnell Aircraft Corp.	St. Louis, Mo.	F. D. McVey	1
		R. C. Brown	1
North American Aviation, Inc.	Columbus, Ohio	P. H. Davison	1
		E. S. Schum	1
		J. E. Shuter	1
Space General Corp.	El Monte, Calif.	W. Hatalsky	1
Space General Corp.	Glendale, Calif.	Dr. R. F. Brodsky	1
Space Technology Lab.	Redondo Beach, Calif.	H. P. Liepman	1
The Bendix Corp.	Ann Arbor, Mich.	P. T. Pilon	1
The Bendix Corp.	Mishawaka, Ind.	Librarian	1
The Boeing Co.	Seattle, Wash.	D. S. Miller	1

UNCLASSIFIED

Security Classification

DOCUMENT CONTROL DATA - R&D

(Security classification of title, body of abstract and indexing annotation must be entered when the overall report is classified)

1. ORIGINATING ACTIVITY (Corporate author)	2a. REPORT SECURITY CLASSIFICATION
The Johns Hopkins University Applied Physics Laboratory 8621 Georgia Avenue Silver Spring, Maryland 20910	UNCLASSIFIED
	2b. GROUP None

3. REPORT TITLE

An Engineering Method for the Rapid Calculation of Supersonic-Hypersonic Pressure Distributions on Lifting and Non-lifting Pointed Bodies of Revolution and Several Special Cases of Blunt Nosed Bodies

4. DESCRIPTIVE NOTES (Type of report and inclusive dates)

Final

5. AUTHOR(S) (Last name, first name, initial)

Vendemia, R. J., Jr.

6. REPORT DATE	7a. TOTAL NO. OF PAGES	7b. NO. OF REFS
December 1965	66	28

8a. CONTRACT OR GRANT NO.	9a. ORIGINATOR'S REPORT NUMBER(S)
NOw 62-0604-c	TG-752
b. PROJECT NO. Task A31	
c.	9b. OTHER REPORT NO(S) (Any other numbers that may be assigned this report)
d.	None

10. AVAILABILITY/LIMITATION NOTICES

Distribution of this document is unlimited.

11. SUPPLEMENTARY NOTES	12. SPONSORING MILITARY ACTIVITY
None	Bureau of Naval Weapons RMGA Washington, D. C.

13. ABSTRACT This report prescribes a method for calculating pressure coefficients and local Mach numbers for lifting and non-lifting pointed bodies of revolution and for several special cases of blunt-nosed bodies. The method, which utilizes hybrid tandem solutions involving Generalized Newtonian and Shock-Expansion theories, provides accurate results for a variety of nose shapes and fineness ratios over a range of supersonic/hypersonic Mach numbers. The numerical simplicity of the method, which makes it readily applicable for quick hand-calculational procedures, was the prime factor in its selection and publication; the few existing methods which yield accurate results over a comparable range of application, such as the method of characteristics, are not used extensively because of the lengthy numerical calculations involved.

The present method has been compared with exact solutions, various pertinent theories, and experimental data where available and the overall agreement of the results is quite favorable. The investigation for lifting bodies indicates the present method is applicable for bodies of revolution at angles of attack up to about ten degrees.

This report presents numerical examples showing stepwise calculational procedures for obtaining pressure coefficient and local Mach number distributions along the meridians of a body of revolution at angle of attack. In order to make the report immediately useful to the engineer desiring such information, all of the necessary tables and look-up parameters are included in the appendices.

UNCLASSIFIED

Security Classification

14. KEY WORDS	LINK A ROLE	LINK A WT	LINK B ROLE	LINK B WT	LINK C ROLE	LINK C WT
AERODYNAMIC						
CYLINDRICAL AFTERBODY						
ENGINEERING METHOD						
HEMISPHERES						
HYPERSONIC						
ISENTROPIC SPIKES						
LIFTING BODIES OF REVOLUTION						
NON-LIFTING BODIES OF REVOLUTION						
POWER SERIES NOSE SHAPES						
PRESSURE DISTRIBUTIONS						
SUPERSONIC						
TANGENT OGIVE NOSE SHAPES						
VON KARMAN NOSE SHAPES						
OGIVAL NOSE SHAPES						
LOW DRAG NOSE SHAPES						

INSTRUCTIONS

1. **ORIGINATING ACTIVITY:** Enter the name and address of the contractor, subcontractor, grantee, Department of Defense activity or other organization *(corporate author)* issuing the report.

2a. **REPORT SECURITY CLASSIFICATION:** Enter the overall security classification of the report. Indicate whether "Restricted Data" is included. Marking is to be in accordance with appropriate security regulations.

2b. **GROUP:** Automatic downgrading is specified in DoD Directive 5200.10 and Armed Forces Industrial Manual. Enter the group number. Also, when applicable, show that optional markings have been used for Group 3 and Group 4 as authorized.

3. **REPORT TITLE:** Enter the complete report title in all capital letters. Titles in all cases should be unclassified. If a meaningful title cannot be selected without classification, show title classification in all capitals in parenthesis immediately following the title.

4. **DESCRIPTIVE NOTES:** If appropriate, enter the type of report, e.g., interim, progress, summary, annual, or final. Give the inclusive dates when a specific reporting period is covered.

5. **AUTHOR(S):** Enter the name(s) of author(s) as shown on or in the report. Enter last name, first name, middle initial. If military, show rank and branch of service. The name of the principal author is an absolute minimum requirement.

6. **REPORT DATE:** Enter the date of the report as day, month, year; or month, year. If more than one date appears on the report, use date of publication.

7a. **TOTAL NUMBER OF PAGES:** The total page count should follow normal pagination procedures, i.e., enter the number of pages containing information.

7b. **NUMBER OF REFERENCES:** Enter the total number of references cited in the report.

8a. **CONTRACT OR GRANT NUMBER:** If appropriate, enter the applicable number of the contract or grant under which the report was written.

8b, 8c, & 8d. **PROJECT NUMBER:** Enter the appropriate military department identification, such as project number, subproject number, system numbers, task number, etc.

9a. **ORIGINATOR'S REPORT NUMBER(S):** Enter the official report number by which the document will be identified and controlled by the originating activity. This number must be unique to this report.

9b. **OTHER REPORT NUMBER(S):** If the report has been assigned any other report numbers *(either by the originator or by the sponsor)*, also enter this number(s).

10. **AVAILABILITY/LIMITATION NOTICES:** Enter any limitations on further dissemination of the report, other than those imposed by security classification, using standard statements such as:

(1) "Qualified requesters may obtain copies of this report from DDC."

(2) "Foreign announcement and dissemination of this report by DDC is not authorized."

(3) "U. S. Government agencies may obtain copies of this report directly from DDC. Other qualified DDC users shall request through
________________."

(4) "U. S. military agencies may obtain copies of this report directly from DDC. Other qualified users shall request through
________________."

(5) "All distribution of this report is controlled. Qualified DDC users shall request through
________________."

If the report has been furnished to the Office of Technical Services, Department of Commerce, for sale to the public, indicate this fact and enter the price, if known.

11. **SUPPLEMENTARY NOTES:** Use for additional explanatory notes.

12. **SPONSORING MILITARY ACTIVITY:** Enter the name of the departmental project office or laboratory sponsoring *(paying for)* the research and development. Include address.

13. **ABSTRACT:** Enter an abstract giving a brief and factual summary of the document indicative of the report, even though it may also appear elsewhere in the body of the technical report. If additional space is required, a continuation sheet shall be attached.

It is highly desirable that the abstract of classified reports be unclassified. Each paragraph of the abstract shall end with an indication of the military security classification of the information in the paragraph, represented as *(TS)*, *(S)*, *(C)*, or *(U)*.

There is no limitation on the length of the abstract. However, the suggested length is from 150 to 225 words.

14. **KEY WORDS:** Key words are technically meaningful terms or short phrases that characterize a report and may be used as index entries for cataloging the report. Key words must be selected so that no security classification is required. Identifiers, such as equipment model designation, trade name, military project code name, geographic location, may be used as key words but will be followed by an indication of technical context. The assignment of links, rules, and weights is optional.

UNCLASSIFIED

Security Classification

The Johns Hopkins University
APPLIED PHYSICS LABORATORY
Silver Spring, Maryland

AD 630342

October 25, 1966

To: Distribution List of APL/JHU TG-752, "An Engineering Method for Rapid Calculation of Supersonic-Hypersonic Pressure Distributions on Lifting and Non-Lifting Pointed Bodies of Revolution and Several Special Cases of Blunt-Nosed Bodies of Revolution," (Unclassified) by R. J. Vendemia, Jr., dated November 1965.

From: Editorial Project Supervisor, Technical Reports Group

Subject: APL/JHU TG-752; correction to

The equation that defines p/p_1 on page 38 of the subject report inadvertently has a sign error in the exponential term. To insure proper accuracy of the work reported, the following revised pages are attached: 37-38, 39-40, 43-44, 45-46, 47-48. You are therefore requested to remove the corresponding pages from your copy of the report and insert the corrected ones.

Paul E. Clark
Paul E. Clark

PEC/job

Enclosures

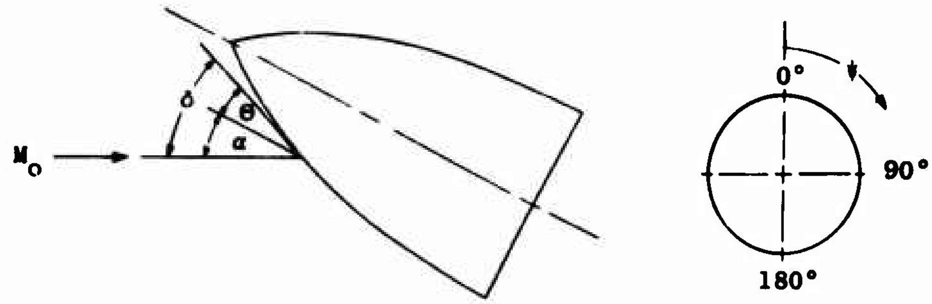

For $\alpha = 0°$, $\sin \delta = \sin \theta$.

The value for $C_{p_{max}}$ on the desired meridian, ψ, may be determined either experimentally or theoretically. The NASA[21,22] zero and small angle of attack cone #tables can be used for the starting values on a cone fitted to the nose vertex if experimental data are lacking; the procedure is as follows: The general expression for pressure coefficient is:

$$C_p = \frac{p_o}{q_o}\left(\frac{p}{p_o} - 1\right) \text{ and } \frac{p}{p_o} = \frac{p}{p_1}\,\frac{p_1}{p_o}$$

where p_1 refers to conditions at zero angle of attack and the quantity p_1/p_o may be obtained directly from the zero angle of attack cone tables[22]. The ratio of p/p_1 which is the ratio of static pressure at angle of attack to static pressure at zero angle of attack can be calculated using the theory of Stone[23] wherein the velocity, pressure, and density are expanded in the following series and higher order terms in α are neglected:

$$M^* = M_1^* - \alpha M_2^* \cos \psi$$

$$p = p_1 - \alpha p_2 \cos \psi$$

$$\rho = \rho_1 - \alpha \rho_2 \cos \psi$$

where the flow quantities M_1^*, p_1, and ρ_1 refer to conditions at zero angle of attack and M_2^*, p_2, and ρ_2 are the flow quantities related to the effect of angle of attack. Reference 23 provides solutions for the above equations yielding,

#The necessary tables required in the calculational procedures of this sub-section have been reproduced from the references and included in Appendix 1.

among others, the following expression:

$$p/p_1 = \left[\frac{(\gamma+1) - (\gamma-1) M^{*2}}{(\gamma+1) - (\gamma-1) M_1^{*2}}\right]^{\frac{\gamma}{\gamma-1}} e^{\alpha (S_2/R) \cos \psi}$$

References 21 and 22 have provided tabulated values of M_1^*, M_2^*, and S_2/R for use in determining p/p_1 and subsequently, C_p. Since conditions at the nose vertex were used to calculate the pressure coefficient, this value of C_p becomes C_{p_N} from whence $C_{p_{max}}$, Equation (7), may be determined. Starting values of $C_{p_{max}}$ must be calculated for each value of ψ at the desired angle of attack. Once this is done, the Generalized Newtonian theory, Equation (6), is used to calculate the values of C_p along each meridian up to the point where the shock expansion method is used to extend the impact theory; for the cylindrical afterbody, Equation (5a) or (5b) is used for the pressure coefficient distribution.

The local Mach number at the nose vertex (where $M = M_N$) may be determined from the relation[24]:

$$M^2 = \frac{2 M^{*2}}{(\gamma+1) - (\gamma-1) M^{*2}}$$

On the leeward side of the body, certain portions of the surface will lie in the "aerodynamic shadow" and the Newtonian theory cannot predict the pressures in this region. This shadow area on the body, shown pictorially here,

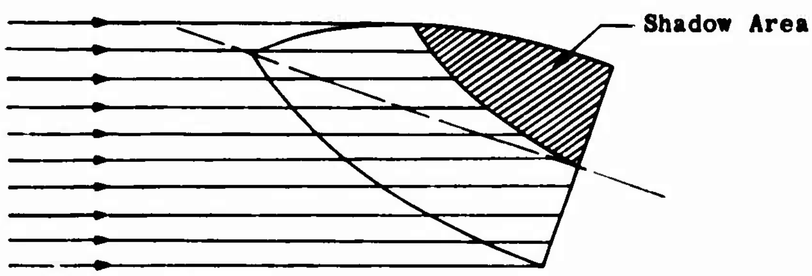

can be determined quite easily along any leeward meridian by setting $\sin \delta = 0$ and solving for Θ. For any meridian in general, the Θ at which the shadowed area starts is:

$$\Theta = \tan^{-1} (\tan \alpha \cos \psi)$$

for $\psi = 0°$ $\quad \Theta = \alpha$

Thus the shadow area begins along the $\psi = 0°$ meridian at the point where the body surface angle is equal to the angle of attack.

On all meridians, the matching point (where the shock-expansion method is used to extend the impact theory) is obtained directly from plots presented in prior sections of this report, e.g., Fig. 6, page 16. When the matching point lies within the shadowed area, the shock-expansion method should be started at the x/ℓ value where $\sin \delta = 0$.

A numerical example is presented in Appendix 1 wherein the pressure coefficient distribution has been calculated for a tangent ogive-cylindrical afterbody combination at $M_o = 2.0$ and $\ell/d = 3$ at an angle of attack of 5 degrees. Tables are included which provide the necessary parameters for determining the pressure and local Mach number distribution. For the numerical example, starting values of C_{p_N} were determined for seven meridians beginning at $\psi = 0°$ and proceeding in 30 degree increments up to $\psi = 180°$. The pressure distribution along the $\psi = 180°$ meridian is the only one for which the C_p calculation is shown since the procedure is similar for each meridian. The calculation of the cylindrical afterbody pressure distribution using Equation (5b) has also been included for the $\psi = 180°$ meridian.

The pressure distributions calculated by the present method for the numerical example of Appendix 1 are presented in Figure 23 where experimental

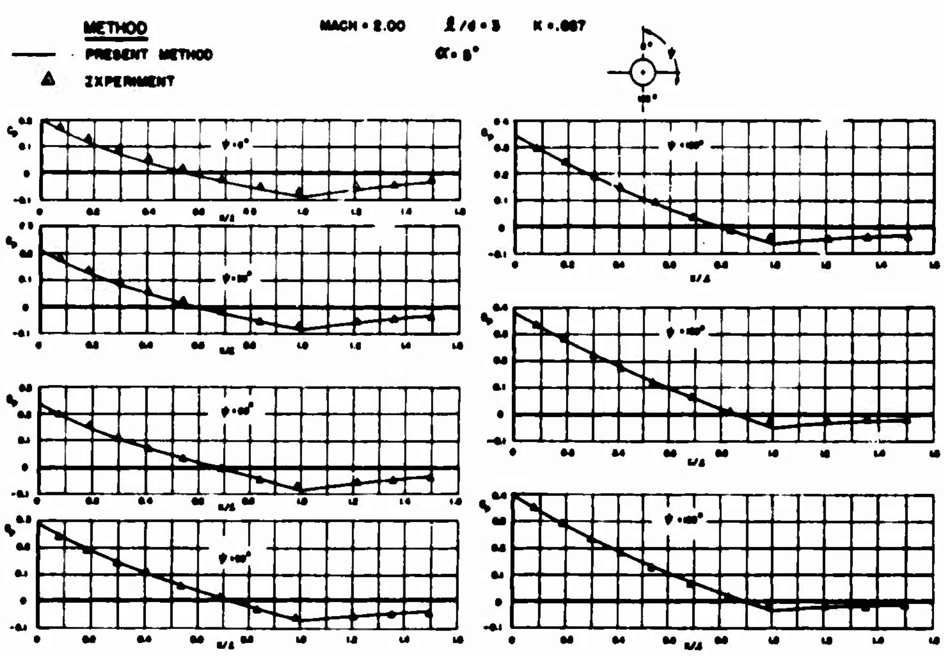

Fig. 23 PRESSURE COEFFICIENT DISTRIBUTION FOR A TANGENT OGIVE-CYLINDRICAL AFTERBODY COMBINATION AT $\alpha = 5°$, $\psi = 0°, 30°, 60°, 90°, 120°, 150°$, and $180°$

values[25] have been included for comparison purposes with the subsequent indication of good agreement.

2. Bodies of Revolution at Large Angles of Attack

The calculation of pressure distributions for angles of attack greater than about 5 degrees requires somewhat more time since the starting values of C_{p_N} must be determined from the MIT[26,27,28] cone tables (or comparable information) unless experimental data are available. Once the starting values have been obtained, the procedure is similar to that used for the small angles of attack.

Since the MIT cone tables are being used to obtain starting values at the nose vertex, the symbols and nomenclature adopted by this widely used reference will not be altered to conform to the nomenclature of this report. Any attempt to redefine or re-reference the parameters would inevitably tend to compound the existing complexity of the equations. The symbols and nomenclature from the MIT cone tables which are used in the present study are defined on page 4 of this report. In addition, the parameters required for calculating C_{p_N} have been picked from the MIT cone tables and are tabulated in Appendix 2 for ready use. If any intermediate values of the parameters are required, they can be obtained much more readily when nomenclature consistent with the reference source is used.

The theory of Stone[23] is used once again to determine the flow parameters which have been expanded in the following series; for large angles of attack, the higher order terms in α cannot be neglected, i.e.,

$$p/\bar{p} = 1 + \alpha A_1 \cos \psi + \alpha^2 (A_2 + A_3 \cos 2\psi)$$

$$\rho/\bar{\rho} = 1 + \alpha B_1 \cos \psi + \alpha^2 (B_2 + B_3 \cos 2\psi)$$

where $p/\bar{p}$ and $\rho/\bar{\rho}$ are the pressure and density on the cone surface at angle of attack divided by the corresponding values at zero angle of attack, A_1 and B_1 specify the first order effects of α, and A_2, A_3, B_2, and B_3 represent the second order effects of α. Proceeding further:

$$A_1 = -\eta/\bar{p}$$

$$A_2 = p_o/\bar{p} + \frac{\gamma}{2} \frac{\bar{u}^2}{\bar{a}^2} + \frac{\eta}{2\bar{p}} \cot \theta_s$$

$$A_3 = p_2/\bar{p} + \frac{\gamma}{2} \frac{\bar{u}^2}{\bar{a}^2} - \frac{\eta}{2\bar{p}} \cot \theta_s$$

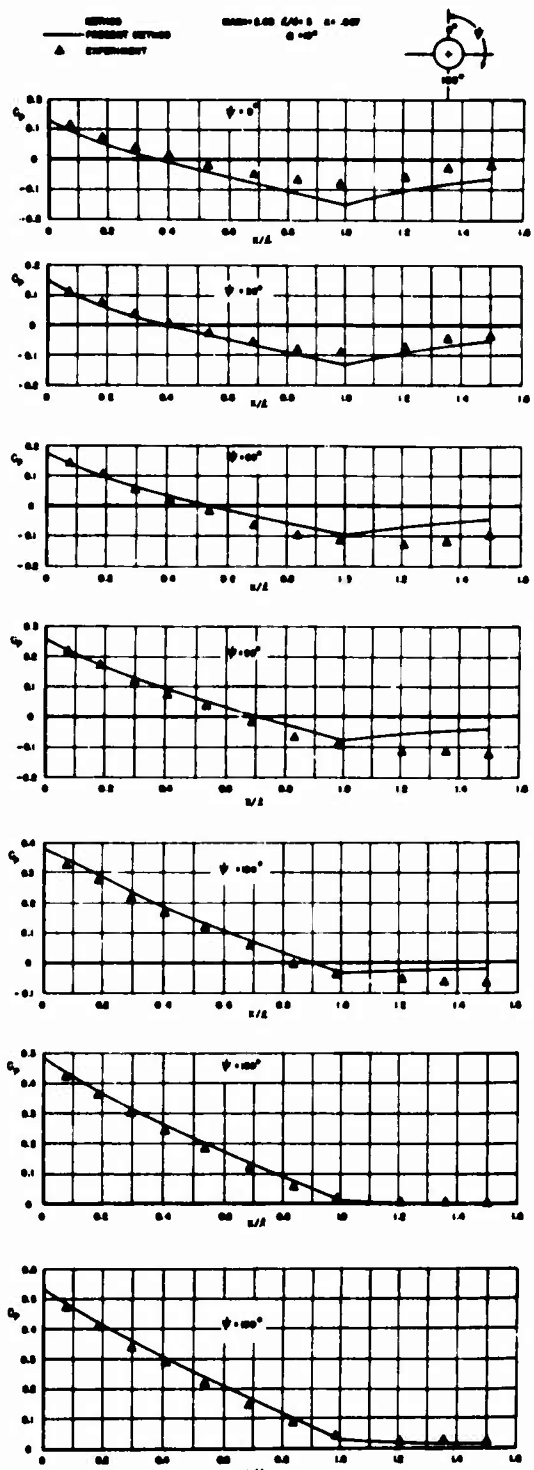

Fig. 24 PRESSURE COEFFICIENT DISTRIBUTION FOR A TANGENT OGIVE-CYLINDRICAL AFTERBODY COMBINATION AT $\alpha = 10°$, $\phi = 0°, 30°, 60°, 90°, 120°, 150°,$ and $180°$

APPENDIX I

CALCULATION OF PRESSURE COEFFICIENT DISTRIBUTION FOR A TANGENT OGIVE-CYLINDRICAL AFTERBODY COMBINATION AT AN ANGLE OF ATTACK OF 5 DEGREES

A. CONDITIONS

FREE STREAM MACH NUMBER	—	$M_o = 2$
NOSE FINENESS RATIO	—	$\ell/d = 3$
NOSE SEMI-VERTEX ANGLE	—	$\theta_N = 18.925°$
HYPERSONIC SIMILARITY PARAMETER	—	$K = .67$
RATIO OF SPECIFIC HEATS	—	$\gamma = 1.405$

B. PRESSURE COEFFICIENT AND MACH NUMBER STARTING VALUES, $X/\ell = 0$

$$C_p = (P_o/q_o)(P/P_o - 1) = (P_o/q_o)\left[(P/P_1)(P_1/P_o) - 1\right] \qquad \text{EQ. AI-1}$$

$$P/P_1 = \left[\frac{(\gamma+1)-(\gamma-1)M^{*2}}{(\gamma+1)-(\gamma-1)M_1^{*2}}\right]^{\frac{\gamma}{\gamma-1}} e^{\alpha(S_2/R_1)\cos\psi} \qquad \text{EQ. AI-2}$$

$$M^* = M_1^* - \alpha M_2^* \cos\psi, \qquad \alpha \text{ IN RADIANS} \qquad \text{EQ. AI-3}$$

$$M = \left[\frac{2M^{*2}}{(\gamma+1)-(\gamma-1)M^{*2}}\right]^{1/2} \qquad \text{EQ. AI-4}$$

WHERE $P_1/P_o = 1.8336$ FROM APPENDIX I, TABLE 8, PAGE 50 .

$M_1^* = 1.4241$ " " " TABLE 9, " 51 .

$M_2^* = -.7258$ " " " TABLE 10, " 52 .

$S_2/R_1 = .0651$ " " " TABLE 11, " 53 .

$P_o/q_o = .3571 = \dfrac{2}{\gamma M_o^2}$

NUMERICAL SOLUTIONS FOR EQUATIONS AI-1, AI-2, AI-3, AND AI-4 ARE SHOWN IN COLUMNS 8, 6, 4, AND 9 RESPECTIVELY OF TABLE 2, PAGE 46 .

APPENDIX I

TABLE 2. PRESSURE COEFFICIENT AND MACH NUMBER STARTING VALUES, $X/\ell = 0$, $\alpha = 5°$

1	2	3	4	5	6	7	8	9	10
ψ	$\cos\psi$	$\alpha M_2^* \cos\psi$	M^* EQ. AI-3	$e^{\alpha (S_2/R) \cos\psi}$	P/P_1 EQ. AI-2	P/P_0 = 1.8336 ⑥	$C_p = C_{p_N}$ EQ. AI-1	$M = M_N$ EQ. AI-4	*$(P/P_t)_N$ TABLE 18
0	1.0000	-.0633	1.4874	1.0075	.8519	1.5620	.2007	1.713	.1987
30	.8660	-.0549	1.4790	1.0065	.8710	1.5970	.2132	1.697	.2036
60	.5000	-.0317	1.4568	1.0037	.9248	1.6956	.2484	1.656	.2164
90	0	0	1.4241	1.0000	1.0000	1.8336	.2976	1.606	.2332
120	-.5000	.0317	1.3925	.9963	1.0774	1.9754	.3488	1.547	.2544
150	-.8660	.0549	1.3693	.9936	1.1354	2.0818	.3863	1.510	.2686
180	-1.0000	.0633	1.3606	.9926	1.1569	2.1212	.4004	1.496	.2740

C. SINE OF FLOW DEFLECTION ANGLE, δ, ALONG $\psi = 180°$ MERIDIAN

$$\sin\delta = \sin\theta \cos\alpha - \cos\psi \cos\theta \sin\alpha$$

TABLE 3. VALUES OF SINE δ, $\alpha = 5°$

1	2	3	4	5	6	7
X/ℓ	θ	$\sin\theta$	$\cos\theta$	$\sin\theta\cos\alpha$	$\cos\psi\cos\theta\sin\alpha$	$\sin\delta$
0	18.925	.32433	.94594	.32309	-.08245	.40554
.1	16.972	.29190	.95645	.29079	-.08336	.37415
.2	15.038	.25946	.96575	.25847	-.08417	.34264
.3	13.122	.22703	.97388	.22617	-.08488	.31105
.4	11.221	.19460	.98088	.19386	-.08549	.27935
.5	9.333	.16217	.98676	.16155	-.08601	.24756
.6	7.464	.12973	.99155	.12924	-.08642	.21566
.7	5.584	.09730	.99525	.09693	-.08675	.18368
.8	3.719	.06487	.99789	.06462	-.08698	.15160
.9	1.859	.03243	.99947	.03231	-.08711	.11942
1.0	0	0	1.00000	0	-.08716	.08716

* VALUES OF $(P/P_t)_N$ ARE OBTAINED FROM TABLE 18 USING THE APPROPRIATE VALUES OF M_N IN COLUMN 9, TABLE 2.

APPENDIX I

D. PRESSURE COEFFICIENT AND LOCAL MACH NUMBER DISTRIBUTIONS ALONG $\psi = 180^\circ$ MERIDIAN (SEE FIGURE 23)

CONDITIONS AT NOSE VERTEX

$M_N = 1.498$ — COLUMN 9, TABLE 2

$(P/P_t)_N = .2740$ — " 10, "

$C_{p_N} = .4004$ — " 8, "

$C_{p_{MAX}} = 2.4346$ — EQ. 7

1. C_p VALUES (COLUMN 3, TABLE 4) FROM THE NOSE VERTEX UP TO THE MATCHING POINT, $(X/\ell)_m$, ARE OBTAINED USING EQ. 6. (THE MATCHING POINT SOLUTION IS DISCUSSED ON PAGE 18).
2. C_p VALUES (COLUMN 4, TABLE 4) FROM $(X/\ell)_m$ TO $X/\ell = 1$ ARE CALCULATED USING THE PROCEDURE OUTLINED ON PAGES 15 AND 16. FOR THIS PARTICULAR EXAMPLE, $C_p = 2.7646\,(P/P_t) - .3571$ (EQ. 3)
3. ALL LOCAL MACH NUMBER VALUES (COLUMN 9, TABLE 4) ARE OBTAINED FROM TABLE 18, APPENDIX 3, USING THE APPROPRIATE VALUE OF P/P_t (COLUMN 8, TABLE 4) CALCULATED FROM EQ. 3a.

TABLE 4. PRESSURE COEFFICIENT DISTRIBUTION AND MACH NUMBER ALONG $\psi = 180^\circ$ MERIDIAN, $\alpha = 5^\circ$

1	2	3	4	5	6	7	8	9
X/ℓ	$\sin^2\delta$	C_p GN EQ. 6	C_p SEM EQ. 3	θ	$\Delta\theta$	ν	P/P_t	M TABLE 18
0	.16446	.4004	—	—	—	—	.2740	1.498
.1	.13999	.3408	—	—	—	—	.2524	1.552
.2	.11740	.2858	—	—	—	—	.2325	1.608
.3	.09675	.2355	—	—	—	—	.2144	1.662
.4	.07804	.1900	—	—	—	—	.1979	1.716
.5	.06129	.1492	—	—	—	—	.1831	1.767
.6	.04651	.1132	—	—	—	—	.1701	1.816
$.7_m$	.03374	.0821	.0821	5.584	—	22.426	.1589	1.855
.8	—	—	.0399	3.719	1.865	24.291	.1436	1.925
.9	—	—	.0009	1.860	1.860	26.151	.1295	1.992
1.0	—	—	-.0350	0	1.859	28.010	.1165	2.060

GN = GENERALIZED NEWTONIAN

SEM = SHOCK EXPANSION METHOD

θ = BODY SURFACE ANGLE

$.7_m$ = MATCHING POINT OF GENERALIZED NEWTONIAN AND SHOCK EXPANSION METHOD

M = M CORRESPONDING TO P/P_t FROM PRANDTL-MEYER TABLES

ν = PRANDTL-MEYER FLOW DEFLECTION ANGLE CORRESPONDING TO M

APPENDIX I

E. CYLINDRICAL AFTERBODY PRESSURE COEFFICIENT DISTRIBUTION ALONG $\psi = 180°$ MERIDIAN

USING EQ. 5b

$$C_p = C_{p\,(x/\ell=1)}\, e^{-\frac{\Delta x/\ell}{K}}$$

VALUES OF C_p ON THE CYLINDRICAL AFTERBODY ARE CALCULATED AS SHOWN IN TABLE 5.

$C_{p(x/\ell=1)} = -.0350$, FROM COLUMN 4, TABLE 4.

TABLE 5. PRESSURE COEFFICIENT DISTRIBUTION ON CYLINDRICAL AFTERBODY, $\alpha = 5°$

1	2	3	4
x/ℓ	$\Delta x/\ell$	$e^{-\frac{2}{K}}$	$C_p = -.0350 \; 3$
1.0	0	1.0000	-.0350
1.1	.1	.8607	-.0301
1.2	.2	.7408	-.0259
1.3	.3	.6376	-.0223
1.4	.4	.5488	-.0192
1.5	.5	.4724	-.0165

TABLE 6. Values of Surface Pressure Coefficient, C_{p_N}, at $\alpha = 0°$

M_o \ θ_N	2.5	5.0	7.5	10.0	12.5	15.0	17.5	20.0	22.5	25.0	27.5	30.0
1.5	.012338	.039662	.077386	.123798	.178117	.240031	.309545	.386979	.473154	.569989		
1.75	.011441	.036329	.070429	.112270	.161201	.216923	.279290	.348246	.423819	.506190	.595857	.694052
2.0	.010786	.033946	.065581	.104458	.150085	.202234	.260761	.325531	.396413	.473302	.556160	.645120
2.5	.009830	.030586	.058960	.094131	.135861	.184034	.238526	.299159	.365710	.437919	.515504	.598189
3.0	.009135	.028240	.054519	.087475	.127024	.173101	.225581	.284262	.348884	.419129	.494637	.575031
3.5	.008592	.026475	.051302	.082818	.121020	.165859	.217199	.274818	.338425	.407669	.482154	.561453
4.0	.008149	.025088	.048865	.079393	.116712	.160770	.211415	.268404	.331425	.400103	.474018	.552714
4.5	.007779	.023968	.046962	.076789	.113504	.157044	.207243	.263837	.326496	.394830	.468399	.546733
5.0	.007462	.023047	.045443	.074757	.111045	.154232	.204131	.260466	.322892	.391003	.464350	.542452
6.0	.006947	.021623	.043189	.071829	.107580	.150338	.199887	.255923	.318080	.385936	.459028	.536858
7.0	.006544	.020585	.041621	.069858	.105309	.147838	.197204	.253086	.315105	.382829	.455786	.533474
8.0	.006221	.019802	.040486	.068472	.103744	.146141	.195404	.251260	.313140	.380789	.453669	.531271
10.0	.005736	.018718	.038988	.066703	.101792	.144060	.193221	.248931	.310793	.378363	.451160	.528672
12.0	.005392	.018021	.038076	.065665	.100674	.142885	.192002	.247675	.309500	.377032	.449790	.527256
15.0	.005038	.017365	.037263	.064766	.099723	.141897	.190986	.246631	.308431	.375937	.448664	.526095
20.0	.004681	.016779	.036577	.064031	.098960	.141113	.190185	.245813	.307594	.375079	.447785	.525193